An *XMM* Search for Quiescent Low-Mass X-ray Binaries in Globular Cluster using X-ray Spectral Identification

Sebastien Guillot

Master of Science

Department of Physics

McGill University

Montreal,Quebec

September 3, 2009

Thesis submitted to McGill University in partial fulfillment of the requirements of the degree of Master of Science

DEDICATION

À mon père.

ACKNOWLEDGEMENTS

I would like to use this page to thank the people who showed great support during those two great years of research. First, I want to thank my supervisor, Bob Rutledge, to whom I owe a lot, for his availability, his patience to answer my questions with great detail, his dedication and his time spent reading my written work. I would also like to acknowledge my co-authors on the two manuscripts I published this year: Vyacheslav Zavlin, George Pavlov, Edward Brown and Lars Bildsten.

I am very grateful with my family for their care and support, especially my mom, my sister and my grand-father. Finally, I also want to thank Marie for her patience listening to the ups and downs concerning the advancement of my research project.

ABSTRACT

Low-mass X-ray binaries (LMXBs) are now routinely used for neutron star (NS) radius measurements. Observations of these systems in their quiescent stage (qLMXB) is one method leading to precise measurements. However, the dominant source of uncertainty on the NS radii remains the distance to the binary systems. Globular clusters (GCs) are therefore the places to look for more qLMXBs, due to their known or measurable distances and their abundance of binary systems. This thesis reports the discovery of seven candidate qLMXBs in six GCs, using observations from the *XMM-Newton* satellite, based on X-ray spectral consistency with NS hydrogen atmosphere models. The goal of this program of observations is to increase the population of known GC qLMXBs, for which longer follow-up exposures will permit high precision radius measurements. Nine candidates were initially identified based on their X-ray spectra with signal-to-noise ratio $S/N > 3$. Two candidates in NGC 6304 were tentatively confirmed, with consistent best-fit parameters, in a follow-up *Chandra* observation. One low-S/N candidate in NGC 6540 ($S/N = 7$) was subsequently excluded by a deeper, higher S/N ($S/N = 17$) observation. One other candidate was also excluded on the basis of the spatial velocity of the associated companion star, precluding cluster membership. Thus, the present work has added seven new qLMXB candidates to the eleven previously known.

RESUMÉ

Les systèmes binaires X à faible masse (LMXB) sont de plus en plus utilisés pour mesurer le rayon des étoiles à neutrons. L'observation de ces systèmes au repos (en quiescence, qLMXB) est l'une des méthodes utilisées pour obtenir des mesures précises du rayon. Cependant, l'incertitude dominante reste la distance du système binaire. Les amas globulaires (AGs) sont donc les emplacements pour chercher des qLMXBs, grâce à leur distance connues ou facilement mesurables et leur abondance de qLMXBs. Cette thèse présente la découverte de sept qLMXBs candidates dans six AGs à partir d'observations du satellite *XMM-Newton*, basée sur leurs compatibilité avec des modèles d'atmosphère d'hydrogène d'étoiles à neutrons. Le but de ce programme d'observations est d'augmenter la population des qLMXBs connues, pour lesquelles de plus longues observations permettront des mesures de rayons plus précises. Neuf candidates ont été l'objet de découvertes basées sur leur spectre X avec un rapport signal-sur-bruit $S/B > 3$. Deux d'entre elles, dans l'amas NGC 6304, ont été confirmées, avec des paramètres compatibles, grâce à des observations du satellite *Chandra*. Une candidate dans NGC 6540, ayant un faible S/B ($S/B = 7$), a été exclu après l'analyse de données avec un $S/B = 17$. Une autre a également été révoqué à cause du mouvement propre de sa compagne optique, excluant toute appartenance à l'AG. Par conséquent, le travail présenté ici a ajouté sept candidates qLMXB aux onze déjà connues.

TABLE OF CONTENTS

LIST OF TABLES

LIST OF FIGURES

STATEMENT OF ORIGINAL RESEARCH

Part of this thesis consists of two manuscripts, one published in *M.N.R.A.S.* and one accepted for publication in the July 2009 issue of *ApJ*:

- S. Guillot, R. E. Rutledge, L. Bildsten, E. F. Brown, G. G. Pavlov, and V. E. Zavlin. *X-ray spectral identification of three candidate quiescent low-mass X-ray binaries in the globular cluster NGC 6304*. M.N.R.A.S., 392:665–681, January 2009a.
- S. Guillot, R. E. Rutledge, E. F. Brown, G. G. Pavlov, and V. E. Zavlin. *Chandra Observation of Quiescent Low-Mass X-ray Binaries in the Globular Cluster NGC 6304*. ArXiv e-prints, March 2009b. Accepted in ApJ.

The following sections were used in parts using the text of the two articles: § 1.2.2, § 2.2, § 2.3, § 3.2, § 4.1 and chapter 5. The figures 4–1 to 4–9, also published in the two cited articles were used in this thesis, with the proper citations. Finally, the tables 2–1, 4–2, 5–2, 5–3 and 5–4 were, in parts or in their entirety, based on tables and data published in Guillot et al. (2009) and **?**.

I would like to acknowledge the contributions of the co-authors for the preparation of these two manuscripts:

- Vyacheslav Zavlin for providing the neutron star atmosphere tabulated model and for his very useful comments and suggestions.
- George Pavlov for his very useful comments and suggestions.
- Edward Brown for his very useful comments and suggestions and for the clarifications he provided on the paragraph mentioning the nuclear physics involved in the crust of neutron stars.
- Lars Bildsten for his very useful comments and suggestions and for useful discussions.
- Robert Rutledge for his patience reading the manuscripts and for providing many improvements to the original text. I would also like to thank him for giving me the opportunity to analyze the *XMM-Newton* data presented in this thesis.

CHAPTER 1
Introduction

1.1 Neutron Stars - The Remnants of Supernova Explosions

The history of neutron star discoveries has been reviewed by several authors (see Rosswog and Bruggen 2000; Carroll and Ostlie 1996).

The first mention of neutron stars (NSs) as astrophysical objects can be traced more than 70 years ago, only one year after the discovery of the neutron (Chadwick 1932). At that time, it was suggested that supernova explosions of stars would lead to stellar compact objects consisting mainly of neutrons (Baade and Zwicky 1934). However, there were more than 40 years between this first theoretical postulate and the emergence of observational evidence of the existence of NSs. In 1967, X-ray and optical emissions of Scorpius X-1 (Sco X-1) were interpreted as coming from an accreting NS in a binary system (Shklovsky 1967). The subclass of radio pulsating neutron stars (pulsars) was discovered the following year when the radio pulsations from the pulsar PSR 1919+21 were attributed to a rapidly rotating magnetized NS (Hewish et al. 1969).

It is now widely accepted that typical NS radii are of the order of 10 km and typical NS masses of about $1.4\,M_\odot$ (for a review, see Lattimer and Prakash 2004, LP04 hereafter). Their core densities reach values above the density of nuclear matter, above any type of matter formed in laboratories and beyond the *neutron drip density*: $\rho_{\rm drip} = 4\times10^{11}\,{\rm g\,cm^{-3}}$, above which nuclei are immersed in a bath of neutrons (Rosswog and Bruggen 2000). Since the initial theoretical picture of a NS described as a sphere of neutron matter, the knowledge of nuclear physics has expanded and NSs are now believed to be composed of four major components (see Figure 1–1, and for a more precise description on the internal structure of NSs, see LP04; Rosswog and Bruggen 2000):

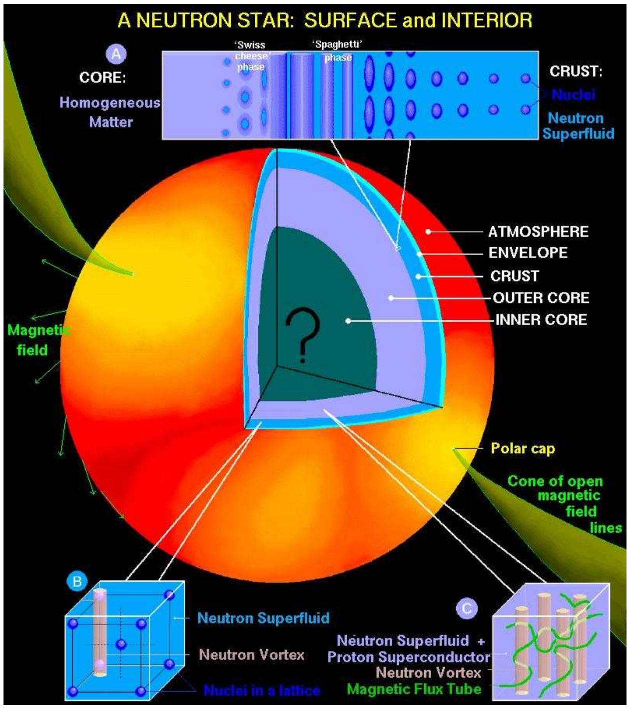

Figure 1–1: The structure of a NS, and the possible composition of the interior. Image from http://www.astroscu.unam.mx/neutrones/

- The core accounts for about $\sim$ 99% of the mass and has densities above $10^{14}\,\mathrm{g\,cm^{-3}}$. At such densities, individual nuclei are not found. Instead, baryons exist in the form of an homogeneous neutron-proton fluid. The inner part of the core may contain more exotic matter like pions and kaons.

- The crust ($\sim 1-2\,\mathrm{km}$ thick) has density in the range $\rho \sim 10^9 - 10^{14}\,\mathrm{g\,cm^{-3}}$, varying with depth. It is mostly composed of nuclei in a crystalline lattice.
- The envelope surrounding the crust only has a small contribution to the total mass of the NS, but it is important for the release of the thermal energy and its transport through the surface layers.
- The atmosphere has a thickness of a few centimeters and also contains a negligible mass. However, its composition directly affects the emission of the NS by shaping the observed photon spectrum through radiative transfer.
  In the specific case of NSs in accreting X-ray binaries, the atmosphere is composed of ionized hydrogen transfered from a stellar companion since heavier accreted elements gravitationally settle through the envelope on short timescales of $\sim$ few seconds (Bildsten et al. 1992)

As it was initially postulated in 1934, NSs are the remnants of core-collapse supernovae (Baade and Zwicky 1934). We now have a better understanding of this phenomena, from observations and from theoretical approaches. These energetic explosions, releasing $\sim\ 10^{51}\,\mathrm{erg\ s^{-1}}$, occur when a massive star ($M \gtrsim 8\,M_{\odot}$, depending on its metallicity, Heger et al. 2003) has consumed all the hydrogen fuel in its core and evolved through the different stages of expansion/contraction and shell burning of the giant phase of stellar evolution. The gravitational pressure in the core exceeds the electron degeneracy pressure and the inner core collapses (Carroll and Ostlie 1996). The outer parts of the core then infalls on the contracted core and bounces off, creating a shock wave within 2 sec of the core collapse, that will expel the matter surrounding the core, leaving a proto-NS.

Different observational classes of NSs are known based on their emission mechanisms and on the observational methods used to detect them, even if they all fall under the classification of NS. The following short discussion intends to clarify the nomenclature of the most widely-accepted types. First, rotation-powered pulsars are isolated fast-rotating NSs – with rotation period P between $P \approx 1.4\,\mathrm{msec}$ (Hessels et al. 2006) and $P \approx 8.5\,\mathrm{sec}$ (Young et al. 1999) – with a relatively large magnetic field ($\sim 10^{12}\,\mathrm{G}$), emitting beamed radio pulses that can be directed toward us, at regular intervals set by the rotation period. The source of the emitted energy is rotational kinetic energy, as these pulsars are observed to spin down, while the emission mechanism appears related to the dipolar magnetic field. The category of magnetars is composed of NSs which have magnetics fields up to $B \sim 10^{15}\,\mathrm{G}$ (Woods and Thompson 2006). They are observed as soft gamma-ray repeaters or anomalous X-ray pulsars. A significant fraction of their observed luminosities is likely related to the process of magnetic field decay. Rotation-powered pulsars which do not have their radio pulses directed toward the observer simply appear as isolated NSs. A second category includes all NSs in binary systems. These are generally powered by the accretion from a stellar companion. The phases of accretion have been observed to be persistent or transient, with regular or irregular recurrence. This category includes low-mass X-ray binaries (LMXB), high-mass X-ray binaries and accreting millisecond pulsar (MSPs). The following section presents X-ray binaries in general and their use for NS radii measurements and § 1.3.2 provides more details about LMXBs and MSPs.

1.2 X-ray Binaries

The observational discovery of NSs may be traced to the X-ray observation performed with a sounding rocket flight above the atmosphere (Giacconi et al. 1962). This was the first observation of an X-ray source outside the solar system, Sco X-1. The NS classification of this source was proposed a few years later when a bright main-sequence star companion was confirmed, suggesting an accreting X-ray system (Shklovsky 1967). This discovery occurred before the first observation of a radio pulsar in 1968 (Hewish et al. 1969). However, it was the rapid rotation of radio pulsars – evidenced by their short period – which first produced the unequivocal interpretation that the source is NS. A few years later, the first X-ray sources discovered in globular clusters were reported in the *UHURU* catalogue (Giacconi et al. 1972, 1974). Since then, hundreds of X-ray binaries have been discovered in the field of the Galaxy and few tens in globular clusters (GCs) (Pooley et al. 2003). The population of NS X-ray binaries in GCs has now become useful for the purpose of determining the equation of state of dense matter, as described in the present work.

1.2.1 The Equation of State and Radius Measurements of Neutron Stars

At the densities expected inside NSs, the behavior of matter is not understood. The pressure and the density are linked by the dense matter equation of state (EoS). However, the unknown interactions between particles at nuclear densities are so uncertain that a large number of different dense matter EoSs are predicted (Lattimer and Prakash 2007, LP07 hereafter). One can only rely on theoretical models since cold NS matter (neutron dominated) cannot be reproduced in laboratories. Each EoS model describing NS matter produces a specific curve on a mass-radius diagram (Fig. 1–2). While most of the EoSs describe normal matter with neutrons and protons, some EoSs correspond to a more exotic composition, involving quarks, hyperons or kaons. As seen on Fig. 1–2, causality provides an upper limit on the NS mass since the sound speed is limited by the speed of light. The lower bound to the possible NS masses is constrained by their rotation. The mass-shedding limit is defined by the rotational frequency at which the velocity of a particle orbiting just above the surface of the NS equals the velocity of the NS surface (LP04). This is defined by the Keplerian velocity $v_{\mathrm{K}} = (2\pi)^{-1}\sqrt{GM/R^3}$, in the case of a Newtonian sphere.

The study of NSs is motivated in part by the need to determine the dEoS. Nuclear physics provides the models for the dEoS which can only be confirmed or refuted by observing NSs and by obtaining precise measurements of NS radii and masses (LP07).

Independent measurements of NS masses using presently available techniques can only be obtained from binary systems. The most accurate values are attained with double NS binaries (Weisberg and Taylor 2005; Kramer et al. 2006). NS-White Dwarf (WD) binary systems are also providing measurements for the NS masses, which, on average, tend to be larger than that of other types of binary systems (LP07). In the best case, the masses of the two NSs in the binary pulsar system PSR 1913+16 have been measured with an accuracy of $\sim 0.014\%$ (Weisberg and Taylor 2005). However, the inclination angle of binary systems is not always well constrained and adds an additional uncertainty to the masses

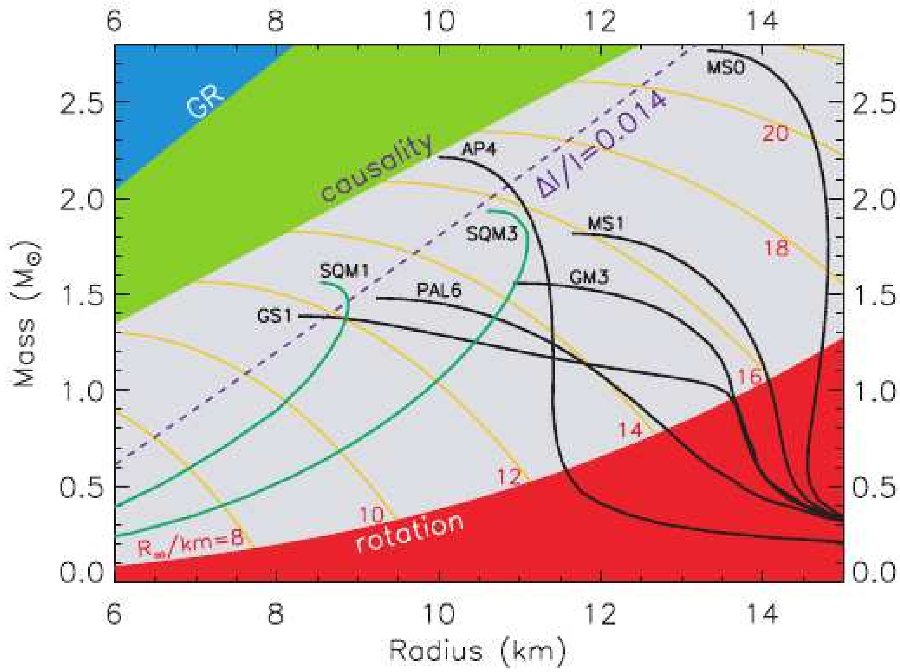

Figure 1–2: This figure shows a typical mass-radius diagram for NSs (from LP04). The black curves correspond to the normal matter EoSs while the green curves are for strange quark matter EoSs. The yellow lines represent the contours of constant radiation radius R_∞ (for EoSs notations, see Lattimer and Prakash 2001).

measured. Nevertheless, even without knowing precisely the mass of a NS, a 5% uncertainty on the radius can exclude up to 2/3 of the EoS models (LP07). Several observational methods exist to measure the radii of NSs.

During strong type-I X-ray burst (thermonuclear), the atmosphere of the NS undergoes a photospheric expansion phase. The flux of those bursts reaches the Eddington limit which depends on the mass and the gravitational redshift: $L_{\rm Edd} \propto M/g_{\rm R}$ (Lewin et al. 1995), from which the radius is calculated. Type-I

X-ray burst luminosity measurements and spectral fits produce NS radii for which a 10–15% uncertainty is claimed (Özel et al. 2009).

Another method to determine the radius is gravitational redshift measurements from X-ray spectral features like emission or absorption lines (Lattimer and Prakash 2001; Cottam et al. 2002). Broad spectral lines due to pressure broadening (Stark effect) can also be useful to measure the radii of NSs since the line width is given by $\Delta \propto M_{\rm NS}/R_{\rm NS}^2$ (Paerels 1997). To date, no such absorption line has been observationally confirmed.

Millisecond pulsar pulse profiles can be explained by polar-cap emission from an optically thick hydrogen atmosphere. Such models depends on the hot-spots' emission area as well as the NS physical radius. Fitting the X-ray pulse profiles of millisecond pulsars provides constraints on NS radii (Bogdanov et al. 2008).

The study of quasi-periodic oscillations at kilohertz frequencies is another method to measure the extent of the inner most stable orbit in binary systems with an accreting NS (Miller et al. 1998). However, these types of measurements only provide upper limits on the mass and radius of the NS and are not restrictive enough for EoS determination (Lattimer and Prakash 2007).

The thermal emission from non-magnetized low-mass X-ray binaries also provides reliable measurements of the radii. The large gravity on the surface of NSs ($g \sim 10^{14}\,{\rm cm\,s^{-2}}$) redshifts the luminosity. In consequence, one measures the effective temperature and emission area affected by the gravitational redshift $g_{\rm R}$:

$$T_\infty^{\rm eff} = g_{\rm R} T^{\rm eff} \quad \text{and} \quad R_\infty = R_{\rm NS}/g_{\rm R} \tag{1.1}$$

The subscript ∞ indicates that the effective temperature and radius as measured from a distant observer. The gravitational refshift g_{R} is given by:

$$g_{\mathrm{R}} = \sqrt{1 - \frac{2GM_{\mathrm{NS}}}{R_{\mathrm{NS}}c^2}} \tag{1.2}$$

Here, M_{NS} and R_{NS} are the baryonic mass and physical radius of the NS.

The blackbody approximation for this type of thermal spectrum was shown to result in radius estimates well below the accepted canonical values for typical NSs: $R_\infty \lesssim 1\,\mathrm{km}$ (Rutledge et al. 1999). In addition, this approximation unrealistically represents the opacity in the atmosphere. A blackbody emitter assumes that the opacity does not depend on the photon energy, but the ionized hydrogen atmosphere of a qLMXB is dominated by free-free transitions, which are photon energy dependent. Thus, a more realistic model to describe the thermal emission of those objects is that of an atmosphere composed of pure fully-ionized hydrogen. The following section explains the emission mechanism for this type of thermal spectrum, while section § 2.2 describes the currently used H-atmosphere NS models.

1.2.2 Quiescent Low-Mass X-ray Binaries and Deep Crustal Heating

LMXBs have specific characteristics within the class of X-ray binaries. They consist of a compact object (NS or stellar mass black hole) in a binary system with a low-mass companion star ($M \lesssim 1\,M_\odot$). As the star evolves and expands, it fills up its Roche-lobe – the line of critical gravitational equipotential between the companion star and the NS – and mass is transfered from the companion star onto the NS via an accretion disk [1] .

Transient LMXBs were originally discovered while in an outburst phase during which thermal accretion instabilities result in an increase in luminosity by a factor $\sim 10^5 - 10^6$ (Lewin et al. 1995). The subclass of transiently accreting LMXBs in quiescence (qLMXBs) was first observed during the post-outburst periods of the transient LMXBs Cen X-4 and Aql X-1, in which the low luminosity ($L_{\mathrm{X}} \sim 10^{32} - 10^{33}\,\mathrm{erg\ s^{-1}}$), interpreted as a thermal blackbody, had emission areas a factor of 100 smaller than implied by the projected area of a 10 km NS. At that time, it was suggested that some low-level mass accretion onto the compact object was required to power the observed luminosity, although what set the low-mass accretion rate ($\dot{M}$) was unclear (van Paradijs et al. 1987; Verbunt et al. 1994).

An alternate explanation to low-$\dot{M}$ accretion has become the dominant explanation for the quiescent emission of qLMXBs (Brown et al. 1998, BBR98 hereafter). In this different interpretation of the quiescent thermal emission, the luminosity is provided not by accretion onto the compact object, but by heat deposited in the NS crust by pressure-sensitive nuclear reactions. These reactions (Gupta et al. 2007; Haensel and Zdunik 1990, 2003, 2008), referred to as deep crustal heating (DCH), occur as matter is piled at the top of the NS

[1] The Roche-Lobe overflow can also occur due to shrinkage of the orbit due to loss of angular momentum in close orbit with period $P \lesssim 7\,\mathrm{h}$. In this case, the companion star does not need to have expanded (Ergma et al. 1997; Verbunt and Bassa 2003).

surface, forcing the column below to greater density and electron Fermi energies. The resulting series of electron captures, neutron emissions, and pycnonuclear reactions, through the depth of the crust, continues until the matter reaches the density of undifferentiated equilibrium nuclear matter, at which point it is no longer constituted of differentiable nuclei. In doing so, this reaction chain deposits 1.3–1.9 MeV per accreted nucleon, distributed throughout the crust (Haensel and Zdunik 2008). In a steady-state, these reactions give rise to a time-average luminosity, which is directly proportional to the time-average $\dot{M}$ (BBR98):

$$\langle L\rangle = 9\times 10^{32}\,\frac{\langle \dot{M}\rangle}{10^{-11}\ M_{\odot}\ \mathrm{yr}^{-1}}\,\frac{Q}{1.5\,\mathrm{MeV/amu}}\ \mathrm{erg\ s}^{-1} \tag{1.3}$$

where Q is the average heat deposited in the NS crust per accreted nucleon.

The energy source of the quiescent thermal luminosity aside, the thermal spectrum can be explained (BBR98) as due to a realistic NS H-atmosphere (NSA) model (Rajagopal and Romani 1996; Heinke et al. 2006; Zavlin et al. 1996, Z96 hereafter), rather than a blackbody approximation imposed in previous works. In the case of qLMXBs, the atmosphere has been accreted from the low-mass post-main sequence stellar companion (BBR98). Optical observations have shown in the spectrum of post-main sequence companions evidence of strong hydrogen emission lines, weak helium lines and traces of heavier elements (van Paradijs et al. 1980, for example,). When accretion onto the NS shuts off, metals will settle gravitationally on a timescale of $\sim$seconds (Bildsten et al. 1992), leaving a pure H-atmosphere. The emergent photon spectra of NS H-atmospheres are physically different – although parametrically similar – to that of blackbody thermal spectra

(Z96), which dramatically changes the derived emission area radii from the $\lesssim 1\,\mathrm{km}$ derived from the blackbody assumption, to radii which are consistent with the entire area of the NS (Rutledge et al. 1999). The optical spectroscopic information on the companion, the detection of qLMXB outburst, together with the theoretical prediction of deep crustal heating provide strong evidence that the NS in qLMXB systems possess atmospheres composed of hydrogen. As will be described in chapter 2, precise NS radii measurements can be obtained from qLMXBs in GCs. These clusters of stars are first introduced in the following section.

1.3 Globular Clusters

1.3.1 General Properties of Globular Clusters

Globular clusters consist of a large set of gravitationally bound stars (up to 10^6 stars), orbiting around a galaxy. In the Milky Way Galaxy, there are 150 GCs catalogued (Harris 1996, last update in 2003). The stars forming the GCs generally have low metallicities (compared to our Sun). Typical GCs are composed of a single population of old stars. More specifically, a simple picture consists in GC stars being born at the same time from the same cloud of gas (Caputo 1985). This results in a group of stars with roughly the same distance, the same composition, the same age but with different initial masses [2] .

The easiest observable to obtain from GC stars is their stellar magnitudes. Using different photometric bands, one can produce a colour-magnitude diagram

[2] High-precision photometry has now shown that some GCs exhibit the characteristics of two stellar populations (for example in ωCen, Bedin et al. 2004).

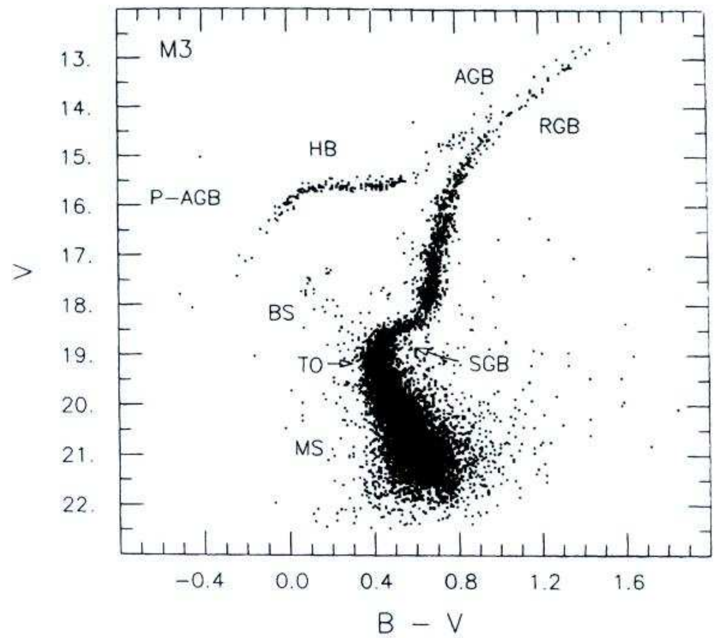

Figure 1–3: This figure shows the colour-magnitude diagram of the globular cluster M3. The different stages of stellar evolution are labelled (diagram and abbreviations from Renzini and Fusi Pecci 1988).

(CMD), where the colour is a difference of magnitudes (for example $m_B - m_V$). The colour is a distance independent value which has a one-to-one correspondence to the effective temperature of the star. Thus, a CMD describes the distribution of GC stars in a Luminosity-Temperature space (see Fig. 1–3). Since it is assumed that a single population of stars is present, the distribution should follow that of the theoretical curves of stellar evolution (called isochrones). Some properties of GCs can be deduced from the fitting of theoretical isochrones to the CMDs, such as the metallicity or the age (Caputo 1985).

The structural parameters of GCs are deduced from star counting and luminosity density profiles of the clusters. From those, the stellar density, the size and the mass can be estimated. Typical characteristics of GCs are central densities of the order $\rho_0 = 10^3 - 10^4\ L_\odot\,\mathrm{pc}^{-3}$ (Harris 1996), masses of $\sim 10^4 - 10^6\,M_\odot$ (Caputo 1985) and sizes of $\lesssim 10\,\mathrm{pc}$ (half-light radius, van den Bergh 2008). While direct stellar collisions are extremely rare events, GCs are the host place of many stellar interactions that can lead to the formation of binary systems. It was recognized in 1975 that GCs have more variable X-ray sources per unit mass than the rest of the Galaxy (Clark 1975). More specifically, it was noted that the ratio of X-ray sources to the surrounding stellar density is two orders of magnitude larger for GCs than for the field of the Galaxy. For example, 12 out of ~ 100 known bright X-ray sources were lying within GCs while the population of GCs represents only $\sim 10^{-4}$ of the total mass of the Milky Way (Hut et al. 1992).

1.3.2 X-ray Sources in Globular Clusters

An extended review of X-ray sources in GCs can be found elsewhere (Verbunt and Bassa 2003). X-ray sources in GCs can be separated into two categories: the binary systems and the isolated X-ray sources.

The isolated X-ray sources can either be normal stars or compact objects like NSs. The coronae of main-sequence stars can have temperature exceeding $T \sim 10^6\,\mathrm{K}$ and therefore be X-ray bright sources (Haisch and Schmitt 1996). Radio millisecond pulsars inside globular clusters have been observed with X-ray telescopes. For example, PSR B1821-24 has X-ray emission that is tentatively explained by cyclotron radiation in the corona above the pulsar surface (Becker et al. 2003), however this conclusion is not universally accected. Also expected is the presence of old radio-quiet isolated neutron stars accreting material from the interstellar medium, but so far, none have been identified in GCs.

Currently, the dominant population of GC X-ray sources is that of X-ray binaries which can be divided into two groups: the "bright" and the "dim" X-ray sources, with luminosities $L_{\rm X} \gtrsim 10^{35}\,{\rm erg\ s^{-1}}$ and $L_{\rm X} \sim 10^{31} - 10^{33}\,{\rm erg\ s^{-1}}$, respectively (Verbunt and Bassa 2003). The observed brightness is linked to the accretion rate of matter from the companion star. Thirteen bright X-ray sources are known to belong to the Galactic GCs. They have been observed to exhibit thermonuclear bursts (fusion of hydrogen into helium and helium into carbon) on the surface of the NS.

Many more dim X-ray sources have been discovered in GCs with the current generation of X-ray telescopes: *XMM-Newton* and the *Chandra X-ray Observatory*. The populations of X-ray binaries observed in GCs include:

- Cataclysmic Variables (CVs): These systems consist in a WD accreting matter from a companion star via Roche-Lobe overflow. The term *variable* originates from the historical variability observed – They were initially called *novae*, because their outbursts appeared as new stars to the unaided eyes of the ancient astronomers. They are believed to represent the largest portion of X-ray binaries in GCs (Di Stefano and Rappaport 1994). The X-ray emission (with luminosity $L_{\rm X} = 10^{31} - 10^{32}\,{\rm erg\ s^{-1}}$, Di Stefano and Rappaport 1994) usually comes from the accretion disk, with a hard spectrum having a power-law photon index $\alpha \sim 1 - 2$, which depends on the accretion rate (Verbunt and Bassa 2003). Their spectrum can also be described by thermal bremsstrahlung emission (Webb et al. 2006).

- Millisecond pulsars: These are NSs that have been spun-up by accretion of matter from a companion star. They are observed to be the evolutionary step of binary systems following the stage of LMXB (Lewin et al. 1995). The observed X-ray emission is composed of a thermal component (from a hot spot, near the magnetic pole) and of a hard non-thermal emission from relativistic electrons in the magnetosphere. The typical luminosity of millisecond pulsars is up to $L_{\rm X} \sim 10^{32}\,{\rm erg\ s^{-1}}$ (Verbunt and Bassa 2003).
- Magnetically Active binaries: These are close binaries composed of two stars in co-rotation. Their rapid rotation and the convection in low-mass stars ($M_\star \lesssim 0.8\,M_\odot$ as found in GCs) create a dynamo effect that increases the magnetic field. The X-ray emission emerges from the magnetic loops containing hot gas (Verbunt and Bassa 2003). Their typical luminosities range from $L_{\rm X} \sim 10^{28}\,{\rm erg\ s^{-1}}$ for BY Dra systems to $L_{\rm X} \sim 10^{32}\,{\rm erg\ s^{-1}}$ for RS CVn systems (van den Berg et al. 2004).
- Low-Mass X-ray binaries: These systems are composed of a NS (or a black-hole) in orbit with a stellar companion, which has a low mass $M_\star \lesssim 1\,M_\odot$. They were discussed in § 1.2.2.

This introductory chapter reviewed the discovery history of NS as well as their formation mechanism. It also introduced X-ray binaries and the different methods for radii measurement of NSs. Finally, GCs and the different populations of X-ray sources inside them were described. Of interest to the subject of this thesis are the transient accreting LMXBs in quiescence. The following chapter will discuss the observation of qLMXBs, starting with a review of X-ray astronomy and a presentation of the two X-ray satellites used in this thesis work. Chapter 3 reports on the data sets used and describes the method to obtain the results that are presented in chapter 4. Chapter 5 discusses the results and chapter 6 concludes the thesis.

CHAPTER 2
X-ray Observations of Quiescent Low-Mass X-ray Binaries

The thermal emission of qLMXBs peaks at the intrinsic energy of $\sim 0.1\,\mathrm{keV}$, but due to the additional effect of instellar absorption, the peak is observed at $\sim 1.0\,\mathrm{keV}$. This type of emission therefore requires the use of telescopes in the X-ray pass-band to be characterized. We begin this chapter with a brief history of X-ray astronomical observations, followed briskly by a description of modern instrumentation, and its application to the subject of this thesis – X-ray spectral identification of qLMXBs. The chapter then surveys the state of knowledge of qLMXBs prior to the present work, in anticipation of chapter 3, where the X-ray observations supporting the present work will be described.

2.1 X-ray Observatories

2.1.1 Brief History of X-ray Astronomy

In 1949, the first astronomical X-ray source, our Sun, was detected, using a detector in the nose of a sounding V-2 rocket (Garmire 1966). In 1962, Geiger counters on-board a rocket were used to detect the first X-ray source outside the solar system (Giacconi et al. 1962). Following this series of firsts, *UHURU* (also called the X-ray explorer satellite, or SAS-1) was the first X-ray detector dedicated to astronomy. It performed a survey of the whole sky using a pair of proportional counters of effective area $\sim 0.084\,\mathrm{m}^2$ each (Giacconi et al. 1971). It was followed by SAS-2 and SAS-3 in the late 1970's. Other satellites which contributed significantly to X-ray astronomy were *Einstein* (Giacconi et al. 1979), *EXOSAT* (Pallavicini and White 1988), *ROSAT* (Snowden and Schmitt 1990), *ASCA* (Inoue 1993) and *BeppoSAX* (Scarsi 1993).

Einstein was the first satellite with X-ray imaging capabilities with Wolter-I X-ray focusing optics (Giacconi et al. 1979). The *ROSAT* satellite was the first to use this technology for a full sky survey, cataloguing $\sim 105\,000$ sources (Voges et al. 2000, compared to ~ 300 known X-ray sources before *ROSAT*). *ASCA* introduced the use of Charge Coupled Device (CCD) detectors in the field of X-ray astronomy. Finally, *BeppoSAX* had instrumentation covering more than 3 decades of energy, from 0.1 keV to 300 keV, using concentrator spectrometers (up to 10 keV), a gas scintillator proportional counter (up to 120 keV) and a Phoswich Detection System (PDS, up to 300 keV).

The current generation of X-ray telescopes makes use of X-ray focusing optics to focus the X-ray photons to the focal plane. The European satellite *XMM-Newton* is one of them and was primarily used for the thesis work. Data from the *Chandra X-ray Observatory* were also analyzed in this work.

2.1.2 *XMM-Newton*

The European Space Agency (ESA) launched the *X-ray Multi-Mirror* satellite in December 1999. Its highly elliptical orbit around the Earth allows for long continuous exposures of X-ray sources, up to ~ 135 ks. The focal planes of the three X-ray telescopes are composed of two instruments. The Reflection Grating Spectrometer (RGS) is used for high-resolution spectrometry over the low-energy range 0.33–2.5 keV. The European Photon Imaging Camera (EPIC) instrument consists of three CCDs operating in photon counting modes. This instrument is described in detail below. *XMM-Newton* is composed of three individual X-ray focusing optics, one for each CCD of the EPIC instrument. The description of *XMM-Newton* and its instruments is based on information available on the *XMM-Newton* Science Operation Centre website at http://xmm.esac.esa.int/.

X-ray Focusing Optics

X-ray focusing systems (also called Wolter-I design) are based on the grazing incidence principle (Wolter 1952). X-ray photons can only be reflected off a mirror at small grazing angle $\theta_g \lesssim 2°$ (or large angle of incidence). To focus X-rays toward the focal plane, the Wolter-I design uses multiple paraboloid and hyperboloid mirrors (see Fig. 2–1). The effective area of a single mirror used at grazing incidence represents only a small fraction of the actual surface area of the mirror [1] . Multiple thin nested concentric mirrors are therefore used to increase the total effective area of the telescope. *XMM-Newton* has 58 Wolter-I mirrors with thicknesses ranging from 0.47 mm for the most inner one to 1.07 mm for the most outer one. The motivation for using shells of paraboloid and hyperboloid mirrors is to reduce the overall focal length of the telescope (down to 7.5 m for *XMM-Newton*), as compared to shells of paraboloid mirrors only (see Fig. 2–1).

The performance of this optical design is highly dependent on the number of mirrors. Adding more mirrors increases the effective area but becomes prohibitive for space missions, due to the extra mass. Similarly, reducing the thickness of

[1] The effective area is given by $A_{\rm eff} \approx \cos(90° - \theta_g)\, A_{\rm surface}$.

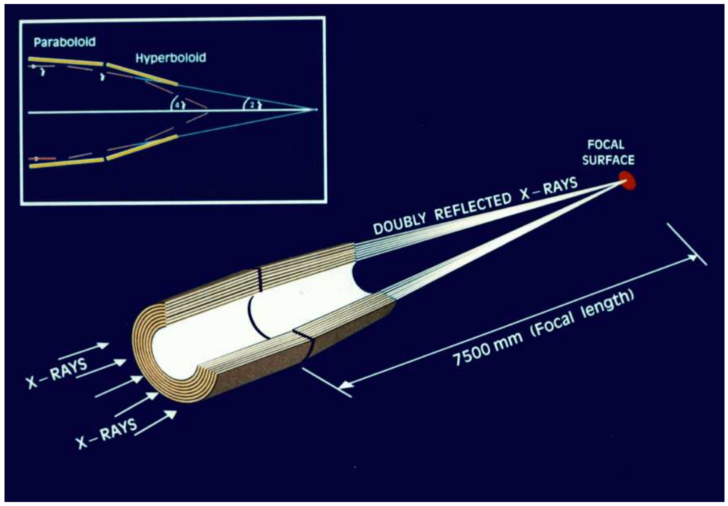

Figure 2–1: This diagram shows the Wolter-I design of the mirror system of *XMM-Newton*. The X-ray photons are focused by nested paraboloid and hyperboloid mirors. Source: http://xmm.esac.esa.int/

each mirror shell results in a gain of effective area but in more important mirror deformations, altering the point spread function (PSF). The trade-off chosen by ESA was a large collective area at the expense of image quality [2] . Finally, the optics of *XMM-Newton* is protected from X-ray stray-light with baffles surrounding the optical system.

For *XMM-Newton*, the optical design allows for a large effective area of $\sim 1000\,\mathrm{cm}^2$, with a modest angular resolution (PSF=$6''$ FWHM). These parameters can vary slightly depending on the photon energy and on the detector used as described below.

[2] The image quality of a telescope can be quantified by the point spread function which depends on the energy of incoming photons, and on the off-axis angle.

On-board Instrumentation: The EPIC Instrument

EPIC is the imaging instrument of *XMM-Newton*. The three CCDs, each one at the focal plane of one of the three X-ray telescopes (see Fig 2–2), are used for highly sensitive imaging over the whole field of view ($\sim 30'$) and the whole energy range (0.15–15 keV) with moderate spectral resolution ($E/\Delta E \sim 20 - 50$). All three CCDs can operate in the *full-frame*, *partial window* or *timing* modes which trade a large field of view (FOV) with limited time resolution for a smaller FOV with higher time resolution. These restrictions are dictated by telemetry limitations.

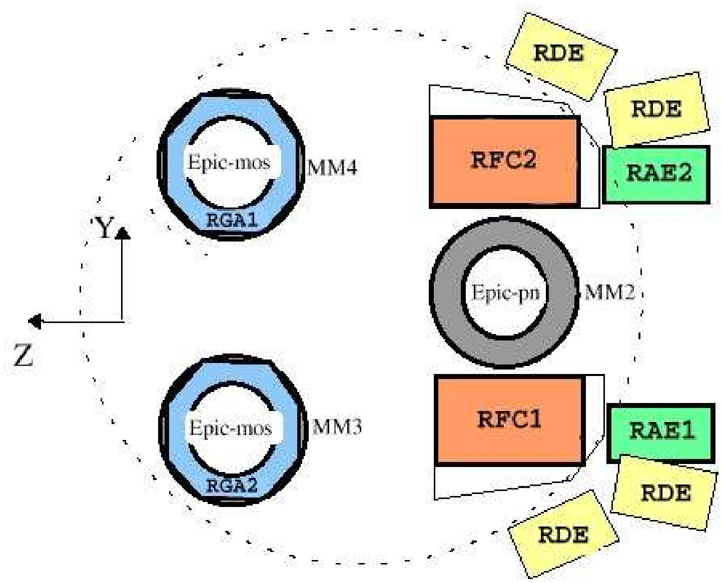

Figure 2–2: This diagram shows the focal plane instrumentation of *XMM-Newton*. Each of the three CCDs (the two MOS cameras and the pn) is each located at the focal points of the three X-ray telescopes. The modules RFCs, RDEs and RAEs belong to the RGS detectors. Source: http://xmm.esac.esa.int/

Two of the three CCDs are Metal Oxide Semi-conductor (MOS) arrays, consisting of 7 front-illuminated CCD chips, for a total of 600×600 pixels. The pixel size of $40\,\mu$m corresponds to $1.1''$ on the sky allowing the camera to fully sample the PSF of the telescope (PSF $= 6''$ FWHM) according to the Nyquist theorem. They share their respective focal paths with the two RGS detectors, and collect only 44% of the incoming flux, the rest being deflected and dispersed by gratings to the RGS detectors. Due to the presence of the RGS gratings, the MOS CCDs have lower sensitivity at 1 keV, where the spectra of qLMXBs peak, compared with the other EPIC detector: the pn camera (see Figure 2–3).

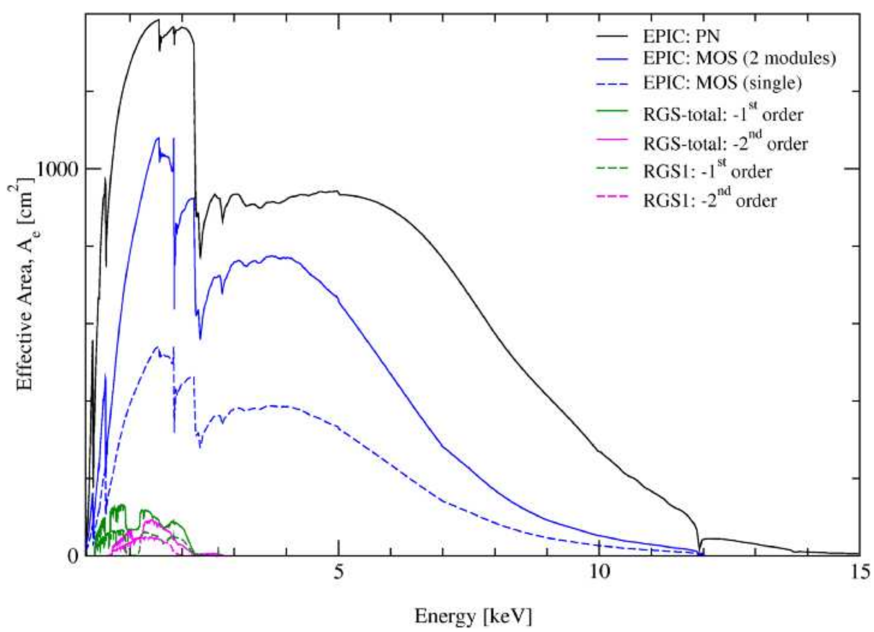

Figure 2–3: This graph shows the on-axis effective area of the RGSs, MOS, and pn detectors at the focal planes of the three X-ray telescopes on-board *XMM-Newton*. The value of effective area comprises the collective area of the X-ray optics system and the quantum efficiency of each detector. At ∼1 keV where the spectra of qLMXBs peak, the pn camera is preferred due to its superior effective area. Source: http://xmm.esac.esa.int/

The pn CCD is at the focal plane of the third telescope, on its own. It is composed of two rows of six rectangular back-illuminated pn-CCDs for a total of 400×384 pixels. *Back-illuminated* refers to the fact the detectors have been flipped over so that the X-ray photons hit the detector from the rear side, increasing the sensitive thickness, and therefore the detector sensitivity at photon energy $\sim 1\,\mathrm{keV}$. The quantum efficiency of the pn camera is significantly better than the MOS cameras by a factor $\times 2$ at $1\,\mathrm{keV}$. The pixel size ($150\,\mu\mathrm{m}$) covers $4.1''$ on the sky and therefore slightly under-samples the PSF. The detector is slightly shifted off-centre to avoid the optimal PSF position to fall on a CCD gap at the centre of the camera. The major drawback of the pn-camera is the mediocre pixel quality (see Fig. 2–4). The large quantity of hot pixels and dead columns (which number has increased during the mission) can prevent the thorough analysis of crowded fields.

Both types of detector (MOS and pn) can suffer from the effect of pile-up in the case of large count-rates. The arrival of more than one X-ray photon during the same readout time frame ($\sim$ sec in *full frame* imaging mode) affects the PSF and the spectral response of the CCD. Fortunately, the effect is well understood and can be spectrally modelled to apply the necessary corrections. Also, the faint sources observed during the course of this thesis work are negligibly affected by pile-up.

Thus, due to its large effective area, and useful energy resolution near the spectral peak of qLMXBs, the best instrument on-board *XMM-Newton* for spectral characterization of qLMXBs is the EPIC/pn camera.

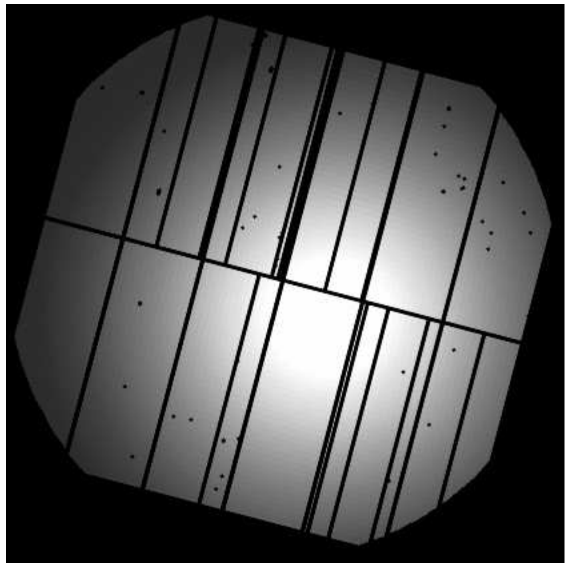

Figure 2–4: This exposure map (made from the observation of NGC 7089) shows the numerous unusable columns and pixels. Also visible is the effect of vignetting on the photon exposure (see § 3.2.3).

2.1.3 The *Chandra X-ray Observatory*

The *Chandra X-ray Observatory* was also used for follow-up observations of the work presented in this thesis. The following description was compiled from the *Chandra* X-ray Centre website at http://cxc.harvard.edu. *Chandra* was launched by NASA a few months before *XMM-Newton* in July 1999, on a similar orbit. It is equipped with a single Wolter-I X-ray telescope called the High Resolution Mirror Assembly (Figure 2–5). The optics system is composed of four grazing incidence spherical mirrors focusing X-rays to the focal plane, with a focal length of 10.1 meters. The small number of mirrors offers mechanical stability of the optical system and provides an unmatched angular resolution ($0.6''$) but a smaller collecting area ($\sim 340\,\mathrm{cm}^2$ at $1\,\mathrm{keV}$), compared with *XMM-Newton*.

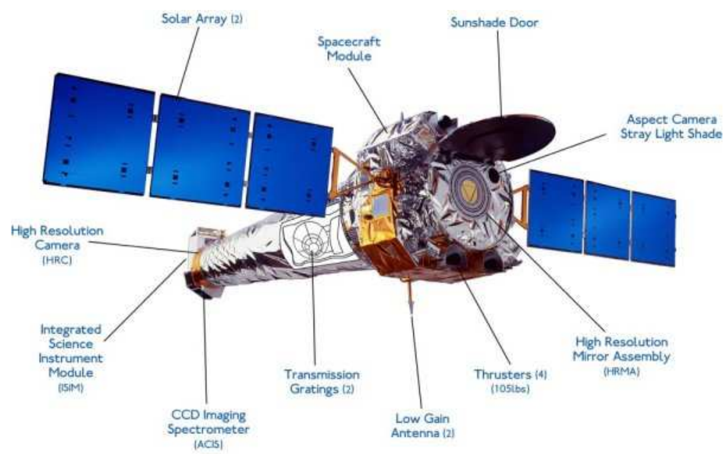

Figure 2–5: This figure shows the different parts of the *Chandra* telescope. Source: http://cxc.harvard.edu/

The instruments on-board *Chandra* are designed for imaging and spectroscopy (Fig 2–6). The focal plane is equipped with the Advanced CCD Imaging Spectrometer (ACIS) and the High Resolution Camera (HRC). The choice of instrumentation for a planned observation is made possible by the mobile focal plane, allowing to align the detector at the focal point. Two optional transmission gratings, the High Energy Transmission Grating (HETG) and the Low Energy Transmission Grating (LETG), can also be used if placed in the optical path.

The ACIS instrument was used for one complementary observation analyzed in this work. It offers the possibility of high angular resolution ($0.6''$, on-axis), together with moderate spectral resolution: $E/\Delta E \sim 20 - 50$ for the front-illuminated chip, and $E/\Delta E \sim 9 - 35$ for the back-illuminated chips. While the ACIS camera is not as affected by vignetting as *XMM-Newton* is, the PSF degrades rapidly as a function of off-axis angle, so that it is $\sim 10''$ at a distance of $\sim 10'$ from the on-axis position.

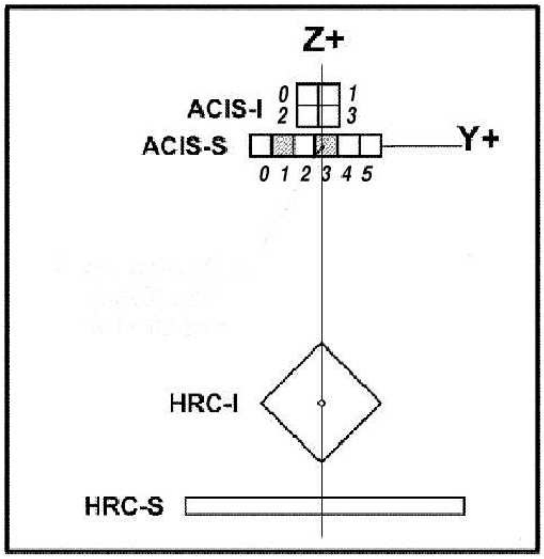

Figure 2–6: This diagram shows the arrangement of the different instruments available on-board the *Chandra X-ray Observatory*. The `I` and `S` after ACIS and HRC indicate that the CCDs are designed for imaging and spectroscopy, respectively. The shaded squares on ACIS correspond to the two back-illuminated chips. Source: http://cxc.harvard.edu/

Chandra and *XMM-Newton* are often presented as two complementary observatories. For example, the typical luminosity of qLMXBs ($L_{\rm X} \sim 10^{32} - 10^{33}\,{\rm erg\ s^{-1}}$) and the typical distances to GCs require the effective area of *XMM-Newton* to collect high signal-to-noise (S/N) data for spectral analyses, within modest integration times. On the other hand, *Chandra*'s angular resolution permits spatial resolution of adjacent sources in cores of GCs, which *XMM-Newton* is not able to differentiate otherwise. Due to the PSF degradation as a function of off-axis angle, *Chandra*'s optimal use is to detect and spatially resolve X-ray sources in moderately small fields (few arcminutes).

The following section describes the method used to observe qLMXBs.

2.2 X-ray Imaging and Spectroscopy to Study Quiescent Low-Mass X-ray Binaries

X-ray CCD imaging spectroscopy is the ideal tool for the study of qLMXBs. The low-flux of these objects precludes the use of dispersion gratings like the RGS on-board *XMM-Newton* or the LETG on-board *Chandra*, which have effective collecting area a factor of ~ 10 or more below that of CCDs with the same focusing optics. While such instruments have large spectral resolution ($E/\Delta E \sim 100-1000$, depending on the energy), their small effective areas ($\sim 100\,\mathrm{cm}^2$) would require prohibitively long integration times. To obtain the number of counts per source necessary to spectrally characterize a qLMXB, one seeks a large effective area like that of *XMM-Newton* despite the limited spectral resolution $E/\Delta E \sim 20-50$. Finally, in the case of survey observations like those described in this thesis work, the combined imaging on large field of views and spectroscopic capabilities are required to detect and characterize X-ray sources.

As explained in § 1.2.2, qLMXBs exhibit thermal emission that is best interpreted by an H-atmosphere NS model. Three models are publicly available for spectral fit within *XSPEC* (Arnaud 1996). They all have similar parameters, like the temperature and the NS mass and radius. The first one, `nsa` (Z96), uses the distance to the object as the normalization and also has the magnetic field strength as a parameter. `nsagrav` (Z96) assumes a negligible magnetic field and differs from `nsa` in the fact that different values of the surface gravitational acceleration were used for the model calculation: in the range $g = (0.1-10)\times10^{14}\,\mathrm{cm\,s^{-2}}$ for `nsagrav` and a single value $g = 2.43\times10^{14}\,\mathrm{cm\,s^{-2}}$ for `nsa`. The last model, `nsatmos` (McClintock et al. 2004; Heinke et al. 2006), also assumes a non-magnetic

NS, but uses the distance as one parameter while the model normalization is the fraction of the NS emitting. The model was calculated for a range of surface gravity $g = (0.63 - 6.3) \times 10^{14}\,\mathrm{cm\,s^{-2}}$.

The mass is assumed to be $M_{\rm NS} = 1.4\,M_{\odot}$ and it is kept fixed during the spectral fit. The models therefore obtain the effective temperature and the radius, assuming this mass. *XSPEC* has the capability to run spectral fits on a mass-radius parameter domain, producing confidence regions for the NS physical parameters on a mass-radius diagram and therefore constraining the dEoS.

One drawback of the H-atmosphere model resides in the radius determination. Since it is estimated from the luminosity and the temperature of the NS, the radius is therefore equivalent to the normalization constant in those models. Since the distance to the source also corresponds to a normalization, one faces the problem of a degeneracy between the radius and the distance to the source (see § 2.3.1 for a discussion on the distance uncertainty). The following section presents some of the known qLMXBs, for which emissions are correctly represented by the spectral model described above.

2.3 Well Studied Quiescent Low-Mass X-ray Binaries

The DCH luminosity/H-atmosphere spectral interpretation has been applied in the detection (and non-detections) of a large number of historically transient LMXBs, including [3] : Cen X-4 (Rutledge et al. 2001a; Campana et al. 2004b); Aql X-1 (Rutledge et al. 2001b); 4U 1608−522 (Rutledge et al. 1999); 4U 2129+47

[3] This list is not exhaustive.

(Rutledge et al. 2000); the transient in NGC 6440, SAX J1748−2021 (in't Zand et al. 2001); X1732−304 in Terzan 1 (Wijnands et al. 2002); XTE J2123−058 (Tomsick et al. 2004); EXO 1747−214 (Tomsick et al. 2005); MXB 1659−29 (Cackett et al. 2006); 1M 1716−315 (Jonker et al. 2007a); 2S 1803−245 (Cornelisse et al. 2007); 4U 1730−22 (Tomsick et al. 2007); 1H 1905+000 (Jonker et al. 2007b). Two of these – Cen X-4 and Aql X-1 – will be described in the following section.

2.3.1 Known Quiescent Low-Mass X-ray Binaries in the Field of the Galaxy

The soft X-ray transient Cen X-4 was originally discovered while exhibiting a type-I X-ray burst (Kitamura et al. 1969; Evans et al. 1970). Since then, it has been repeatedly observed during bursts. The quiescence phase has also been studied extensively since 1980 with the satellites *Einstein* (van Paradijs et al. 1987), *EXOSAT* (van Paradijs et al. 1987), *ASCA* (Asai et al. 1996, 1998), *ROSAT* (Campana et al. 1997), *Beppo-SAX* (Campana et al. 2000), *Chandra* (Rutledge et al. 2001a) and *XMM-Newton* (Campana et al. 2004b). The use of H-atmosphere models for a spectral fit was first performed on this source with the *Chandra* observation, producing radius measurements in agreement with the expected values for NSs: $R_{\rm NS} = 12.9{\pm}2.6\,{\rm km}$ assuming $d/1.2\,{\rm kpc}$ and $kT_{\rm eff} = 74^{+12}_{-5}\,{\rm eV}$ (Rutledge et al. 2001a). The most recent measurements using *XMM-Newton* (the largest S/N ever obtained for this source) confirmed those best-fit parameters: $R_{\rm NS} = 9.7{\pm}2.4\,{\rm km}$ assuming $d/1.2\,{\rm kpc}$ (Campana et al. 2004b). Also, long term variability of the quiescence phase was detected, attributing it to accretion onto the NS surface (Campana et al. 2004b).

Aquila X-1 (Aql X-1) has also been observed many times since the discovery with *UHURU* (Giacconi et al. 1972). Recurrent X-ray bursts confirmed the transient nature of the source (Kaluzienski et al. 1977). *ROSAT* (Verbunt et al. 1994), *ASCA* (Asai et al. 1998) and *Beppo-SAX* (Campana et al. 1998) also observed Aql X-1 during quiescence but the H-atmosphere spectral fit was first performed on *Chandra* data with the best-fit parameters ($R_{\rm NS} = 13.4^{+5}_{-4}\,$km $(d/5\,{\rm kpc})$ and $kT_{\rm eff} = 135^{+18}_{-12}\,$eV) consistent with NS values (Rutledge et al. 2001b). Variability during the quiescent phase was detected, and can be accounted for the variability of the observed power-law component, as observed for other qLMXBs (Rutledge et al. 2002a). However, higher S/N is needed to draw such conclusions.

Aql X-1 and Cen X-4 (and many, but not all, other qLMXBs) both have a power-law tail dominating at energies above 2 keV. Although the origin of this high-energy tail is still debated, three theories have been proposed to explain this excess of emission at large energies. A proposed interpretation relates the power-law emission to the residual of a recent accretion episode (Grindlay et al. 2001a). An alternate explanation associates the power law to shock emissions via the emergence of a magnetic field (Campana and Stella 2000). However, neither of these two hypothesis is yet supported by observational evidence. The last model presents the nature of the power-law component as due to intrabinary shock between the winds from the NS and its companion star. The NS wind is initiated by the reactivation of the NS rotation due to accretion, as observed for the LMXB SAX J1808.4−3658 (Campana et al. 2004a) and the binary radio millisecond pulsar PSR J0024−7204 (Bogdanov et al. 2005).

The NS radius measurements of field qLMXBs are usually based on an assumed distance to the source (since the radius and the distance are degenerate parameters). However, the distance to field qLMXBs is difficult to estimate and is often uncertain by up to 50%. Since the observable flux density $F_\nu \propto (R_\infty/d)^2$, this uncertainty in the distance results in a corresponding fractional uncertainty in R_∞. For example, the distance to the qLMXB 4U 2129+47 is controversial (Cowley and Schmidtke 1990) and is also related to the uncertainty in the amount of interstellar absorption (characterized by the hydrogen column density N_H, written $N_{H,22}$ in units of $10^{22}\,\mathrm{cm}^{-2}$ hereafter). The debated values for the distance, between 1 kpc and 6 kpc, lead to best-fit values for the projected radius of $R_\infty = 9.3^{+7.8}_{-4.6}\,\mathrm{km}$ ($d/1.5\,\mathrm{kpc}$ and $N_{H,22} = 0.28$) or $R_\infty = 16^{+11}_{-6.4}\,\mathrm{km}$ ($d/6.0\,\mathrm{kpc}$ and $N_{H,22} = 0.17$) (Rutledge et al. 2000).

Placing observational constraints on the dense matter EoS requires measurements of R_∞ to $\approx 5\%$ accuracy, or better (LP04). The observational solution is to discover new qLMXBs, the distances to which are known with greater certainty than the present group of field sources. GCs are the obvious place to search for these, as they host an over-abundance of LMXBs (see § 1.3.1) and their distances are precisely known or precisely measurable.

2.3.2 Known Quiescent Low-Mass X-ray Binaries in Globular Clusters

Firstly, the typical ages of GCs $\sim 10^9$ yr imply that all massive stars have evolved. It is therefore more likely to find NSs – remnants of massive stars – with low-mass companions, among binary systems. In addition, most distances to GCs are determined with uncertainties $\lesssim 5\%$ allowing precise NS radius measurements.

Finally, the interstellar absorption is also well known. In consequence, for a qLMXB in a GC, one can fix the known distance and N_H to perform spectral fits.

Quiescent LMXBs in GCs are now routinely discovered and studied. A total of 11 are known (some require confirmation). Table 2–1 shows the list of GC qLMXBs with their parameters. The following paragraphs will describe two of them for which tight constraints have been placed on R_∞.

The discovery observation of the qLMXB in the GC Omega Centaurus (ωCen) was performed with *Chandra*-ACIS (Rutledge et al. 2002b). CXOU 132619.7−472910.8 has a thermal spectrum consistent with a non-magnetic NS H-atmosphere at the distance of ωCen. The best-fit parameters are $R_\infty = 14.3^{+2.1}_{-2.1}$ km and $kT_{\rm eff} = 66^{+4}_{-5}$ eV, using a distance of 5 kpc. Consistent results with smaller uncertainties were obtained using a 40 ks observation with the EPIC camera on-board *XMM-Newton*: $R_\infty = 13.6^{+0.3}_{-0.3}$ km and $kT_{\rm eff} = 67^{+2}_{-2}$ eV (Gendre et al. 2003b). The source flux is consistent with being unchanged over the time interval in the two observations. The measured unabsorbed luminosity was $L_{\rm X} = 0.32^{+0.02}_{-0.02} \times 10^{33}$ erg s^{-1} [0.1–5 keV].

A qLMXB was reported in the GC M13 from a 37 ks *XMM-Newton* observation. The low absorption in the direction of M13, $N_{H,22} = 0.01$, permitted accurate measurements of the radius. Indeed, photo-electric absorption of X-rays starts to become important at energies $\sim$ 1.5 keV and below, where the thermal emission of qLMXBs peaks. The best-fit values obtained for this qLMXB are: $R_\infty = 12.8^{+0.4}_{-0.4}$ km and $kT_{\rm eff} = 76^{+3}_{-3}$ eV. The source luminosity is $L_{\rm X} = 0.73^{+0.06}_{-0.06} \times 10^{33}$ erg s^{-1} [0.1–5 keV].

Table 2–1: The known quiescent low-mass X-ray binaries in globular clusters

Object	R_∞ (km)	$kT_{\rm eff}$ (eV)	d (kpc)	$N_{H,22}$ (10^{22} cm^{-2})	$L_{\rm X}$	$F_{\rm X}$	References
ωCen(ACIS)	$14.3^{+2.1}_{-2.1}$	66^{+4}_{-5}	5	(0.09)	0.5 ± 0.2	1.67 ± 0.67 [1]	Rutledge et al. 2002b
ωCen(EPIC)	$13.6^{+0.3}_{-0.3}$	67^{+2}_{-2}	5.3	$0.09^{+0.025}_{-0.025}$	0.32 ± 0.02	0.95 ± 0.06 [1]	Gendre et al. 2003b
M13 (EPIC)	$12.8^{+0.4}_{-0.4}$	76^{+3}_{-3}	7.7	(0.011)	0.73 ± 0.06	1.03 ± 0.08 [1]	Gendre et al. 2003a
47 Tuc X5	$19.0^{+8.8}_{-7.8}$	101^{+21}_{-14}	4.85	$0.09^{+0.08}_{-0.05}$	1.4	4.3 [2,†]	Heinke et al. 2003b
47 Tuc X7	$14.5^{+1.8}_{-1.6}$	$105.4^{+5.6}_{-5.6}$	4.85	$0.042^{+0.018}_{-0.016}$	1.5	5.3 [2,†]	Heinke et al. 2006
M 28 (#26)	$14.5^{+6.9}_{-3.8}$	90^{+30}_{-10}	5.5	$0.26^{+0.04}_{-0.04}$	$1.2^{+0.7}_{-0.4}$	$3.35^{+1.9}_{-1.1}$ [3]	Becker et al. 2003
M 30 A-1	$13.4^{+4.3}_{-3.6}$	94^{+17}_{-12}	9.0 ± 0.5	$0.029^{+0.017}_{-0.012}$	0.71	0.73 [2,†]	Lugger et al. 2007
NGC 6397 U24	4.9^{+14}_{-1}	57–92	2.5	0.1–0.26	0.08	1.06 [4,†]	Grindlay et al. 2001b
M80 CX2	(10)	82 ± 2	$10.3^{+0.8}_{-0.7}$	$0.09^{+0.025}_{-0}$	0.29 ± 0.02	0.23 ± 0.02 [5]	Heinke et al. 2003a
M80 CX6	(10)	76^{+5}_{-6}	$10.3^{+0.8}_{-0.7}$	$0.22^{+0.08}_{-0.07}$	0.09 ± 0.01	0.07 ± 0.01 [5]	Heinke et al. 2003a
NGC 2808 C2	(12)	$81.3^{+5.3}_{-4.9}$	9.6	$0.82^{+0.40}_{-0.40}$	0.26 ± 0.04	0.24 ± 0.04 [2]	Servillat et al. 2008
NGC 3201 16	(10)	172^{+55}_{-42}	5.0	(1.17)	0.34	1.0 [6,†]	Webb et al. 2006

NOTES: This table lists the known GC qLMXBs and their parameters. Error bars are 90% confidence. The unabsorbed X-ray luminosity $L_{\rm X}$ and flux $F_{\rm X}$ are expressed in units of 10^{33} erg s^{-1} and 10^{-13} erg cm^{-2} s^{-1}, respectively, both in the X-ray bands listed below: [1] for 0.1–5 keV, [2] for 0.5–10 keV, [3] for 0.5–8.0 keV, [4] for 0.5–2.5 keV, [5] for 0.5–6.0 keV, [6] for 0.2–10.0 keV and [†] indicates that no errors were provided by the authors. Values in parentheses were held fixed for the spectral fits.

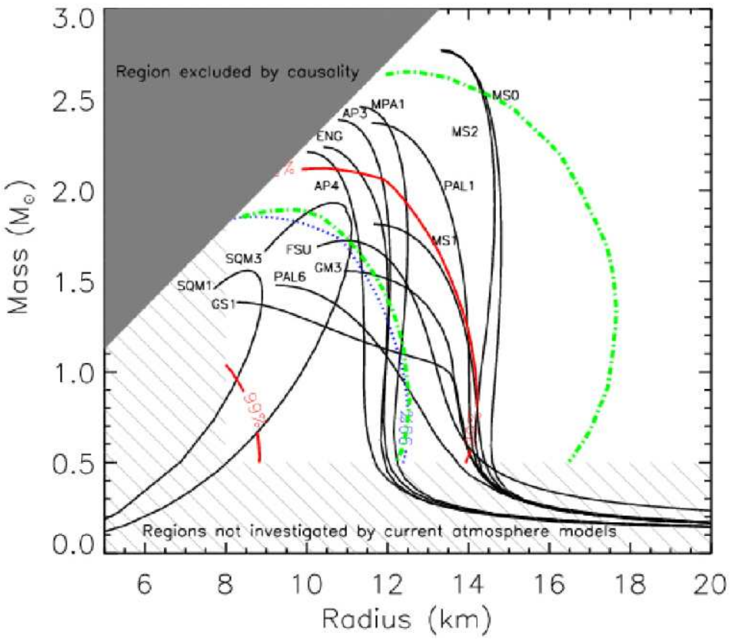

Figure 2–7: This mass-radius diagram is similar to Fig. 1–2. Overplotted are the best mass-radius constraints obtained with the model `nsatmos`, from the qLMXBs in ωCen (red lines), in M13 (blue lines) and in 47Tuc (green lines), 99% confidence. The confidence contours of M13 exclude the EoSs: MS0, MS1, MS2, PAL1 and AP4. Figure from Webb and Barret (2007).

To date these two NSs have the best constraints on their radius measurements (uncertainty of $\lesssim 5\%$) among the population of GC qLMXBs. Figure 2–7 shows the 99% confidence contours on the M-R diagram, plotted over some of the predicted EoSs. The best-fit parameter of the qLMXB in M!3 discard the EoSs like MS0-2 and PAL1 (Webb and Barret 2007). The qLMXB in ωCen is less constraining but still excludes the MS0 EoS.

2.3.3 Known Counterparts of Globular Cluster Quiescent Low-Mass X-Ray Binaries

While the counterparts of field qLMXBs can generally be identified without difficulty (Cen X-4, van Paradijs et al. 1980, Aql X-1, Thorstensen et al. 1978), only a small portion of GC qLMXBs have counterparts in other observational bands. Most of them are located in the core of their host GC, preventing observations of counterparts due to the large stellar densities. In only two cases, X5 in 47 Tucanae (47 Tuc, Edmonds et al. 2002) and ωCen (Haggard et al. 2004), the optical counterpart of the X-ray source was found. The identification followed the spectral classification. The observation of counterparts can lend strong support to the qLMXB spectral classification, although they are observationally challenging due to the the high stellar densities in GCs.

In the case of a detected counterpart, different observational methods can be used to confirm the binary nature of the system and yield measurements of the binary parameters. Radial velocity curves can be obtained from high-resolution optical spectroscopy (Tomsick et al. 2001). From that, one may deduce the orbital period and the mass function of the binary system, which is a relation between the masses of the two objects. Photometry can also be performed to infer the orbital period from variation of the brightness of the companion star due to ellipsoidal variations.

In dense stellar regions like the cores of GCs, the spatial resolution of the Hubble Space Telescope (*HST*) is often required to detect counterparts. For example, a counterpart with magnitude $V = 21.7$ was found for the qLMXB X5 in the GC 47 Tuc (Edmonds et al. 2002). The variability observed seems to show evidence of light coming from the red main-sequence star and an accretion disk. The counterpart to the qLMXB in ωCen was also detected using *HST* data (Haggard et al. 2004). The faint companion star ($R_{625} = 25.2$), is constrained to be a low-mass star $M \lesssim 0.14\, M_{\odot}$, if a main-sequence star. On a CMD, the companion star is located 1.5 mag (in $B_{435} - R_{625}$ colour) and 1.3 mag (in H$\alpha - R_{625}$ colour) to the blue side of the main sequence. These blue and Hα excesses suggest the presence of an accretion disk in the system.

A known infrared (IR) counterpart can also provide insight on the classification of binary systems as qLMXBs. For example, the Two Micron All Sky Survey (2MASS) J-band magnitude gives the J-band flux of the system and therefore allows one to calculate the X-ray to J-band flux ratio, $F_{\rm X}/F_J$. This is a distance independent measurement providing complementary information on the system. Coronally active stars typically have $F_{\rm X}/F_J \lesssim 10^{-2}$ (Shevchuk et al. 2009). For a given association between an X-ray source and its counterpart, a value above this upper limit can exclude the coronally active star classification.

CHAPTER 3
Observations of Globular Clusters with *XMM-Newton*

3.1 Program of Observations with *XMM-Newton*

A program of short-integration *XMM-Newton* observations, has been undertaken to survey GCs and increase the number of known qLMXBs in GCs. The integration times for each cluster observed were estimated based on the typical luminosity of qLMXBs ($L_{\mathrm{X}} = 10^{32}\,\mathrm{erg\ s^{-1}}$), the distance to the clusters and the expected Galactic absorption. Pre-observations simulations show that to be able to spectrally identify qLMXBs to a useful precision ($\sigma_r/r \sim 12\%$), one requires at least $\sim$ 1500 counts, assuming $N_{H,22} \sim 0.1$. The integration time was then established to produce $\sim$ 1500 counts from a qLMXB at the distance and N_H of the GC, assuming $L_{\mathrm{X}} = 5{\times}10^{32}\,\mathrm{erg\ s^{-1}}$, and a typical blackbody effective temperature $kT_{\mathrm{eff},BB} \sim 190\,\mathrm{eV}$. All observations were performed with the medium filter to diminish the effect of optical/UV light contamination.

3.1.1 Observation of Six Globular Clusters

Six GCs were chosen for this program: NGC 6304, NGC 6540, NGC 6553, NGC 6637, NGC 6681, NGC 7089. The physical properties of these clusters are listed in Table 3–1.

They were selected among the GCs that have not been observed yet with any of the current generation X-ray observatories and thus lack observations capable of

Table 3–1: The six globular clusters of the *XMM-Newton* program of observations

Name	R.A. (J2000)	Dec. (J2000)	d (kpc)	r_c ($'$)	r_{HM} ($'$)	r_t ($'$)	$N_{H,22}$ (cm^{-2})
NGC 6304	$17^h14^m32.1^s$	$-29°27'44.0''$	6.0	0.21	1.41	13.25	0.266
NGC 6540	$18^h06^m08.6^s$	$-27°45'55.0''$	3.7	0.03	0.24	9.49	0.32
NGC 6553	$18^h09^m17.6^s$	$-25°54'31.0''$	6.0	0.55	1.55	8.60	0.35
NGC 6637	$18^h31^m23.2^s$	$-32°20'53.0''$	9.1	0.34	0.83	8.35	0.11
NGC 6681	$18^h43^m12.7^s$	$-32°17'31.0''$	9.0	0.03	0.93	7.91	0.08
NGC 7089	$21^h33^m29.3^s$	$-00°49'23.0''$	11.5	0.34	0.93	21.45	0.043

NOTES: This table shows the positions, distances, core radii, half-mass radii and tidal radii of the globular clusters observed in this thesis work. The uncertainty on the distances are assumed to be negligible and are frozen during spectral fitting. Also shown is the hydrogen column density in the direction of the clusters in units of $10^{22}\,\mathrm{cm}^{-2}$. The values are extracted from the Catalogue of Globular Clusters (Harris 1996).

spectrally identifing qLMXBs. Also, they were carefully chosen for a combination of their properties leading to a propitious environment for detection of qLMXBs.

First of all, their moderate distances ($\sim 5-10\,\mathrm{kpc}$) allow for relatively large fluxes from the qLMXBs with typical X-ray luminosities $L_{\mathrm{X}} \sim 10^{32}-10^{33}\,\mathrm{erg\ s^{-1}}$. Then, the interstellar absorption also plays an important role in the identification of qLMXBs (see § 2.3.2). The GCs were selected based on their low to moderate hydrogen column density. In reality, this condition is linked to the distances. A distant cluster ($\sim 10\,\mathrm{kpc}$) is a good candidate for detection of qLMXBs as long as the N_H is low in its direction ($N_{H,22} \lesssim 0.1$).

Finally, the selection of GCs was also dictated by their physical properties, to maximize the number of new qLMXBs detected. It was recognized that the number of NS binary systems is related to the interaction rate of the cluster. Previous work quantified the linear relation: $N_{\mathrm{qNS}} \propto \Gamma$ (Gendre et al. 2003a;

Heinke et al. 2003c). For a virialized GC, the interaction rate Γ is given by $\Gamma \propto \rho_0^{1.5} r_c^2$ where ρ_0 is the central luminosity density and r_c is the core radius in physical units, not angular distance (Verbunt 2003). Overall, the full program is expected to produce 2–3 new qLMXBs which will be used for precise NS radius measurements.

This thesis work consisted in the data reduction and data analysis of the six GC observations. The following results were obtained:

- A total of seven candidate qLMXBs in the six GCs were identified based on spectral consistency with NS H-atmosphere models.
- Two of the candidates are within the core of their host GCs.
- Five of them are located at large distances ($> 15\, r_c$) from the host GC cores, including two outside the tidal radius of their GCs.
- Two other X-ray sources were first identified as candidates, but a dynamical analysis (spatial velocities) of their associated 2MASS counterpart demonstrated that they cannot be cluster members, therefore refuting the initial classification. For one of them, a high-S/N spectrum, obtained from an archived *XMM-Newton* observation, confirmed this conclusion by showing inconsistency with a qLMXB spectrum.

The data reduction and analysis are presented in the following section. The main focus of this work was the data analysis of the NGC 6304 observations (results in § 4.1, and also published in Guillot et al. 2009 and **?**). The results of the data analysis of the other GCs are in sections § 4.2 to § 4.6.

3.2 Data Reduction and Analysis

The steps for the reduction of *XMM-Newton* data, presented in the following subsections, were executed for all data sets, for each GC. A subsection is dedicated to the data reduction of additional *Chandra* data for the GC NGC 6304. The data analysis process leading to the identification of candidate qLMXBs is also detailed below.

3.2.1 Reduction of X-ray Data from *XMM-Newton*

The data reduction is performed using *XMM-Newton* Science Analysis System v7.0.0 for NGC 6304 and v8.0.0 for the other five data sets, using standard analysis procedures. The command `epchain` performs all the required steps for preliminary data reduction. The data sets are systematically checked for proton flares, which cause a drastic increase in the background and the time interval during a flare to have to be discarded. Then, the spectral quality of the data is quantified using the task `epatplot`, as recommended before choosing the energy band for analysis [1] . In all cases, `epatplot` shows a significant discrepancy below 0.5 keV between the distribution of the various pattern events [2] (single and double) as a function of energy and the expected curves, therefore excluding the use of this low-energy band. The 0.5–10 keV spectral energy range is therefore

[1] From *XMM-Newton* Science Operations Centre XMM-SOC-CAL-TN-0018 (Guainizzi 2008).

[2] A pattern event is a pixel pattern created by an event on the CCD. Patterns from true X-ray photons, like single, double and quadruple patters, can be identified are use for spectral analysis while those from cosmic rays need to be excluded.

chosen for the data reduction, the detection and the subsequent steps of the analysis. Only the event patterns recommended by the *XMM-Newton* Science team are used: single, double and quadruple patterns. An exposure map is then created for source detection, which is performed with `wavdetect` from CIAO v3.4 for the analysis of the NGC 6304 data and v4.1 for the other GCs (Fruscione et al. 2006). `Wavdetect` is a source detection algorithm using "mexican hat" wavelet functions with different pixel scales. It is run with the relative exposure of 0.2, the wavelet scales (1.0 2.0 4.0 8.0) and the significance threshold (2.6×10^{-6}). The minimum source significance to detect sources is adopted to be $\sigma = 3$.

The presented analysis is focussed on the pn camera (Strüder et al. 2001), due to its greater sensitivity in the low photon energy range (0.5–2.0 keV) where qLMXBs are brightest. In the case of NGC 6304, the MOS1 and MOS2 data are also used (see § 4.1). The data reduction process is similar except that `emchain` is used to perform the preliminary data reduction.

3.2.2 Reduction of X-ray Data from *Chandra*

The CIAO V4.1.1 (Fruscione et al. 2006) package is used for the source detection and analysis of the *Chandra* observation of NGC 6304 used in this thesis work. The pre-processed event file (level 2) is analyzed including events in the 0.5–8.0 keV range. The data are checked for flares and the time interval containing flares are excluded, if any. The source detection is performed with the `wavdetect` algorithm, treating each ACIS chip separately, using the following parameters: an exposure threshold *expthresh=0.1* and the wavelet scales *scales="1.0 2.0 4.0 8.0"*. For comparison, the detection is also performed on the full 0.5–8 keV using an exposure map (created with `mkexpmap` following the analysis thread *"Single Chip ACIS Exposure Map"*[3]). Similar detections are obtained, except for a few minor differences. More importantly, the statistical positional uncertainties obtained with the previous detection run (without the exposure map) are smaller than that obtained when the exposure map is used. In consequence, the results with the smallest statistical uncertainties (detection without the exposure map) are presented and used. The astrometry with good precision is needed for the search of possible optical or IR counterparts. The uncertainty in the source positions is the quadratic sum of the statistical uncertainty ($\sim 0.1''$) and the systematic positional uncertainty of $\sim 0.6''$ for *Chandra*[4] .

3.2.3 Spectral Analysis of the Data

For each detected source (according to the $> 3\sigma$ criteria), the X-ray counts are extracted, before being binned for spectral fitting.

Count Extraction

For *XMM-Newton* data, a radius of $25''$ around each source is chosen, accounting for 81% of the total energy from the source at 1.5 keV. The background counts, used for background subtraction, are extracted in a larger region ($100''$) around the source, excluding the source itself and other sources in close proximity. Alternatively, we choose (for NGC 6304 only) an annulus (of $40''$ width) centered at the position of the peak of the exposure map (that is, the image centre), and

[3] Available at http://cxc.harvard.edu/ciao4.1/threads/expmap_acis_single/

[4] From the *Chandra* Calibration web-page available at http://cxc.harvard.edu/cal/

with an average radius equal to the distance between the source being analyzed and the image centre [5] . Finally, since the background region must not contain any X-ray source, a circular area of 35″ around each source ensures that 87% of the overlapping source counts (at 1.5 keV) are excluded.

For *Chandra* data, the extraction region depends on the off-axis angle since the PSF degrades at large off-axis angles. In all cases, the extraction region is chosen so that more than 90% of the energy is included (Encircled Count Fraction $ECF > 90\%$ [6]). For sources at small off-axis angle, i.e. sources in the core of the cluster, the circular extraction region of radius 2.5″ around a source comprises more than 95% of the source energy[7] . Sources at large off-axis angle requires a larger extraction region: for example at 1.5′ away from the on-axis position, a circular 3″-radius region is necessary. In all cases, the background is chosen around the source with a radius of 60″, excluding 5″ (> 99% of the ECF) around the source itself. The script `psextract`, together with the calibration files from CALDB v4.1 (containing the latest effective area maps, quantum efficiency maps and gain maps, Graessle et al. 2007), is used to extract the counts of the X-ray sources, in the energy range 0.5–8.0 keV. Since the analyzed observation

[5] This was originally done to minimize the effect of vignetting (see Fig. 2–4) on the background region, but this effect is actually negligible on the 100″ regions chosen, and for subsequent analyses, we used source-centered annulii.

[6] The extraction radii are determined using the web-tool available at: http://cxc.harvard.edu/cgi-bin/build_viewer.cgi?psf

[7] *Chandra* Observatory Proposer Guide, Chap. 6, v11.0, Jan 2009

of NGC 6304 was performed with the ACIS-S instrument and a focal plane temperature of -120 °C, the response matrices files (RMF) have to be recalculated, according to the recommendations of the CIAO Science Thread *"Creating ACIS RMFs with mkacisrmf"*. It is also crucial to recalculate the ancillary response file (ARF) using the new RMFs in order to match the energy grids between the RMF and ARF files.

Overall, one has to extract the counts in the source and background regions such that the ratio of the areas $A_{\rm src}/A_{\rm bkgd} < 0.1$, which permits a representative background subtraction inside the source region.

Spectral Analysis

The *XMM-Newton* extracted counts were binned using `grppha` into energy bins between 0.5 and 10 keV with 25 counts per bins (or 20 counts per bins for sources with less than 100 counts in excess of the background).

Using *XSPEC* v12.3 (Arnaud 1996), the extracted spectra are fit with a tabulated NS H-atmosphere model (Z96). For this model, similar to `nsa` the radius is measured from the normalization parameter $(R_\infty/\,(d/10\,{\rm kpc}))^2$, assuming a distance d and a mass of $M_{\rm NS} = 1.4\,M_\odot$. If this model provides a statistically acceptable fit (null hypothesis probability $\gtrsim 10^{-2}$) and values of R_∞ and $kT_{\rm eff}$ in the range of previously observed qLMXBs, $5-20$ km and $\sim 50-150$ eV respectively (see Table 2–1), then, the source is classified as a candidate qLMXB. The spectral parameters are then confirmed with the single-component model of NS H-atmosphere included in *XSPEC* (NSA model: `nsa`, Z96). Alternatively, the other models are available in *XSPEC*: `nsagrav` and `nsatmos`. When using any of those models, the mass is kept constant at $1.4\,M_\odot$ and the distance normalization ($1/d^2$) or distance parameter d is kept fixed. The `nsa` model contains a magnetic field parameter that is set to zero while `nsagrav` and `nsatmos` assume non-magnetic atmospheres. In all cases, the models `nsa`, `nsagrav`, and `nsatmos` give consistent parameters. The error region of the reported best fit values are at 90% confidence. The unabsorbed flux is quoted for the best fits, in the range 0.5–10 keV, except when noted otherwise.

In the case where the NSA tabulated model provides an unacceptable fit, a visual inspection and a F-test indicate whether a photon power law should be added to the spectral model. If a significant portion of the high-energy tail is in excess of the NS atmosphere fit, a simple power law is added. This is justified by the fact that qLMXBs sometimes display a hard power-law component which dominates the spectrum above 2 keV (see § 2.3.1). For all model fits, the photo-electric Galactic absorption (the multiplicative model `wabs` in *XSPEC*) with a fixed value of N_H at the position of the GC [8] is included in the spectral fit.

A major technical problem arises during the spectral fitting with the `nsa`, `nsagrav` and `nsatmos` models. All three of them were implemented in *XSPEC* with restrictive parameter spaces. In particular, the radius parameter space is defined only between 5 km and 20 km for `nsa`, between 6 km and 45 km for `nsatmos` and between 6 km and 30 km for `nsatmos`. In this case, while the best fit

[8] From http://cxc.harvard.edu/toolkit/colden.jsp using the NRAO data (Dickey and Lockman 1990)

may be statistically acceptable, and the parameter values obtained are consistent with those expected for a qLMXB, the parameter uncertainty range for low-S/N qLMXB spectra may be greater than that tabulated in the *XSPEC* models and the uncertainty calculation fails due to zero diagonal components in the parameters matrix. The consequence of the imposed cut off in the parameter space would be a misrepresentation of the parameter uncertainties, preventing any conclusions to be drawn from the spectral fit. In those cases, the tabulated model (Z96) and the parameters resulting from the fit are used, since they do not suffer from this constraint. In some cases of identified qLMXBs, the MOS1 and MOS2 spectra are extracted in a similar manner as described above, and used to perform a simultaneous fit. This procedure reduced the uncertainties on the effective temperature and projected radii of the candidate qLMXBs in NGC 6304, by up to 50%, in some cases.

Due to the low-count statistics of the *Chandra* observation available (80 counts for the brightest source), the spectra are left unbinned and the Cash-statistic (Cash 1979) permits to find the best-fit parameters, without spectral binning, assuming that the model used is correct. The results of Monte Carlo "goodness-of-fit" simulations are provided to support the spectral fits. This probability, when close to 50%, suggests a good fit while extremal values indicate that the model poorly describes the data.

The identification of new qLMXBs using the method described in this chapter may introduce an observational selection effect since the spectral identification is based on the consistency with a theoretical model and on the consistency with observations of field qLMXBs. In other words, such objects having properties other than those presented above would not be identified as qLMXBs. However, no other properties of qLMXBs are observed in the field or in LMXBs which have gone into outburst historically. Also, while two qLMXBs identified using this technique have late been observationally confirmed (in ωCen (Haggard et al. 2004) and in 47 Tuc (Edmonds et al. 2002)), no qLMXB candidates identified using this technique have been refuted – although, the approach has no standard for a required S/N or identification, but $\sim 20\%$ uncertainty in R_∞ is a usual standard to consider a target a strong candidate.

CHAPTER 4
Results

This chapter details the results of the systematic search for qLMXBs in the targeted GCs. Table 4–1 shows the parameters of each observation available for the selected targets. Each GCs is treated separately in the following six sections and the analyses pertaining to the candidate qLMXBs are presented one by one. As mentioned before, the primary focus of this thesis work was the analysis of the observation targeted at NGC 6304. The analyses of the three candidates in this GC are therefore more detailed.

Table 4–1: Observational parameters of the available globular cluster observations

Target	Instrument	Starting Time (TT)	Exposure (ksec)	Usable Time (ksec)
NGC 6304	*XMM*/EPIC	2006 Sep. 04 10:39:06	11.0	11.0
NGC 6304	*Chandra*/ACIS	2008 Jan. 28 18:10:38	5.3	5.3
NGC 6540	*XMM*/EPIC	2005 Sep. 21 03:31:47	7.7	7.2
NGC 6540 †	*XMM*/EPIC	2005 Oct. 06 01:22:46	105.1	70.0
NGC 6553	*XMM*/EPIC	2006 Oct. 06 01:41:44	20.4	16.8
NGC 6637	*XMM*/EPIC	2006 Oct. 18 01:28:26	9.9	8.3
NGC 6681	*XMM*/EPIC	2005 Sep. 21 07:02:38	9.0	6.4
NGC 7089	*XMM*/EPIC	2005 Oct. 30 03:10:53	10.2	9.7

NOTES: This table lists the observational parameters of all the available observations used in this thesis work. The starting time is given in Terrestrial Time (TT). The *usable time* is the exposure time available after the subtraction of time intervals with large background flaring. †The long observation of NGC 6540 was actually targeted at a microlensing event, MACHO-96-BLG-5, but the western most half of the GC was on the EPIC field of view.

4.1 NGC 6304

NGC 6304 was observed for an integration time of 11 ks, all of which could be used since no background flares were found. A total of eleven X-ray sources were detected with the pn camera, plus an additional six X-ray sources detected on a MOS1+MOS2 image (Fig. 4–1). The *XMM-Newton* search for qLMXBs in the cluster NGC 6304 revealed three candidate qLMXBs. Two of them are within the FOV of a subsequent observation with *Chandra*. All X-ray sources in the GC were fitted with a fixed value of Galactic absorption, $N_{H,22} = 0.266$.

The *XMM-Newton* frame was realigned to the 2MASS frame using the association between one of the candidate qLMXBs and its possible counterpart (see § 4.1.3). Before the astrometric correction, *XMM-Newton*'s absolute astrometry uncertainty is $2''$ (Guainizzi 2008). After the frame alignment, the residual uncertainty of $1.2''$ (1σ) originates from the relative astrometry between the three EPIC detectors that were used for the correction (Jeffries et al. 2006).

The analyses of the three candidates in this cluster: XMMU J171433−292747, XMMU J171421−292917 and XMMU J171411−293159 are in the following sections.

4.1.1 The Core Source: XMMU J171433−292747

Analysis of *XMM-Newton* Data

This X-ray source is located near the centre of the cluster, at a distance $d_c < 1\,r_c$. The spectral fit of the pn data with the tabulated NS atmosphere model is statistically acceptable (χ^2_ν/dof (prob.) $= 1.24/21$ (0.20)) and is producing values for R_∞ and $kT_{\rm eff}$ in the range expected for a NS in quiescence. However, there

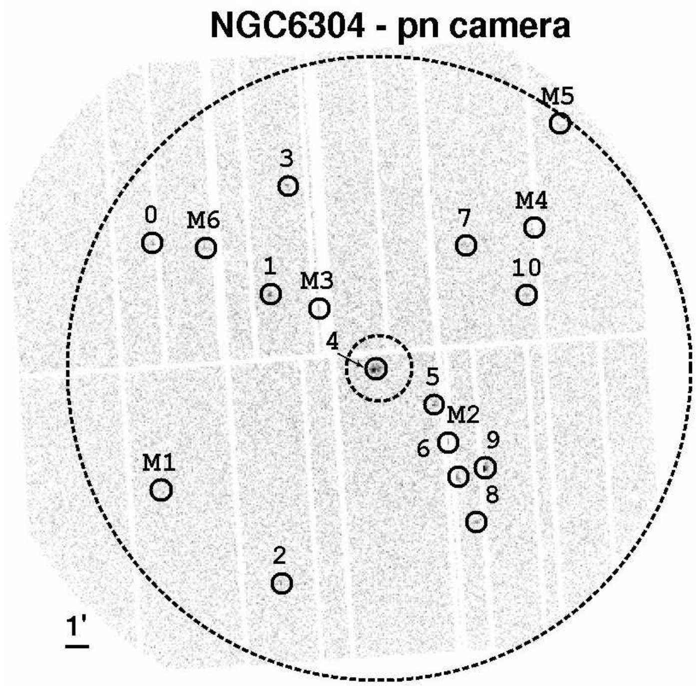

Figure 4–1: This EPIC/pn image of NGC 6304 shows the sources detected with the pn camera (labelled 0 to 10), and exclusively with the MOS cameras (M1 to M6). The small and large dashed circles respectively represent the half-mass and tidal radius. In this figure, north is up and R.A. increases to the left. The candidate qLMXBs are the sources #4, #5 and #9 corresponding respectively to XMMU J171433−292747, XMMU J171421−292917 and XMMU J171411−293159. Figure from Guillot et al. (2009).

exists a systematic excess of counts above the best-fit model at photon energies larger than 3 keV suggesting an additional high-energy spectral component, which is accounted for by the addition of a power law. The low-probability value of the F-test (prob=0.014) suggests that adding a power-law component better describes the data than the absorbed H-atmosphere model alone. The best-fit NSA tabulated model with the power-law component has a fit statistic χ^2_ν/dof (prob.) = 0.69/19 (0.83) (see Fig. 4–2). The slope of the power law is $\alpha = 1.5^{+0.9}_{-0.8}$ and this component of the model contributes to $48ud1819\%$ of the total unabsorbed flux of the source. Also, $R_\infty = 8.1^{+8.3}_{-2.5}$ km and $kT_{\rm eff} = 127^{+31}_{-29}$ eV. These values are in agreement with other known qLMXBs (Table 2–1).

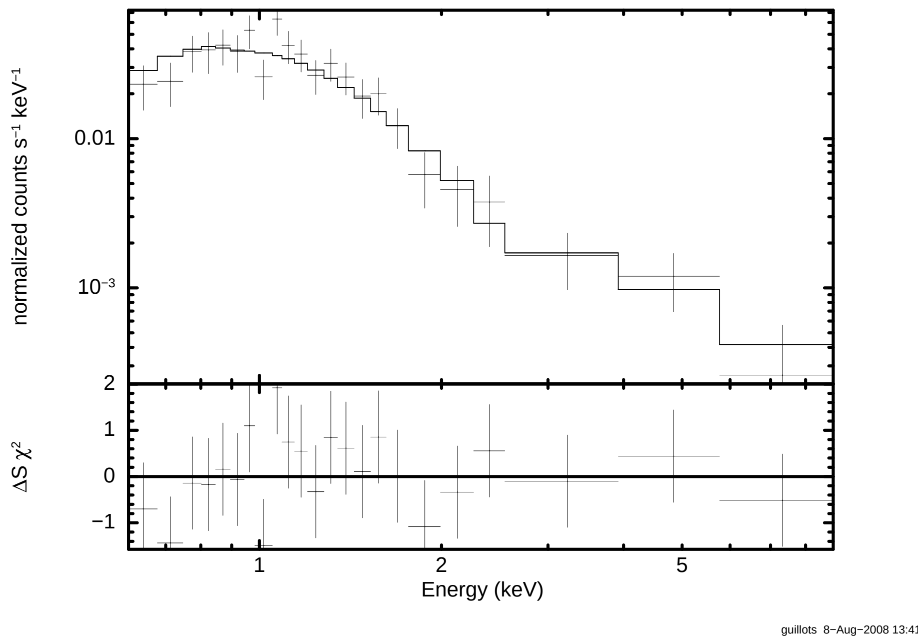

Figure 4–2: This spectrum is that of XMMU J171433−292747, consistent with a `nsa + powerlaw` model. Fixed absorption is taken into account in the spectral fit using $N_{H,22}$=0.266. Due to the low S/N at large energies (above 2.5 keV), the last 9 bins were grouped into three separate bins. Figure from Guillot et al. (2009).

The 0.5–10 keV lightcurve exhibits no variability (Fig. 4–3). More specifically, the average number of counts per 100 sec bin is 7.2±3.2 (1σ). All bins have count numbers consistent within 3σ of the average except one bin with 21 counts. The Poisson probability of finding a bin with such a peak in the lightcurve with a mean of 7.2 is 2.0%. Also, the peak does not represent a variation by more that a factor of 10 of the mean number of source counts. No detailed variability analysis can be performed due to the highly variable background. Thus, no variability is detected

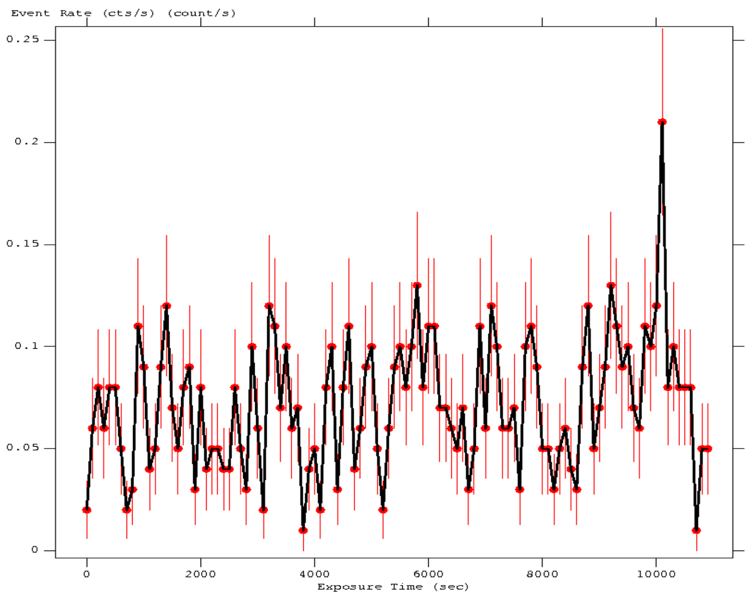

Figure 4–3: This lightcurve of XMMU J171433−292747 shows the detected 0.5–10 keV countrate as a function of time. Each bin is 100 sec long and the mean countrate per bin is 7.2±3.2 (1σ) counts. No variability is detected with weak constraints.

on a $\lesssim 100$ sec time-scale with weak constraints. The absence of significant intensity variability over the timescale of the observation further supports the classification of this source as a candidate qLMXB. Moreover, the luminosity is consistent with being the same as that observed during the *ROSAT* observation 14 yr earlier (see § 5.2 and Table 5–2). This is consistent with the expected stable thermal luminosity from a qLMXB on this timescale (BBR98, Ushomirsky and Rutledge 2001).

While the presence of PL component has been observed for field qLMXBs (Cen X-4, Aql X-1, amongst other), no such component has been observed for gC qLMXBs. More specifically, it is not searched for since the identification is based on the consistency with the theoretical model of a NS H-atmosphere. The PL component could be explained by the presence of two unresolved sources – one spectrally hard and one spectrally soft. This possibility is investigated by separating the data into soft ($< 1.5\,\mathrm{keV}$) and hard ($> 1.5\,\mathrm{keV}$) images and performing a source detection as described in § 3.2.1. XMMU J171433−292747 is detected in both bands, with 24.6σ and 4.5σ significances in the soft and hard bands respectively (the 1.5 keV division was selected as the lowest possible photon energy which provides a significant source detection – a cutoff of 2.0 keV finds no source with $> 3\sigma$ significance above 2.0 keV). A positional offset of $3'' \pm 0.9''$ is measured between the positions of the source in the two images, which is marginally consistent with a single source. It is possible that an unresolved hard X-ray source lies close to the candidate qLMXB and was interpreted as a high-energy tail in the spectrum of source XMMU J171433−292747. In fact, a short archived *Chandra* observation was analyzed to investigate this alternative.

Analysis of *Chandra* Data

In the short *Chandra* observation, two sources, CXOU J171432.93−292748.0 and CXOU J171431.86−292745.5, are detected (with significance $\sigma > 3$) within the core radius of NGC 6304, separated by an angular distance of $\sim 13''$. The brightest one – CXOU J171432.93−292748.0, accounting for 74 counts (including about 2 background counts) – is positionally consistent with the *XMM* candidate qLMXB XMMU J171433−292747, within 2σ. The relative offset between the *XMM-Newton* and *Chandra* positions of the source is $2.9''\pm1.6''$; the error on the *XMM-Newton* astrometry (statistical and systematic errors) accounts for 1.5″ (1σ). Since *XMM-Newton* cannot resolve the two sources in the core, the centroid position obtained previously with `wavdetect` on the pn data is in between the two sources detected with *Chandra*/ACIS (Fig. 4–4).

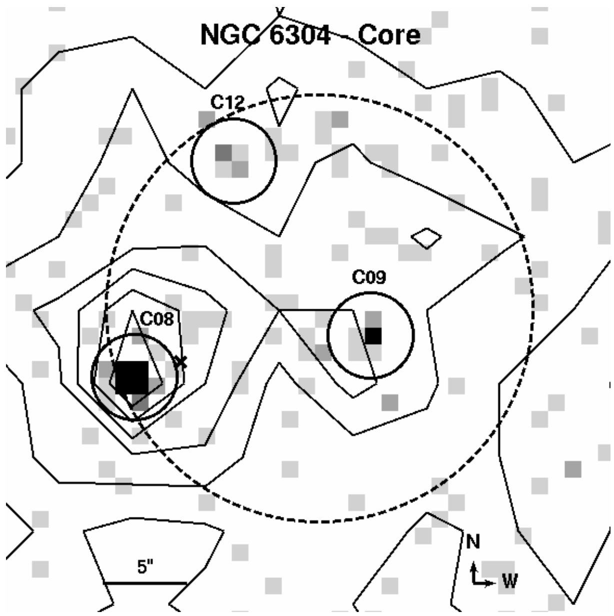

Figure 4–4: This *Chandra*/ACIS-S3 image of the core of the globular cluster NGC 6304 was created from the level-2 pre-processed file in which the events were spatially binned by a factor ×2. The dashed line represents the core radius of NGC 6304. The cross shows the position of the *XMM-Newton* detected source, and the contour lines represent the overlapped event distribution of the *XMM-Newton* data. The three solid circles are the 2.5″ extraction radii of the *Chandra*/ACIS sources: C08 = CXOU J171432.93−292748.0, C09 = CXOU J171431.86−292745.5 and C12 was found with `wavdetect` with a low significance: 2.3σ. Figure from Guillot et al. (2009)

The source CXOU J171432.93−292748.0 (C08) is spectrally soft with all events having energies below 2.5 keV. It is assumed to correspond to the candidate qLMXB XMMU J171433−292747, and therefore a NS H-atmosphere model is used for the spectral fitting, together with Cash-statistic: $kT_{\rm eff} = 127^{+34}_{-27}$ eV and $R_\infty = 7.5^{+8.3}_{-3.7}$ km. The goodness-of-fit probability is 35% indicating that the model is likely to describe the data.

For this X-ray source – the only one in this *Chandra* observation – the number of counts allows for spectral binning ($\sim$ 15 counts per bins), while having an acceptably approximate Gaussian uncertainty in each bin. A 5-bin spectra is obtained in the 0.5-8.0 keV range. For the tabulated NS H-atmosphere model, the best-fit parameters of this χ^2_ν-fit are: $kT_{\rm eff} = 128^{+40}_{-30}$ eV and $R_\infty = 7.3^{+10.5}_{-3.7}$ km. Although the counting statistics are poor, the best-fit values are in agreement with the *XMM* results, and the model fitted is statistically acceptable (χ^2_ν/dof (prob.) = 0.12/3 (0.95)). For completeness, the spectrum is fit with an absorbed power law, leading to a best-fit photon index $\alpha = 3.5^{+0.5}_{-0.4}$ with χ^2_ν/dof (prob.) = 1.3/3 (0.27), which indicates a soft source, as expected for a typical qLMXB. This provides further support to the argument that CXOU J171432.93−292748.0 is the candidate qLMXB detected in XMMU J171433−292747. The best-fit H-atmosphere parameters for CXOU J171432.93−292748.0 are consistent with typical values for quiescent NSs and with the best-fit values obtained with *XMM-Newton*. The unabsorbed flux is also consistent with the flux of the thermal component of the *XMM-Newton* observation (as will be demonstrated statistically below).

The second *Chandra* source in the core, CXOU J171431.86−292745.5, $C09$ on Figure 4–4 (18 counts including about 2 background counts), appears spectrally harder, and its best-fit photon index ($alpha = 0.8^{+0.7}_{-0.7}$) is consistent with the hard power-law component in the spectrum of source XMMU J171433−292747

($alpha = 1.2^{+0.7}_{-0.8}$). For completeness, the spectrum is fit with a NS atmosphere model, for which the best-fit projected radius $R_\infty \leq 1\,\mathrm{km}$ is inconsistent with the typical radii of NSs. In addition, the goodness of this fit (99.9% of Monte-Carlo simulations from the NS atmosphere model give better statistics than the best fit) indicates that the spectrum is not that of a NS H-atmosphere model. These results provide further support that this second source in the core is not the candidate qLMXB. In fact, the photon index of CXOU J171431.86−292745.5 is consistent with typical photon indices of CVs (Richman 1996).

As a last check of statistical consistency, a simultaneous fit is performed using the *XMM*/pn, *XMM*/MOS1, *XMM*/MOS2 for XMMU J171433−292747 and *Chandra*/ACIS spectra for both CXOU J171432.93−292748.0 and CXOU J171431.86−292745.5. While fitting, the temperature, the radius and the photon index parameters of each individual data set are kept tied together and N_H is kept fixed at the value cited above. Again, the fit is statistically acceptable, χ^2_ν/dof (prob.) = 0.76/42 (0.86), and the obtained best-fit parameters are in agreement with typical values for accreting quiescent NS. These best-fit values of the NSA model are the ones quoted in Table 4–2 for CXOU J171432.93−292748.0. The flux cited for this source is that of the thermal component contribution.

To characterize the variation in flux for the qLMXB, a second simultaneous spectral fit using the EPIC/pn data alone for XMMU J171433−292747 and with the ACIS-S data for CXOU J171432.93−292748.0 and CXOU J171431.86−292745.5 is performed; a multiplicative factor for the spectral normalization is used, fixed at 1 for the *XMM-Newton*/pn spectrum and left as a free parameter for the

Chandra/ACIS spectrum. The best-fit factor is $0.8^{+0.2}_{-0.2}$ (90% confidence), which is marginally consistent with the fluxes being the same.

It is therefore concluded that XMMU J171433−292747, observed in the core of NGC 6304 in the *XMM* data, is a composite of the candidate qLMXB CXOU J171432.93−292748.0 and the X-ray source CXOU J171431.86−292745.5 of unknown classification, which were not distinguishable at the resolution of *XMM-Newton*, but which are spatially resolved at the resolution of *Chandra*.

4.1.2 XMMU J171421−292917

This faint candidate qLMXB has been characterized as such from the *XMM-Newton* data but it is also present in the *Chandra* observation mentioned above.

Analysis of *XMM-Newton* Data

The NS H-atmosphere tabulated model applies for this low-S/N source. The fit is statistically acceptable (χ^2_ν/dof (prob.) $= 1.09/16$ (0.36)) and the parameters are consistent with expected values ($kT_{\rm eff} = 70^{+28}_{-20}$ eV and $R_\infty = 23^{+69}_{-10}$ km; see Fig 4–5). The `nsa`, `nsagrav` and `nsatmos` models are then used to confirm the first fit. Even though acceptable, the fits of this low-S/N spectrum using the *XSPEC* models do not allow for representative error estimates, as explained in §3.2.3. Also, the simultaneous fitting of the pn, MOS1 and MOS2 spectra did not provide an improvement of the uncertainties, due to the small number of counts of this source in the MOS CCDs, ~ 60 counts. In consequence, the best-fit values using the tabulated model are reported in Table 4–2.

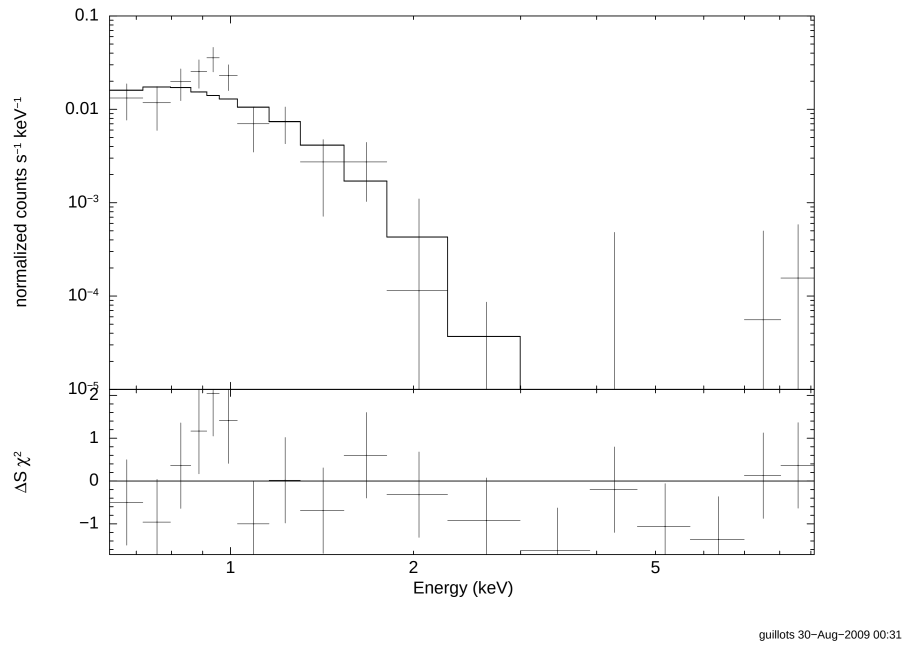

Figure 4–5: The low-S/N spectrum of XMMU J171421−292917 has been fit with the absorbed tabulated NSA model, using the hydrogen column density $N_{H,22}$=0.266. The fit was statistically acceptable with χ^2_ν/dof (prob.) = 1.09/16 (0.36). Figure from Guillot et al. (2009).

Analysis of *Chandra* Data

This low-S/N candidate qLMXB is also detected in the *Chandra*/ACIS observation as CXOU J171420.88−292916.1. An offset of $1.2'' \pm 1.6''$ is measured between the *Chandra*/ACIS and the *XMM-Newton* observation, consistent within 1σ. CXOU J171420.88−292916.1, is located $\sim 1.5'$ off-axis and requires a $3''$-radius extraction region. The source has 19 counts (including about 3 background counts) and its unbinned spectrum is fit, using the Cash-statistic, with a NS atmosphere model. The best-fit parameters are consistent with the previously measured values:

$R_\infty = 9.3^{+410}_{-4.6}$ km and $kT_{\rm eff} = 89^{+49}_{-46}$ eV, with a "goodness-of-fit" probability of 77.2%, indicating a moderately good fit.

As was previously done (§ 4.1.1), a simultaneous χ^2_ν-fit is performed for this candidate qLMXB, using the *XMM-Newton* and *Chandra* spectra. The *Chandra*/ACIS spectrum has only one bin, containing the 19 counts. The fit is statistically acceptable (χ^2_ν/dof (prob.) $= 1.11/22$ (0.33)) and the best-fit parameters ($R_\infty = 30^{+66}_{-15}$ km and $kT_{\rm eff} = 65^{+23}_{-16}$ eV) are consistent with the *XMM*-alone best-fit values.

To characterize the variation in flux of the candidate qLMXB, a simultaneous spectral fit is performed using the EPIC/pn data alone for XMMU J171421−292917 and with the ACIS-S data for CXOU J171420.88−292916.1. A multiplicative factor for the spectral normalization is used, fixed at 1 for the *XMM-Newton*/pn spectrum and left as a free parameter for the *Chandra*/ACIS spectrum. The best-fit factor of the ACIS spectrum ($0.54^{+0.30}_{-0.24}$, 90%) suggests that the flux has changed between the *XMM-Newton* observation and the *Chandra*/ACIS observation. Higher S/N data will permit confirmation of the apparent variability in the flux of this candidate qLMXB.

The 2MASS counterpart to XMMU J171421−292917

Using the online 2MASS Point Source Catalogue (2MASS–PSC), a possible counterpart, 2MASS J17142095−2929163 ($m_J = 13.063(29)$, $m_H = 12.645(33)$ and $m_K = 12.510(35)$, where the numbers in parentheses are the 1σ uncertainties in the preceding digits), is identified at an angular distance of $0.45''$. The probability that another star as bright or brighter lies as close or closer to this

X-ray source is 0.084% (179 stars with magnitude $m_J \leq 13.063$ are found in an annulus of inner radius $2'$ and outer radius $4'$ around the optical centre of NGC 6304), implying an association with 99.916% confidence. The *Chandra* source position is located $0.9''\pm0.6''$ from the possible identified 2MASS counterpart 2MASS J17142095−2929163. This offset is consistent (1.4σ) with the X-ray and 2MASS sources being associated where the uncertainty is due to *Chandra*'s systematic and statistical uncertainties; the error on the 2MASS position is assumed to be negligible. Also, the probability that another source as bright or brighter lies as close or closer to the X-ray position is 0.34%, providing further support to the association, with 99.66% confidence.

To obtain the bolometric luminosity of 2MASS J17142095−2929163 at the distance of NGC 6304, the reddening $E(K-V)$ is first calculated using $E(K-V)/E(B-V) = -2.744$ (Rieke and Lebofsky 1985), where $E(B-V) = 0.53$ for NGC 6304. Using the V-band magnitude $V = 14.85(5)$ (S. Ortolani, private communication, 2008), the intrinsic colour is $(V-K)_0 = (V-K) + E(K-V) = 2.34 - 1.45$. Using bolometric corrections obtained from 2MASS photometry (Masana et al. 2006) as a function of $(V-K)_0$ and of the average metallicity of the cluster $[m/H] = -0.56$ (Valenti et al. 2007), the K-band bolometric correction is $BC_K = 0.50$. Using a K-band extinction correction, $A_K = 0.36\,E(B-V)$ (Fitzpatrick 1999), $m_{\rm bol} = m_K - A_K + BC_K = 12.82$ is calculated to find the bolometric luminosity. Taking a zero absolute bolometric magnitude $M_{\rm bol} = 0$ star to correspond to a luminosity of 2.97×10^{35} erg s^{-1} (Harwit 2006) and the distance modulus, the absolute bolometric magnitude is $M_{\rm bol} = -1.07$, for a bolometric luminosity of $7.96{\times}10^{35}\,{\rm erg\ s^{-1}}$.

If the X-ray emission is coming from the star 2MASS J17142095−2929163, the X-ray to bolometric flux ratio for this giant star is therefore $F_{\rm X}/F_{\rm bol} = 10^{-4.05}$. From the *ROSAT* All Sky Survey catalogue of bright late-type giants and supergiants (Hunsch et al. 1998), the mean calculated X-ray to bolometric flux ratio for all 450 stars observed in that catalogue is $F_{\rm X}/F_{\rm bol} = 10^{-5.6\pm0.6}\,(1\sigma)$. The 0.1–2.4 keV range was used to estimate the X-ray flux. The 2MASS counterpart and the associated X-ray source are consistent with being a giant star (2.6σ). However, if X-rays from XMMU J171421−292917 were due to a typical giant star, then similar X-ray fluxes from other giant stars in this GC would be expected; yet no other giant star on the outskirts of this GC exhibit similar X-ray fluxes.

For main-sequence stars, the typical X-ray to bolometric flux ratio seems to reach an upper limit and saturates at 10^{-3} (Vilhu and Walter 1987). For the association of XMMU J171421−292917 with 2MASS J17142095−2929163, the X-ray to bolometric flux ratio is ratio, $F_{\rm X}/F_{\rm bol} = 9{\times}10^{-5}$, and is therefore consistent with a main-sequence foreground star.

The X-ray emission from dMe stars (M-class red dwarfs) is spectrally comparable to those of RS CVn (Singh et al. 1996). Typically, RS CVn exhibit a two-temperature Raymond-Smith plasma model[1] (Dempsey et al. 1993). Since the number of counts is not sufficient for such a fit with all parameters left free, the spectrum of XMMU J171421−292917 is fitted twice with a two-temperature Raymond-Smith plasma model keeping the high-temperature component fixed at the lowest ($kT_2 = 0.93$ keV) and highest value ($kT_2 = 3.45$ keV) from the sample of RS CVn (Dempsey et al. 1993). The metallicities are also held fixed at the solar value, $Z = 0.0177$. The normalization of the Raymond-Smith model in *XSPEC* model provides the emission measure (EM $= \int n_e n_H dV$), a distance dependent value. The best-fit parameters for those two statistically acceptable fits are $N_{H,22} = 1.5^{+1.3}_{-0.4}$, $kT_1 = 0.11^{+0.22}_{-0.06}$ keV, $\mathrm{EM}_1 = 2.4^{+12.9}_{-2.1}\times10^{59}\,\mathrm{cm}^{-3}$ and $\mathrm{EM}_2 \leq 3.9\times10^{55}\,\mathrm{cm}^{-3}$ for the first fit (χ^2_ν/dof (prob.) $= 1.25/14$ (0.23)) corresponding to $kT_2 = 0.93$ keV and $N_{H,22} = 1.12^{+1.12}_{-0.53}$, $kT_1 = 0.11^{+0.19}_{-0.06}$ keV, $\mathrm{EM}_1 = 2.1^{+18.5}_{-1.5}\times10^{59}\,\mathrm{cm}^{-3}$ and $\mathrm{EM}_2 \leq 5.5\times10^{54}\,\mathrm{cm}^{-3}$ for $kT_2 = 3.45$ keV (χ^2_ν/dof (prob.) $= 1.25/14$ (0.23)).

The value of EM_1 lies $\sim$ 6 orders of magnitude above the typical values ($\mathrm{EM}_1 = 0.1 - 3\times10^{53}\,\mathrm{cm}^{-3}$), for the fits performed with the maximum and minimum kT_2 respectively, assuming 2MASS J17142095−2929163 lies in NGC 6304. Moreover, the ratio of the two emission measures $\mathrm{EM}_2/\mathrm{EM}_1$ is a distance independent value, that is in all cases ≥ 1 for coronally active stars (Dempsey et al. 1993).

[1] RS CVn refers to the class of active stars showing similar properties as the canonical object *RS Canum Venaticorum*, and does not refer to Raymond-Smith plasma.

In both cases, the derived 90% confidence upper limits of EM_2/EM_1 lie below values observed from coronally active systems. Therefore, the observed X-ray spectrum is inconsistent with the typical two-temperature plasma of a coronally active star, independently of the distance of the X-ray source with its associated IR counterpart.

As a conclusion, XMMU J171421−292917 is not a coronally active foreground star. And since the X-ray source is spectrally consistent with a qLMXB at a distance of 6 kpc, the X-ray source is identified as a candidate qLMXB in NGC 6304 with an IR companion star.

4.1.3 XMMU J171411−293159

This X-ray source was present in the *XMM-Newton* observation but was outside the field of view of the available *Chandra* observations. A possible IR counterpart was found using 2MASS-PSC.

The X-ray Spectrum

The fit with the tabulated NS atmosphere model is statistically acceptable and does not require an additional power law (Fig. 4–6). The χ^2_ν-statistic is χ^2_ν/dof (prob.) $= 1.29/16$ (0.20), the projected radius is $R_\infty = 15.3^{+15.5}_{-5.2}$ km and the effective temperature is $kT_{\rm eff} = 100^{+24}_{-19}$ eV. The confirmation with any of the models `nsa, nsagrav` and `nsatmos` fails because the fit, while statistically acceptable, produces error regions larger than the allowed parameter space in *XSPEC*. It is therefore impossible to derive the uncertainty region for the spectrum of XMMU J171411−293159 using these models. In consequence, the results of the tabulated model are quoted and show that the model fit is consistent with the thermal spectrum of a qLMXB at the distance of the NGC 6304. Moreover, no significant variability over the timescale of the observation is observed, with weak constraints. To better improve the statistics and uncertainties, the MOS1, MOS2 and pn spectra are fitted simultaneously. The resulting fit is statistically acceptable (χ^2_ν/dof (prob.) $= 1.20/31$ (0.21)) and the obtained parameters are: $kT_{\rm eff} = 115^{+21}_{-16}$ eV and $R_\infty = 10.7^{+6.3}_{-3.1}$ km. These values are reported in Table 4–2.

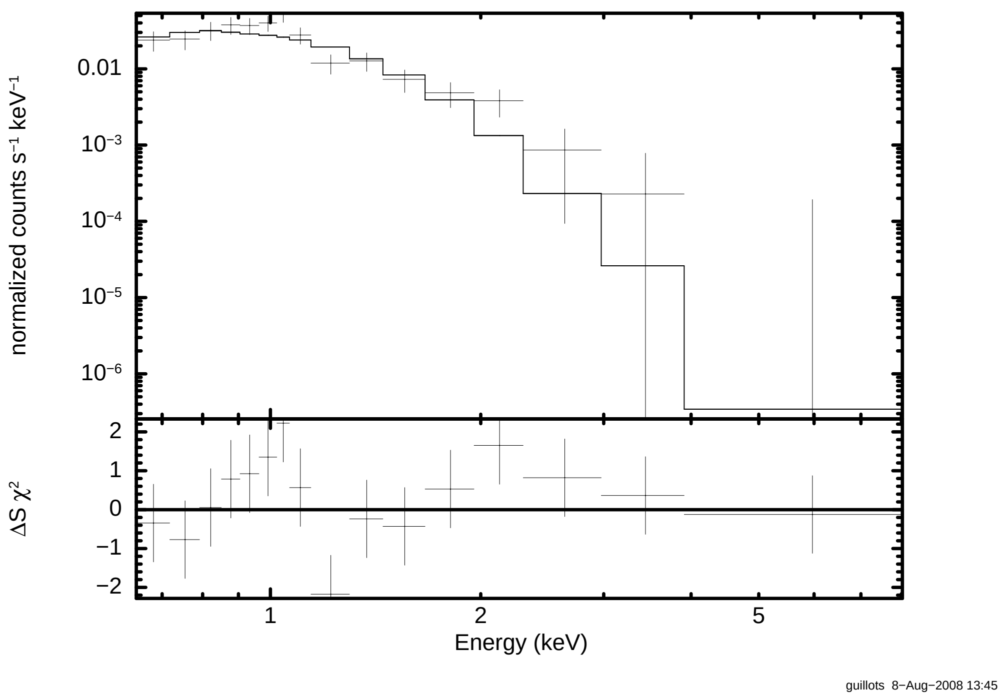

Figure 4–6: This spectrum is that of XMMU J171411−293159, spectrally consistent with the tabulated NSA model. The hydrogen column density $N_{H,22}$=0.266 accounts for the absorption in the spectral fit. Due to the low S/N at large energies, the last three bins were grouped into a single bin above 4 keV. Figure from Guillot et al. (2009).

For completeness, additional spectral fits are provided. First, a single power law gives an acceptable fit (χ^2_ν/dof (prob.) $= 1.37/14$ (0.16)) with a soft photon index, $\alpha = 3.51^{+0.40}_{-0.37}$. A single temperature Raymond-Smith plasma fit with variable absorption and solar metallicity also produces an acceptable fit (χ^2_ν/dof (prob.) $= 1.03/13$ (0.42)) with the following best-fit parameters: $N_{H,22} = 0.19^{+0.14}_{-0.15}$ and $kT_{\rm eff} = 0.76^{+0.26}_{-0.17}$ keV. Thus, the spectrum of this (highest S/N) X-ray source is consistent with other spectral interpretations; however, such a steep power law ($\alpha = 3.5$) is usually interpreted as indicating a thermal spectrum.

The 2MASS Counterpart of XMMU J171411−293159

A probable 2MASS counterpart (2MASS J17141152−2931594; m_J = 8.796(22), m_H = 8.361(18), m_K = 8.213(20)) is found located at a distance of 1.77″ (before astrometric correction to the 2MASS frame), which is consistent with the absolute astrometry uncertainty of 2″ (Guainizzi 2008). The probability that another source as bright or brighter lies as close or closer to the X-ray source is 0.012%. Therefore, the association between XMMU J171411−293159 and 2MASS J17141152−2931594 is identified on the basis of spatial proximity, with 99.988% confidence. Also, the USNO-B1.0 catalogue (Monet et al. 2003) lists an object at this location (separated by <0.5″) with $B = 11.66$ and $B = 11.28$ (both with 1-σ error of $\sim 0.3''$. In the V-band, this star has an observed magnitude of $V = 10.65$ (S. Ortolani, private communication, 2008).

The colour-magnitude diagrams (Figs. 4–7 & 4–8) containing theoretical isochrones (Marigo et al. 2008) for ages in the range $t = 10^{8.55} - 10^{10.15}$ yr and

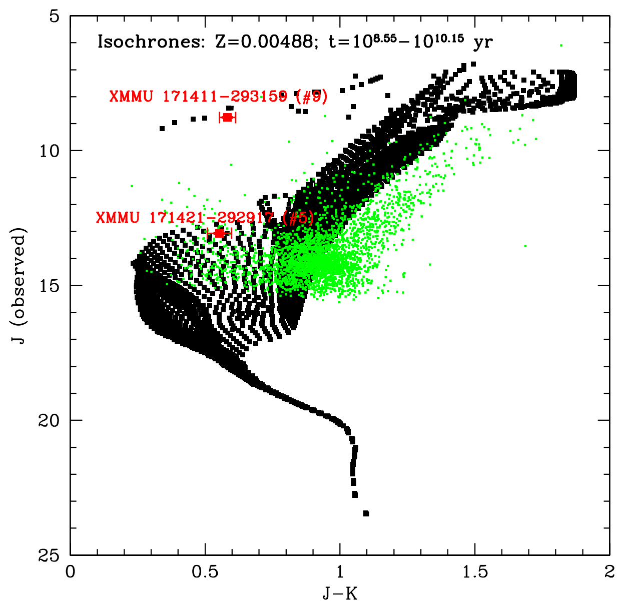

Figure 4–7: This colour (J–K) magnitude (J) diagram was made from all the 2MASS stars (small dots) within 6.5′ of the core of NGC 6304, down to a magnitude of m_K∼15. It also shows theoretical isochrones (small squares) for ages in the range t=$10^{8.55}$–$10^{10.15}$ yr and Z=0.00488 (Marigo et al. 2008). The counterpart 2MASS J17141152−2931594 appears to belong to the post-asymptotic giant branch. Figure from Guillot et al. (2009).

metallicity Z=0.00488 [2] show that the optical counterpart is consistent with a post-asymptotic giant branch (post-AGB) star, both in V and J bands. Even if the lifetime of the post-AGB stage is short, finding such an object in a GC is not unlikely. Based on previous work, 16 planetary nebulae (PNe) are expected to be found in the GCs of the Galaxy (Jacoby et al. 1997). This corresponds to

[2] The value of the cluster metallicity is calculated from [m/H]=−0.56 (Harris 1996) and $Z_\odot = 0.0177$ (Montalbán et al. 2004)

$6.7{\times}10^{-7}\,\mathrm{PN}\,{L_\odot}^{-1}$, from the total luminosity of all GCs, $\sim\,2.4{\times}10^{7}\,L_\odot$ (Secker 1992). Using the estimated mass of NGC 6304 (Gnedin et al. 2002) [3] and the average mass-to-light ratio of GCs, $M/L\,=\,1.7$ (Caputo 1985), 0.25 PNe are expected in this cluster. Since the lifetime of a PN, $\sim 10^{4}\,\mathrm{yr}$ (Jacoby et al. 1997), is comparable to that of a post-AGB object, $\sim\,10^{3}-10^{4}\,\mathrm{yr}$ (Siódmiak et al. 2008; Bloecker 1995), the number of post-AGB stars should be compared to the predicted number of PNe ($\sim$ 0.25) making the discovery of one such system not unlikely.

Using the procedure described in § 4.1.2, the bolometric magnitude and luminosity of the IR counterpart are calculated from the V-band magnitude. The values found are $m_{\mathrm{bol}} = m_K - A_K + BC_K = 8.914$, implying an absolute bolometric magnitude $M_{\mathrm{bol}}\,=\,-4.96$. The bolometric luminosity is $L_{\mathrm{bol}}\,=\,2.9{\times}10^{37}\,\mathrm{erg\ s^{-1}}$, when the bolometric luminosity for the zero absolute bolometric magnitude is $2.97{\times}10^{35}\,\mathrm{erg\ s^{-1}}$. Therefore the X-ray to bolometric flux ratio, $F_{\mathrm{X}}/F_{\mathrm{bol}} = 2{\times}10^{-5}$, is consistent ($1.4\sigma$) with that of a bright late-type giant (Hunsch et al. 1998), as detailed in § 4.1.2.

The Foreground Star Hypothesis

The hypothesis that 2MASS J17141152−2931594 is a field dwarf star is investigated. First, this star (TYC 6824-713) is listed in the Tycho-2 catalogue (issued from a re-analysis of the Hipparcos data), providing proper motion, but no parallax information (Høg et al. 2000). The proper motion observed for this star is

[3] Online data at http://www.astro.lsa.umich.edu/∼ognedin/gc/vesc.dat

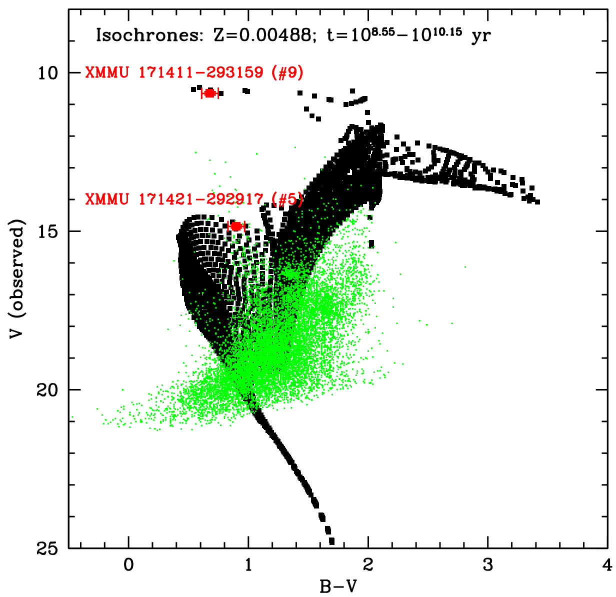

Figure 4–8: This colour (B–V) magnitude (V) diagram was made with all stars (small dots) within 6.5′ of the core of NGC 6304, down to a magnitude of $m_K{\sim}21$ (S. Ortolani, private communication, 2008). The same isochrones as Fig 4–7 are also shown. The figure supports the classification of 2MASS J17141152−2931594 as post-asymptotic giant branch star. Figure from Guillot et al. (2009).

–6.6±2.8 milli-arcseconds per year ($\mathrm{mas\,yr^{-1}}$), marginally consistent (at 2.4σ) with a zero proper motion, as would be expected for a cluster member. This does not resolve the possible cluster membership versus the foreground star hypothesis.

If reddening dust is distributed uniformly between the observer and NGC 6304, the source, assuming it is a main-sequence star, is most consistent with an $M_V = 4.4$ object at a distance 170 pc, with $E(B-V) = 0.03$, based on the absolute magnitude M_V and colour $(B-V)$ values of stars in the Hyades (de Bruijne et al. 2001).

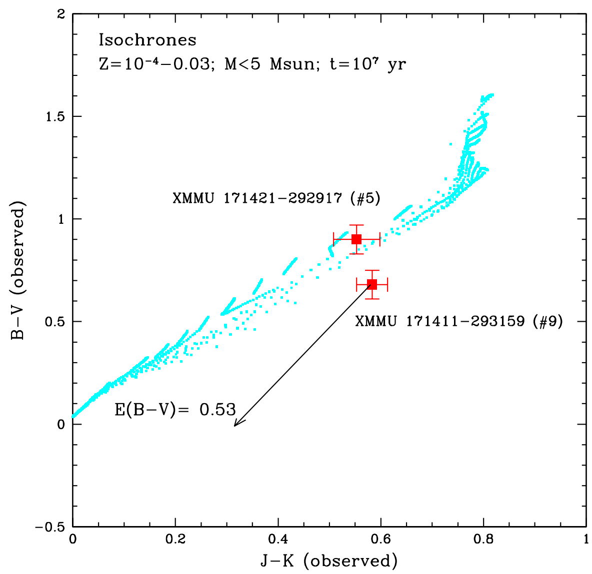

Figure 4–9: This colour (J-K) colour (B-V) diagram shows isochrones of low-mass (M<5 $M_{\odot}$) stars at t=10^7 yr (small points) for a range of metallicities (Z=0.0001–0.03, ΔZ=0.0005). In considering XMMU J171411−293159 as a foreground coronally active star, it lies marginally off the isochrones main-sequence, between 2-3σ) at zero reddening ($E(B$–$V)$=0). The discrepancy worsens if the hypothetical foreground source is at greater reddening; the vector beginning at source #9 terminates at the intrinsic colour 2MASS J17141152−2931594 would be at $E(B$–$V)$=0.53, that of NGC 6304. This does not support the hypothesis that XMMU J171411−293159 is a typical coronally active star, in the foreground of NGC 6304. Figure from Guillot et al. (2009).

In a $(B-V)$ vs. $(J-K)$ colour-colour diagram (Fig. 4–9), XMMU J171411−293159 lies marginally off the main-sequence for a wide range of metallicities (Z = 0.0001 − 0.03), lying closest to stars in the mass range 0.7–0.9 $M_{\odot}$, depending on metallicity, according to theoretical isochrones (Marigo et al. 2008). More specifically, considering XMMU J171411−293159 as a foreground coronally active star, it lies marginally off the main sequence (between 2–3σ) at zero reddening

($E(B-V)=0$). The discrepancy worsens if it is at greater reddening; on Fig 4–9, the vector beginning at the source terminates at the intrinsic colour 2MASS J17141152−2931594 would be at $E(B-V)=0.53$, that of NGC 6304. This does not support the hypothesis that XMMU J171411−293159 is a typical coronally active star, in the foreground of NGC 6304. But this marginal offset from the theoretical isochrones does not definitely exclude the possibility that the star is in the foreground.

An analysis similar to the one performed in § 4.1.2 excludes the possibility that the system is coronally active. The results of the spectral fits with a 2-temperature Raymond-Smith (RS) plasma are as follows. For $kT_2 = 0.93\,\mathrm{keV}$ (χ^2_ν/dof (prob.) $= 0.79/12$ (0.66)), $N_{H,22} = 1.3^{+0.6}_{-0.4}$, $kT_1 = 0.11^{+0.04}_{-0.04}\,\mathrm{keV}$, $\mathrm{EM}_1 = 1.9^{+11.2}_{-1.8}\times10^{60}\,\mathrm{cm}^{-3}$ and $\mathrm{EM}_2/\mathrm{EM}_1 = 1^{+5}_{-1}\times10^{-5}$. In the case of $kT_2 = 3.45\,\mathrm{keV}$, $N_{H,22} = 0.14^{+0.24}_{-0.10}$, $kT_1 = 0.84^{+0.18}_{-0.25}\,\mathrm{keV}$, $\mathrm{EM}_1 = 1.3^{+0.4}_{-0.4}\times10^{56}\,\mathrm{cm}^{-3}$ and $\mathrm{EM}_2/\mathrm{EM}_1 = 1^{+5}_{-1}\times10^{-5}$. The distance independent value $\mathrm{EM}_2/\mathrm{EM}_1$ is in both cases lower than the value $\mathrm{EM}_2/\mathrm{EM}_1 \geq 1$ observed for known coronally active stars (Dempsey et al. 1993). Thus, the X-ray spectrum of this source is inconsistent with that of typical coronally active stars.

In conclusion, the optical/IR colours and proper motion of the counterpart are in marginal agreement with those of a main sequence object located in the foreground of NGC 6304. However, the X-ray spectrum of XMMU J171411−293159 is inconsistent with those of typical coronally active stars, independently of the source distance. At the same time, the X-ray spectrum is consistent with an H-atmosphere qLMXB at the distance of NGC 6304; and the V vs. $(B-V)$

and J vs. $(J - K)$ CMDs support interpretation of the 2MASS counterpart as a post-AGB star in NGC 6304, which is evolutionarily consistent with the X-ray spectrum of a qLMXB. Without excluding classification as a foreground star, XMMU J171411−293159 is identified as a candidate qLMXB in NGC 6304; however, an optical/IR spectrum of the 2MASS counterpart should be obtained to confirm that the IR source is an actual post-AGB star in NGC 6304, and not a marginally spectrally unusual, optically variable main-sequence star (0.7–0.9 $M_{\odot}$) at a distance of ~few 100 pc.

4.2 NGC 6540

The integration time of the NGC 6540 observation was 7.7 ks (pn-camera) and 9.4 ks (MOS cameras). Only 7.2 ks of the pn-data could be used due to background flaring. Ten sources are detected in this observation, three of them close together in the core of the cluster (Fig 4–10). Their proximity requires careful source extraction, excluding the nearby sources with smaller radii than the usual 25″. None of the core sources show statistical consistency with NS H-atmosphere spectra at the distance of NGC 6540. However, one candidate qLMXB was identified on the outskirts of the GC, XMMU J180530−274212. An additional *XMM-Newton* archived data set covering the western half of the GC observed the candidate. The long integration time (105 ks) provides a high S/N, allowing for a more reliable spectral fit which contradicts the initial qLMXB classification. Also, the spatial velocity of the IR associated counterpart demonstrates that the star cannot be a cluster member, refuting the qLMXB candidacy of the X-ray source. The full analysis of this source is described in the following section.

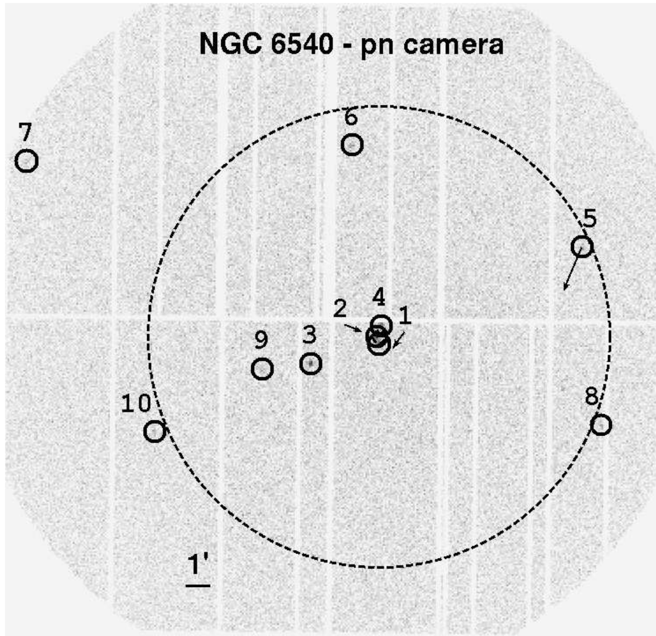

Figure 4–10: This EPIC/pn image of NGC 6540 shows the 10 sources detected in the pn camera. The large dashed circles represents tidal radius. The circle for the half-mass radius $r_{\rm HM}$=0.24′ is barely visible in the middle of the three core sources. In this figure, north is up and R.A. increases to the left. The vector for source #5 shows the proper motion of the counterpart 2MASS J18053074−2742128; the magnitude corresponding to the displacement in the sky over 10000 years. The calculated spatial velocity (222±47 km s^{-1} at 3.7 kpc) demonstrates that the star cannot be a cluster member (see § 4.2.1).

4.2.1 XMMU J180530−274212

The Short *XMM-Newton* observation

Using the tabulated NSA model, the spectrum of the detected source XMMU J180530−274212 (7σ) is fitted; the best-fit parameters are $R_\infty > 8$ km and $kT_{\rm eff} = 58^{+38}_{-22}$ eV with χ^2_ν/dof (prob.) = 0.83/13 (0.63). The error calculation failed to estimate the 90% confidence upper limit to R_∞. The hydrogen column density in the direction of the GC used for the spectral fit was fixed to

$N_{H,22} = 0.32$. The unabsorbed flux is $F_{\rm X} = 1.1{\times}10^{-13}\,{\rm erg\ cm^{-2}\ s^{-1}}$, corresponding to $L_{\rm X} = 0.17{\times}10^{33}\,{\rm erg\ s^{-1}}$ at the distance of the NGC 6540, $d = 3.7\,{\rm kpc}$. As for other candidates before (§ 4.1), this suggests a candidate qLMXB. An absorbed power-law model also supports the thermal source hypothesis since a soft photon index $\alpha = 4.4^{+1.3}_{-1.0}$ is obtained from the spectral fit.

The Possible Infrared Counterpart

The search for an IR 2MASS counterpart leads to the association of the X-ray source with the star 2MASS J18053074−2742128 (with 99.19% confidence using the method described before). The star has magnitudes $m_J = 10.629(31)$, $m_H = 10.362(41)$ and $m_K = 10.336(34)$ and is at a distance of $2.42''$ from the X-ray source. The inferred J-band flux is $F_J = 2.7{\times}10^{-11}\,{\rm erg\ cm^{-2}\ s^{-1}}$, implying that the X-ray to J-band flux ratio is $F_{\rm X}/F_J = 0.002$. This flux ratio is consistent with that of X-ray active stars (Shevchuk et al. 2009). Moreover, this star appears in the Tycho-2 catalogue (as TYC 6850-1313) and has a reported proper motion of $6{\pm}2.9\,{\rm mas\,yr^{-1}}$ in R.A. and $-11.1{\pm}2.7\,{\rm mas\,yr^{-1}}$ in Dec. (Høg et al. 2000). This is consistent ($> 4\sigma$) with a non-zero proper motion, corresponding to a spatial velocity of $v_\star = 222 \pm 47\,{\rm km\,s^{-1}}$ at the distance of NGC 6540. This velocity is in excess (4.1σ) of the escape velocity of the GC, $v_{\rm esc} = 27.6\,{\rm km\,s^{-1}}$ (Gnedin et al. 2002). Moreover, the direction of the proper motion is about $\sim 40^\circ$ south of the GC core. Thus, this object is not gravitationally bound to NGC 6540 and the cluster membership is therefore excluded. This irrefutably contradicts the initial qLMXB classification. Two B-band magnitudes are obtained from the USNO-B catalogue (Monet et al. 2003): $B = 11.68$ and $B - 11.55$.

The Archived *XMM-Newton* Observation

The second observation available (archived) allows us to obtain a better S/N for this source (17σ detection). The large amount of flaring in this observation precluded us from using the full time interval: 70 ks are free of background flaring and can be used for spectral fitting. 665 ± 39 counts (background subtracted) from the $25''$ extraction region are binned for the spectral fitting. The best-fit parameters for the tabulated NSA model (including absorption) are $R_\infty = 15.0^{+3.8}_{-7.6}$ km and $kT_{\rm eff} = 73^{+9}_{-10}$ eV with χ^2_ν/dof (prob.) = 1.83/28 (0.0047) (see Fig. 4–11).

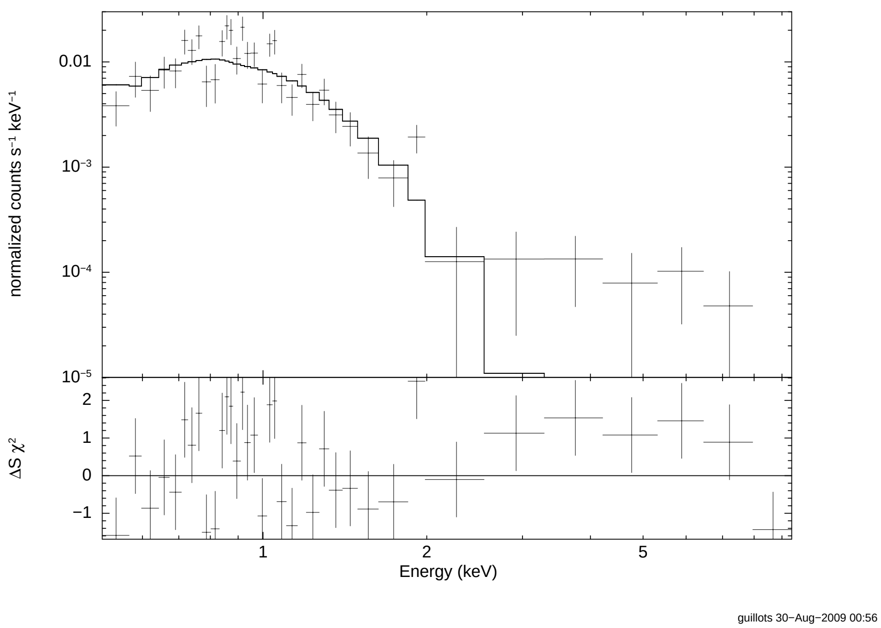

Figure 4–11: This spectrum is that of XMMU J180530−274212. The model used for the spectral fit is the tabulated NSA model. The discrepancies between data and the model can be seen at low energies E ~1 keV. The spectral fit is not statistically acceptable and therefore the model does not describe the data.

Although visual inspection of Fig. 4–11 may suggest the need for a power-law component, due to an excess of counts at high energies, the F-test probability (prob.=0.24) demonstrates that an additional component is not statistically required. R_∞, $kT_{\rm eff}$ and the X-ray luminosity are in the range of values expected for typical qLMXBs, but the null hypothesis probability for this fit (prob. = 0.0047) indicates that it is unlikely that the given model describes the data. Additionally, the models `nsa`, `nsagrav` and `nsatmos` produce fits that are not statistically acceptable either. Letting the hydrogen column density vary also generates a statistically unacceptable fit. The unabsorbed flux corresponding to the fit is $F_{\rm X} = 0.82\times10^{13}\,{\rm erg\ cm^{-2}\ s^{-1}}$, so that $L_{\rm X} = 0.13\times10^{33}\,{\rm erg\ s^{-1}}$.

The statistically unacceptable spectral fit of this high-S/N spectrum confirms the previous conclusion that the association between the X-ray source XMMU J180530−274212 and 2MASS J18053074−2742128 is not a qLMXB system.

4.3 NGC 6553

The full observation of NGC 6553 (20.4 ks) is reduced to 16.8 ks of usable time due to a large proton flare at the beginning of the integration. A total of 44 sources are detected (with significance $> 3\sigma$) in this observation (Fig. 4–12). The only X-ray source detected in the GC core is identified as a candidate qLMXB. Two other candidates are also identified: one on the outskirts of the GC (still inside the tidal radius of $r_t = 8.6''$), and one just outside of the tidal radius. The following sections describe the spectral analysis which led to the identification of those sources. In all cases, the Galactic absorption is included in the model using $N_{H,22} = 0.35$.

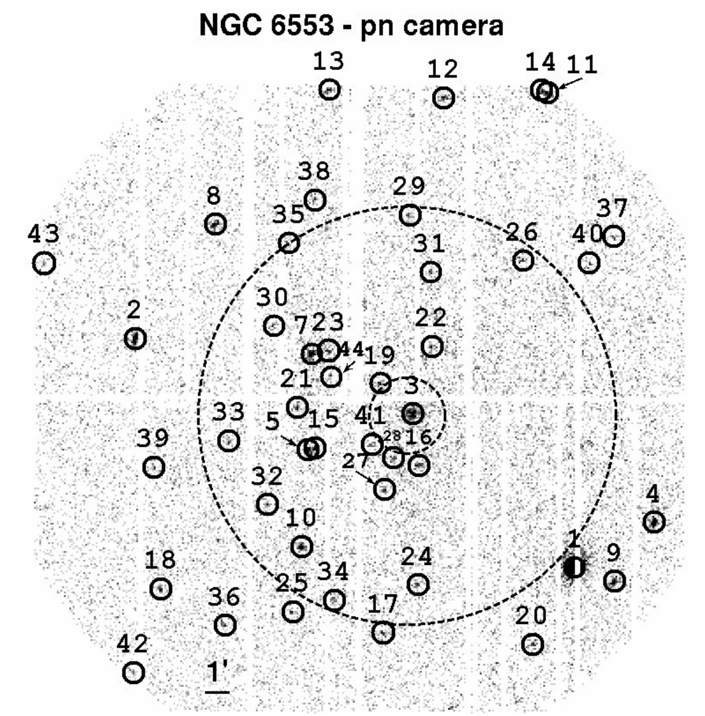

Figure 4–12: This EPIC/pn image of NGC 6553 shows the 44 sources detected on the pn camera. The small and large dashed circles respectively represent the half-mass and tidal radius. A Log grey-scale has been used for the image to due the brightness of source #1. In this figure, north is up and R.A. increases to the left. The three candidate qLMXBs of this GC are the sources #3, #9 and #35, respectively corresponding to XMMU J180916−255426, XMMU J180839−260119 and XMMU J180939−254724.

4.3.1 The Core Source: XMMU J180916−255426

The spectral fit of the pn data is performed using the tabulated NSA model, assuming a distance of 6 kpc. While the fit is statistically acceptable (χ^2_ν/dof (prob.) = 1.20/26 (0.22)), visual inspection of the spectrum suggests the need for a power-law component above 2 keV. This is confirmed using the F-test; the low F-test probability (prob.=0.01) indicates that the additional power-law is required.

Adding a power law to the atmosphere model leads to the following best-fit parameters: $R_\infty = 5.5^{+7.3}_{-2.3}$ km and $kT_{\rm eff} = 137^{+55}_{-35}$ eV for the H-atmosphere component; $\alpha = 2.0^{+0.9}_{-1.3}$ for the power-law component. The χ^2_ν-statistic of such fit is χ^2_ν/dof (prob.) = 0.82/24 (0.71) (see Fig 4–13). The best-fit projected radius R_∞ is on the low end of typical qLMXBs but is not inconsistent with such classification. The unabsorbed flux, $F_{\rm X} = 1.3\times10^{-13}$ erg cm^{-2} s^{-1}, implies a luminosity $L_{\rm X} = 0.6\times10^{32}$ erg s^{-1} at 6.0 kpc that is also consistent with that expected from GC qLMXBs. The fit is confirmed using `nsatmos + power law` and results are in statistical agreement with the previous ones: $R_\infty = 6.4^{+5.7}_{-1.4}$ km and $kT_{\rm eff} = 127^{+7}_{-45}$ eV for the atmosphere component; $\alpha = 2.2^{+0.8}_{-0.7}$ for the power-law component, with χ^2_ν/dof (prob.) = 0.95/24 (0.52).

The contribution of the power-law component, 55^{+11}_{-10}% of the total flux, surpasses that of the atmosphere model. This is unusual for a GC qLMXB and suggests that, as observed for XMMU J171433−292747 in NGC 6304 (see § 4.1), multiple X-ray sources are unresolved in the core. However, the `wavdetect` algorithm used on MOS2 images separated in two different bands (0.5–2.0 keV and 2.0–4.5 keV) does not argue in favour of this interpretation. The pre-processed *XMM-Newton* images in the two X-ray bands are used for this detection analysis. The choice of MOS2 is dictated by a smaller pixel size than the pn camera (see § 2.1.2). On the soft image (0.5–2.0 keV), only one source is detected, with the centroid 0.6″ from that of XMMU J180916−255426. No source is detected on the 2.0–4.5 keV

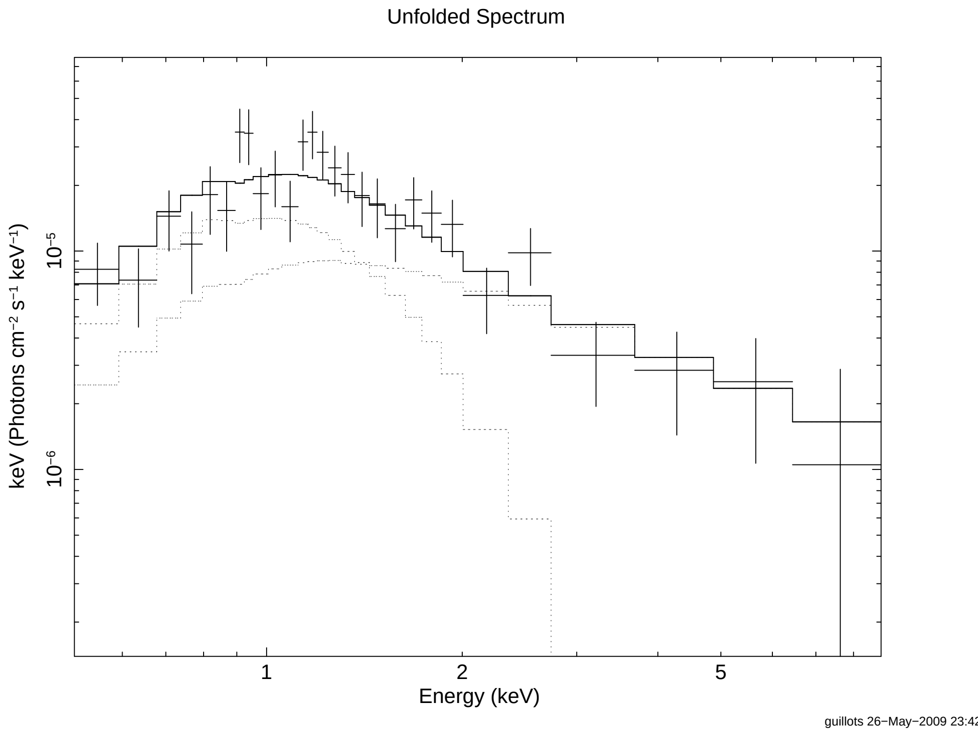

Figure 4–13: This spectrum is that of XMMU J180916−255426. The two components (H-atmosphere and power law) are shown in dashed lines, the power law being the one that dominates at $E \gtrsim 2\,\mathrm{keV}$, both affected by interstellar aborption. The hydrogen column density $N_{H,22}$=0.35 accounts for absorption.

image. This confirms, within the limitations imposed by the angular resolution of *XMM-Newton* and its on-board detectors, that XMMU J180916−255426 is consistent with being a single source. Only higher-resolution observation could differentiate possible multiple sources in the GC core. *Chandra* observations of NGC 6553 taken on October 30, 2008, but which are not yet published, may confirm or refute this hypothesis. Finally, the large stellar density in the GC core precludes finding a possible counterpart in the 2MASS catalogue.

4.3.2 XMMU J180839−260119

The second candidate qLMXB in NGC 6553 could only be fit with the tabulated NSA model; the other *XSPEC* NSA models could not evaluate the errors on the best-fit parameters, despite an acceptable fit. The tabulated model spectral fit is statistically acceptable (χ^2_ν/dof (prob.) = 1.7/13 (0.56)) and the obtained parameters in agreement with typical values. The best-fit projected radius is $R_\infty = 13.2^{+15}_{-6.6}$ km and the best-fit effective temperature is $kT_{\rm eff} = 98^{+26}_{-20}$ eV (see Fig 4–14). The unabsorbed flux $F_{\rm X} = 1.0\times10^{-13}$ erg cm^{-2} s^{-1} represents a luminosity $L_{\rm X} = 0.4\times10^{33}$ erg s^{-1} at $d = 6.0$ kpc, which is a typical luminosity for qLMXBs. A power-law model with fixed $N_{H,22}$ results in a statistically unacceptable fit, with prob. $\lesssim 0.01$. However, letting $N_{H,22}$ be a free parameter in this model leads to a best-fit photon index $\alpha > 4.5$ (χ^2_ν/dof (prob.) = 1.7/12 (0.60) with $N_{H,22} = 0.88^{+0.6}_{-0.3}$) which suggests a soft source, typical for qLMXBs.

Therefore, the X-ray spectrum of this source indicates a candidate qLMXB at the distance of NGC 6553 but the location outside the tidal radius of the GC challenges this classification. The search for a 2MASS possible counterpart results in the possible association with 2MASS J18083961−2601203 ($m_J = 10.146(15)$, $m_H = 9.796(23)$ and $m_K = 9.723(31)$), at a distance $d = 0.8''$ from the X-ray source, with 99.97% confidence. The X-ray to J-band flux ratio ($F_{\rm X}/F_J = 0.002$) is consistent with the source being a coronally active star, therefore this classification cannot be excluded, despite the X-ray spectral identification as a qLMXB. The Tycho-2 counterpart suggests a star with proper motion that is consistent (2.4σ) with zero: -2.7±3.0 mas yr^{-1} in R.A. and -6.6±2.8 mas yr^{-1} in dec. (Høg et al.

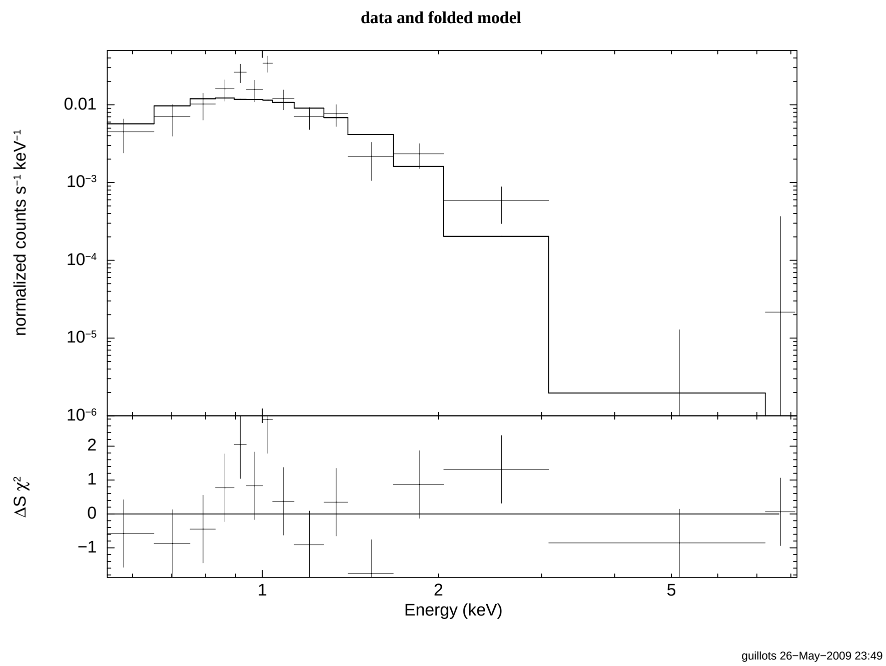

Figure 4–14: The spectrum XMMU J180839−260119 is fit with the tabulated NSA model, including absorption $N_{H,22}$=0.35. Such model describes well the data since the spectral fit is statistically acceptable with χ^2_ν/dof (prob.) = 1.7/13 (0.56).

2000). Therefore, the NGC 6553 membership of the 2MASS counterpart is not excluded.

4.3.3 XMMU J180939−254724

The last candidate qLMXB in this cluster is located just inside the tidal radius. It has low S/N (5.3σ detection) for which the obtained best-fit parameters using the tabulated NSA model are $R_\infty = 9.0\,\mathrm{km}$ and $kT_{\mathrm{eff}} = 88^{+80}_{-42}\,\mathrm{eV}$ (χ^2_ν/dof (prob.) = 0.63/5 (0.68), see Fig. 4–15). The error on the radius cannot be estimated due to the low-count statistics of the spectrum. For the same reasons, the three *XSPEC* models cannot be used. The results of this spectral analysis suggest that this source is consistent with a faint qLMXB at the distance of NGC 6553.

Further support is provided by the soft best-fit photon index ($\alpha = 3.5^{+1.5}_{-1.3}$) when using a power law model (χ^2_ν/dof (prob.) $= 0.82/5$ (0.53)), representative of a thermal source. The unabsorbed luminosity $L_{\rm X} = 0.13{\times}10^{33}\,{\rm erg\ s^{-1}}$ (at $d = 6.0\,{\rm kpc}$) also implies that XMMU J180939$-$254724 is a faint qLMXB.

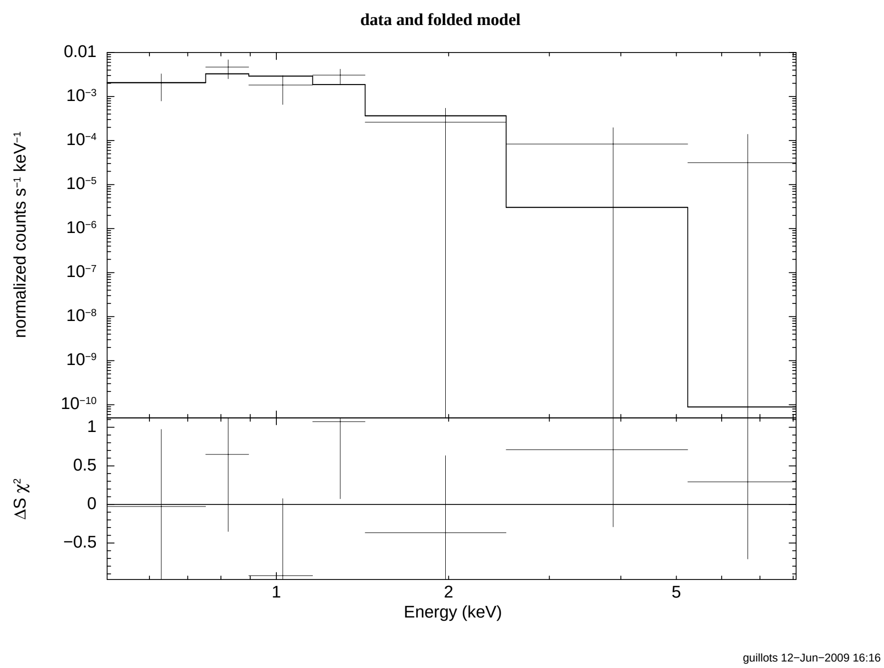

Figure 4–15: The spectrum XMMU J180939$-$254724 is fit with the tabulated NSA model, including absorption $N_{H,22}$=0.35. The count statistics is poor but the model acceptably describes the data: χ^2_ν/dof (prob.) $= 0.63/5$ (0.68).

A faint 2MASS counterpart 2MASS J18093945$-$2547248 is tentatively associated with 81% confidence, at an angular distance $d = 3.9''$ from the X-ray source. The low confidence of the 2MASS/*XMM-Newton* source association prevents any conclusive remarks. Higher S/N X-ray observations are needed to confirm the classification of this source and more precise astrometry is required to associate the X-ray source with a possible stellar counterpart.

4.4 NGC 6637 – M69

NGC 6637 is located at a distance of 9.1 kpc and the Galactic absorption in its direction is $N_{H,22} = 0.11$. Out of the 26 sources sources detected (Fig. 4–16), only six sources have sufficient counts for spectral characterization (> 100 photon events). This is due to the limited usable exposure time: 8.25 ks are available for the pn-camera in this observation due to flaring, while 17 ks were proposed. Among the bright high-S/N sources, one is a candidate qLMXB and its analysis is described in the following section.

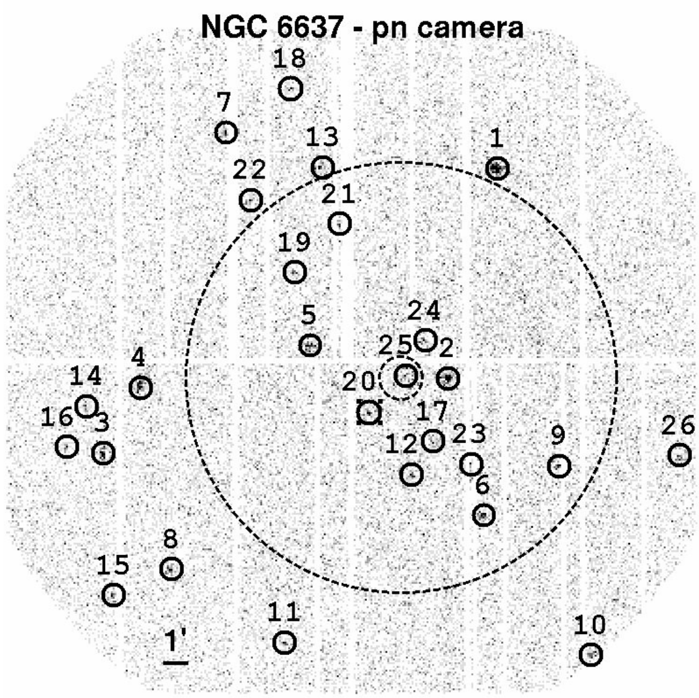

Figure 4–16: This EPIC/pn image of NGC 6637 shows the 26 sources detected on the pn camera. The small and large dashed circles respectively represent the half-mass and tidal radius. In this figure, north is up and R.A. increases to the left. Source #3, located outside the tidal radius, is the candidate qLMXB XMMU J183217−322346.

4.4.1 XMMU J183217−322346

This X-ray source is spectrally consistent with a qLMXB at the distance of the GC. The fit with the tabulated H-atmosphere model: χ^2_ν/dof (prob.) = 1.4/5 (0.22). The best-fit radius and temperature ($R_\infty = 17.4^{+28}_{-6.8}$ km and $kT_{\rm eff} = 99^{+37}_{-25}$ eV) are comparable to other values measured for the known GC qLMXBs. The unabsorbed flux is $F_{\rm X} = 0.84\times10^{-13}$ erg cm^{-2} s^{-1}, so $L_{\rm X} = 0.83\times10^{33}$ erg s^{-1}. While the spectral characteristics of the source suggest a qLMXB at the distance of the GC (see Fig. 4–17), the association of this source with NGC 6637 is questionable since the source is located far outside the tidal radius, at $1.4\, r_t$.

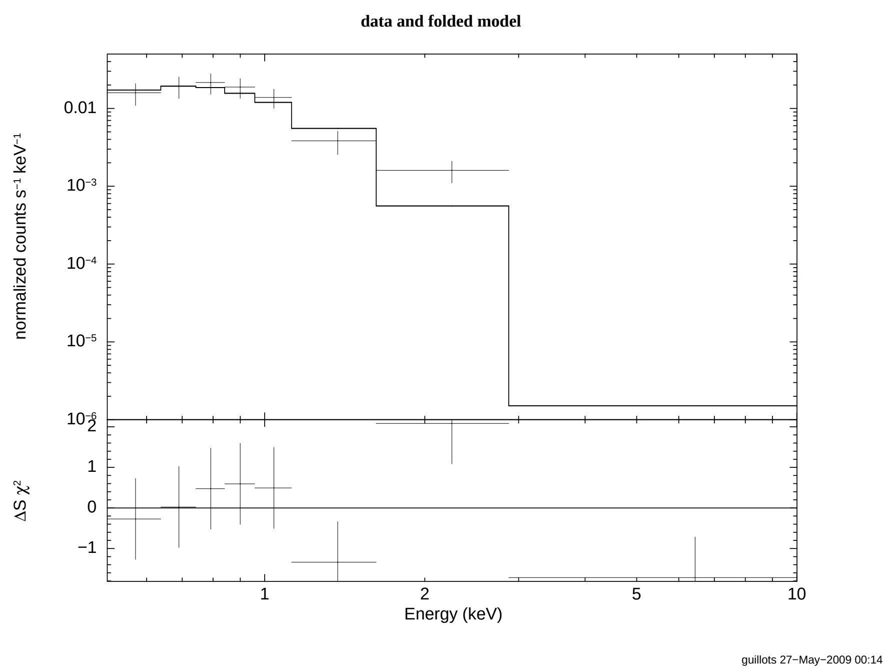

Figure 4–17: This spectrum is that of XMMU J183217−322346, fit with the tabulated NSA model, including interstellar absorption, using $N_{H,22}$=0.266. The spectral fit is statistically acceptable since χ^2_ν/dof (prob.) = 1.4/5 (0.22).

A 2MASS star is tentatively associated with 2MASS J18321804−3223488 (93.4% confidence). The star's magnitude $m_J = 11.844(23)$ implies that $F_{\rm X}/F_J = 0.01$. The statistical confidence in the association between the X-ray source and the IR counterpart is not large enough for any firm conclusion to be drawn from the X-ray to J-band flux ratio.

We conclude, with evidence solely supported by spectral consistency with an H-atmosphere model, that the X-ray source XMMU J183217−322346 is a candidate qLMXB at the distance of NGC 6637.

4.5 NGC 6681 – M70

The GC NGC 6681 is observed with 9.0 ks of integration time. Background flaring reduces the usable time intervals to 6.5 ks. The Galactic absorption used for the spectral fits is $N_{H,22} = 0.08$. The high-background level increases the limiting detectable flux to $\sim 10^{-14}\,\mathrm{erg\ cm^{-2}\ s^{-1}}$ and therefore prevents the detection of faint sources, which are immersed in the background. Only four sources are detected in this observation, one of them being spectrally consistent with a qLMXB. However, the associated 2MASS counterpart has a proper motion inconsistent with that of a cluster member, excluding the classification of the X-ray source as a qLMXB at the distance of NGC 6681 (Fig. 4–18). The analysis leading to this conclusion is detailed in the following section.

4.5.1 XMMU J184311−321409

Using the tabulated NS atmosphere model (see Fig. 4–19), one finds that XMMU J184311−321409 is consistent with a qLMXB at the distance of 9.0 kpc, with a statistically acceptable fit: χ^2_ν/dof (prob.) $= 0.71/25$ (0.85). The best-fit

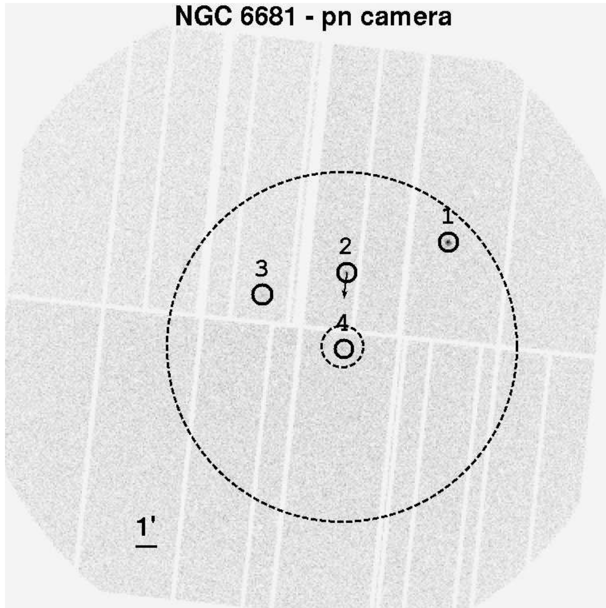

Figure 4–18: This EPIC/pn image of NGC 6681 shows the four sources detected in the pn camera data. The small and large dashed circles respectively represent the half-mass and tidal radius. In this figure, north is up and R.A. increases to the left. The vector for source #2 shows the proper motion direction of the counterpart 2MASS J18431156−3214096; the magnitude corresponding to the displacement in the sky over 10000 years. Source #2 is spectrally characterized as a qLMXB in this cluster, but this classification is excluded by the dynamical analysis of the counterpart 2MASS J18431156−3214096, since $v_\star = 316 \pm 80\,\mathrm{km\,s^{-1}}$ at $d = 9.0\,\mathrm{kpc}$ (see § 4.5.1).

temperature $kT_{\rm eff} = 139^{+51}_{-38}\,\mathrm{eV}$ and the best-fit radius $R_\infty = 7.5^{+11}_{-3.8}\,\mathrm{km}$ are in the expected range for qLMXBs. The source unabsorbed luminosity is also in the range of values typical for qLMXBs: $F_{\rm X} = 0.74{\times}10^{-13}\,\mathrm{erg\ cm^{-2}\ s^{-1}}$, so $L_{\rm X} = 0.71{\times}10^{33}\,\mathrm{erg\ s^{-1}}$. The spectral fit can be confirmed with the `nsatmos` model, with which the fit is statistically acceptable (χ^2_ν/dof (prob.) $= 0.74/25$ (0.82)), with $R_\infty = 10.9^{+12.3}_{-10.9}\,\mathrm{km}$ and $kT_{\rm eff} = 146^{+57}_{-64}\,\mathrm{eV}$. For completeness, the spectrum of XMMU J184311−321409 is fit with an absorbed power law:

$\alpha = 2.5^{+0.5}_{-0.4}$, χ^2_ν/dof (prob.) $= 0.94/25$ (0.54). The best-fit photon index is on the low end of what is typically measured for thermal sources.

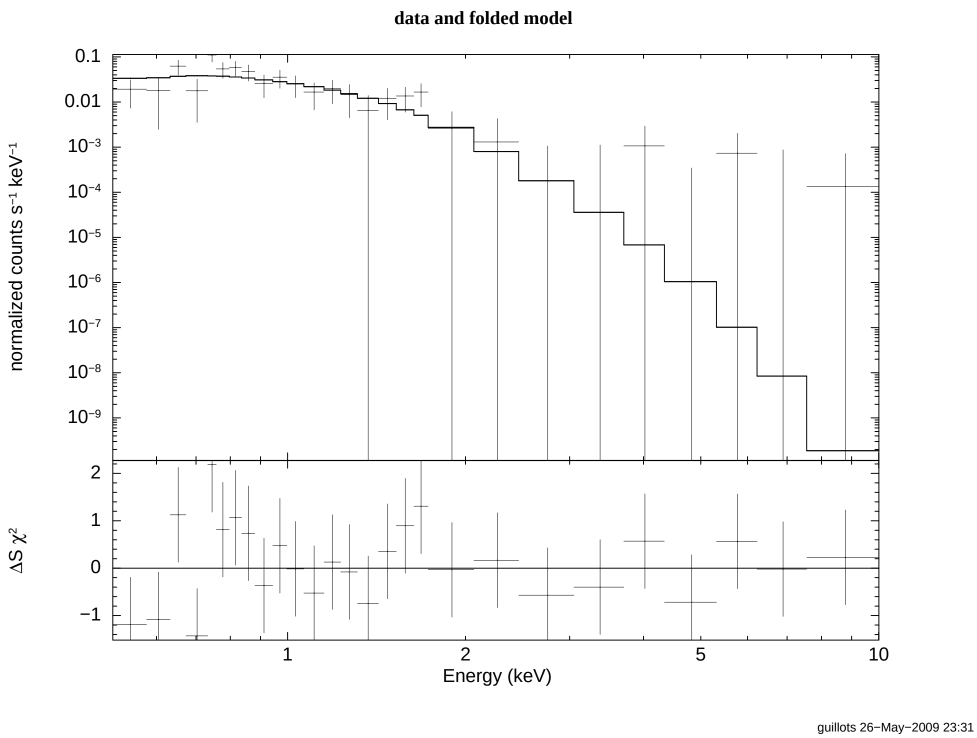

Figure 4–19: This spectrum is that of XMMU J184311−321409. The tabulated NSA model together with the `wabs` absorption model (using $N_{H,22}$=0.266) has been use to obtain the statistically acceptable spectral fit: χ^2_ν/dof (prob.) = 0.71/25 (0.85).

The associated counterpart 2MASS J18431156−3214096 ($>$ 99.99%, at a distance of $0.75''$ from the X-ray source) is a bright star: $m_J = 7.992(11)$, $m_H = 7.463(21)$ and $m_K = 7.303(23)$. In fact, it is the brightest 2MASS point source within $7'$. The star's magnitude sets the X-ray to J-band flux ratio to $F_X/F_J = 0.0002$. Such a value does not exclude the source being a coronally active star. The proper motion measurements of the associated counterpart challenges the classification of the object as a qLMXB in the GC. Indeed, the Tycho-2 star (TYC 7411-00025) corresponding to the 2MASS counterpart has a proper motion consistent with a non-zero value (3.9σ): $0.9\pm1.7\,\mathrm{mas\,yr^{-1}}$ in R.A. and $-7.4\pm1.9\,\mathrm{mas\,yr^{-1}}$ in Dec. (Høg et al. 2000). The velocity of this star at the distance of NGC 6681 is $v_{\star} = 316 \pm 80\,\mathrm{km\,s^{-1}}$. The star velocity is in excess of the escape velocity by 3.45σ, with $v_{\rm esc} = 39.3\,\mathrm{km\,s^{-1}}$ (Gnedin et al. 2002). The direction, toward the GC core within $\sim 2°$, excludes any possibility of cluster membership.

It can be concluded that, despite the spectral characterization consistent with a qLMXB, the X-ray source is not a qLMXB based on the dynamical analysis of its associated counterpart.

4.6 NGC 7089 – M2

NGC 7089 is a GC located at a distance of 11.5 kpc, with an hydrogen column density in its direction of $N_{H,22} = 0.043$. While the proposed duration of the observation was 19.9 ks, the provided length was only 10.2 ks, with 9.7 ks usable due to a background flare at the beginning of the observation. Out of the 44 X-ray sources detected (Fig. 4–20), six have more than 80 counts, allowing each spectrum to have five spectral bins, with $\sim 15-20$ counts per bin. This is the minimum number of counts per bin to have an approximate gaussian distribution of counts in each bin.

None of the X-ray sources with large enough count statistics was consistent with a qLMXB at the distance of 11.5 kpc.

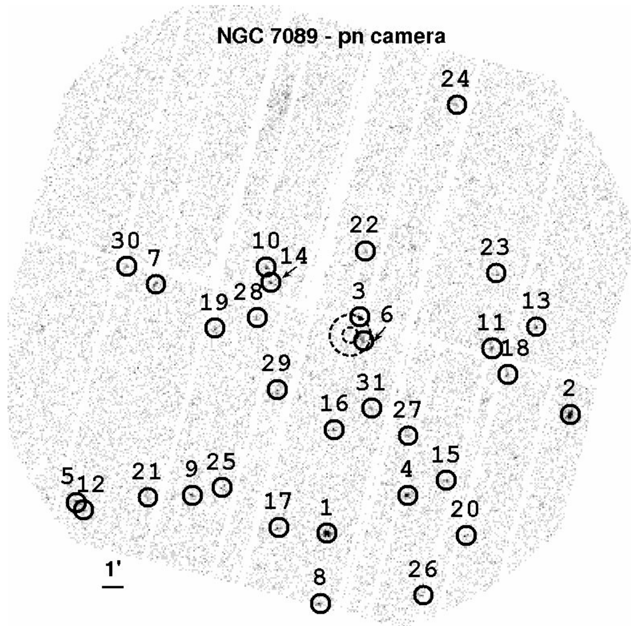

Figure 4–20: This EPIC/pn image of NGC 7089 shows the 44 sources detected on the pn camera. The small and large dashed circles respectively represent the core and half-mass radii, the tidal radius being larger that the FOV. In this figure, north is up and R.A. increases to the left. No candidate qLMXB is found in the FOV of this observation.

This chapter presented all the analyses performed during the course of this thesis work, which led to the spectral identification of seven candidate qLMXBs which best-fit parameters are listed in Table 4–2. The following chapter contains discussions of these results.

Table 4–2: Parameters of the spectrally identified candidate quiescent low-mass X-ray binaries.

Name	Host GC	R_∞ (km)	$kT_{\rm eff}$ (eV)	d (kpc)	$N_{H,22}$ (10^{22} cm^{-2})	$F_{\rm X}$	Section	Reason
CXOU J171432.93−292748.0 [a]	NGC 6304	$7.9^{+6.4}_{-2.2}$	123^{+23}_{-25}	(6.0)	(0.266)	$1.14^{+0.24}_{-0.21}$	4.1.1	
CXOU J171420.88−292916.1 [b]	NGC 6304	23^{+69}_{-10}	70^{+28}_{-20}	(6.0)	(0.266)	$0.32^{+0.13}_{-0.11}$	4.1.2	
XMMU J171411−293159	NGC 6304	$10.7^{+6.3}_{-3.1}$	115^{+21}_{-16}	(6.0)	(0.266)	1.52	4.1.3	
XMMU J180916−255426 [c]	NGC 6553	$6.4^{+5.7}_{-1.4}$	127^{+7}_{-45}	(6.0)	(0.35)	0.65	4.3.1	
XMMU J180839−260119	NGC 6553	$13.2^{+15}_{-6.6}$	98^{+26}_{-20}	(6.0)	(0.35)	1.0	4.3.2	
XMMU J180939−254724	NGC 6553	9.0 †	88^{+80}_{-42}	(6.0)	(0.35)	0.3	4.3.3	
XMMU J183217−322346	NGC 6637	$17.4^{+28}_{-6.8}$	99^{+37}_{-25}	(9.1)	(0.11)	0.84	4.4.1	
XMMU J184311−321409	NGC 6681	$7.5^{+11}_{-3.8}$	139^{+51}_{-38}	(9.0)	(0.08)	0.74	4.5.1	Dynamical

NOTES: This table lists the X-ray sources that were spectrally characterized as candidate qLMXBs. The column "Reason" gives information about the type of analysis performed, other than X-ray spectral fitting, used to exclude a qLMXB classification. "Section" indicates where the analysis can be found in this thesis. For all source parameters, a mass $M_{\rm NS}$=1.4 $M_\odot$ was assumed and all errors are 90% confidence. [a]The values reported for this source (also XMMU J171433−292747) correspond to the simultaneous EPIC + ACIS data fit and the flux is that of the NSA component (see § 4.1.1). [b] The given values are those of the MOS1 + MOS2 + pn data fit (also source XMMU J171421−292917, see § 4.1.2). [c] The flux for this source is that of the NSA component only (see § 4.3.1). † The error estimate for this fit failed due to a low S/N.

CHAPTER 5
Discussions

The following sections discuss the results of the data analysis. First, the number of detected candidate qLMXBs is compared to the expected population in each cluster. Then, a section covers a comparison between the *XMM-Newton* observation of NGC 6304 and a *ROSAT* observation. A discussion regarding the power-law component of qLMXB spectra is developed in the third section. Finally, the locations of the candidate qLMXBs in their host GCs are inspected.

5.1 Comparison with the Expected Number of Quiescent Neutron Stars in Each Globular Cluster

As mentioned in § 3.1.1, the expected number of quiescent NS binaries is linked to the physical properties of the cluster, via the encounter rate. This has been parameterized as a linear relation between the number of quiescent NSs and the encounter rate: $N_{\mathrm{qNS}} \sim 0.04 \times \Gamma + 0.2$ (Gendre et al. 2003a). The authors are using an arbitrary normalization for Γ: $\Gamma_{\mathrm{NGC\ 6440}} = 100$. From this relation and with the same normalization, the encounter rate of each GC can be calculated to estimate the predicted number of quiescent NS binaries. Alternatively, one can use a second empirical estimate which considers the encounter rate of GCs normalized to the Galactic value. This method leads to a different relationship between N_{qNS} and Γ: $N_{\mathrm{qNS}} = 0.993 \times \Gamma - 0.046$ (Heinke et al. 2003c).

For each of the analyzed GC, the probability of finding the number of identified candidate qLMXBs or more, when the average expected number is obtained from the above relations, can be calculated using Poisson statistics. Table 5–1 shows the results of this comparison using the two relations cited in the previous paragraph. Both provide similar results and in all cases the predicted and actual numbers are in agreement (in marginal agreement in the worst case), as demonstrated by the Poisson probability calculations.

Table 5–1: The comparison between the number of candidate quiescent low-mass X-ray binaries identified and the predicted numbers.

Name	$N_{\rm qLMXB}$ Candidates	$N_{\rm qLMXB}$ Predicted †	Proba. (%)	$N_{\rm qLMXB}$ Predicted ††	Proba. (%)
NGC 6304	3	0.46	3.2	0.38	1.8
NGC 6540	0	0.57	100	0.56	100
NGC 6553	3	0.43	2.7	0.34	1.3
NGC 6637	1	0.38	38	0.25	25
NGC 6681	0	0.58	100	0.57	100
NGC 7089	0	0.64	100	0.66	100

NOTES: This table shows the comparison between the number of candidate qLMXBs identified and the predicted population from empirical relations († Gendre et al. 2003a, †† Heinke et al. 2003c). To obtain the predicted numbers, we calculated the encounter rates of the six GC using the two different normalizations used by the two groups of authors. The columns "Proba." indicate the Poisson probability of finding the number of identified candidates or more when the average is given in the "Predicted" columns. The total predicted number of qLMXBs among the six GCs is 3.06 and 2.76, using the two relations, respectively. In all cases, the number of candidate qLMXBs agrees with the predictions.

For NGC 6304, in both cases, the probabilities of finding 3 candidate qLMXBs where 0.46 (0.38) on average are expected (3.2% and 1.8% respectively) is marginally consistent with the predicted numbers. Similarly for NGC 6553, the probabilities (2.7% and 1.3%) suggest only marginal consistency between the predictions and the actual number of identifications. The other GCs, NGC 6540, NGC 6637, NGC 6681 and NGC 7089, have a number of identified candidate qLMXBs consistent with the two predictions.

The sum of the predicted number of qLMXBs among the six GCs is 3.06 and 2.76, using the two relations. The Poisson probability of finding seven qLMXBs or more when 3.06 (2.76) is expected on average, is 49.8% (24.2%). In conclusion, the number of identified candidates is in agreement with the expected numbers.

5.2 Comparison with a *ROSAT* Observation of NGC 6304

NGC 6304 was observed once previously, using *ROSAT*/HRI (Rappaport et al. 1994, R94 hereafter), in which four X-ray sources were discovered. In this section, they are referred to as "the *ROSAT* sources" or the "sources A, B, C and D". Three are spatially coincident with three X-ray sources detected in the presented *XMM-Newton* observation of NGC 6304 (in fact, the three sources correspond to the three candidate qLMXBs in this GC). A fourth *ROSAT* X-ray source, however, appears to have faded significantly; the analyzed *XMM-Newton* observation detects no X-ray source consistent in position with *ROSAT* source D. The following analysis compares the position and fluxes of the four *ROSAT*/HRI sources.

The positions of the sources in R94 have been examined and compared to those of X-ray sources in the present thesis work. No positional uncertainties are given from the *ROSAT* analysis. Using the archived *ROSAT*/HRI data at *HEASARC*, the positional uncertainties required for the comparison with the present *XMM-Newton* data were obtained. The source positions are consistent

Table 5–2: Source comparison between *ROSAT* and *XMM-Newton* observations of NGC 6304

XMM-Newton/pn (11 ks)			*ROSAT* (5.0 ks)		
ID	$kT_{\mathrm{eff,BB}}$ [a]	ECF [b] $\times 10^{-2}$	$\mathrm{ID}_{\mathrm{R94}}$	Counts predicted [c]	Counts Observed [d]
XMMU J171433−292747	260±30	9.35±0.15	A	20.7±1.5	15
XMMU J171421−292917	170±30	8.55±0.65	B	3.9±0.9	7
XMMU J171411−293159	200±30	9.0±0.2	C	11.4±1.0	17
-	–	6.2	D	<1.8	14

NOTES: This table shows a comparison in the luminosities (counts) between the *ROSAT* and *XMM-Newton* observations. For source D, due to the non detection, a 3σ upper limit is calculated.

[a] The $kT_{\mathrm{eff,BB}}$ is the blackbody effective temperature, obtained from fits to the present *XMM* spectra.

[b] The energy-conversion-factor (ECF) is the number of *ROSAT*/HRI counts per *XMM* count for each source, which depends on $kT_{\mathrm{eff,BB}}$ and N_H (assumed to be $N_{H,22}$=0.266). For source D, undetected in the *XMM* observation, an absorbed thermal bremsstrahlung spectrum with $kT = 3\,\mathrm{keV}$ is assumed.

[c] The total counts predicted for the *ROSAT* observation based on the present *XMM* observation, using the source spectrum measured here, the predicted HRI countrate from WebPIMMS, and the *ROSAT* observation duration of 5030 sec.

[d] The total number of source counts from *ROSAT*/HRI observation, corrected for observation at the HRI centre (that is, after subtracting background counts, correcting for vignetting, quantum efficiency and scattering). The uncertainty in this number is not given by R94.

between the two different observations: source A, B and C corresponding to XMMU J171433−292747, XMMU J171421−292917 and XMMU J171411−293159 in this work. The boresight systematic uncertainty ($6''$) has been taken into account. No corresponding source is detected on *XMM-Newton*/pn within $1'$ of the given position of source D. On the pn camera, a total of 304 counts are found in a $25''$ area around the given position, while an average of 294.8±2.2 are due to background using a nearby off-source area. This leaves 9±18 counts due to a possible X-ray source at this position, consistent with no source detection.

There is a 3σ upper limit on the flux from source D of $F_{\rm X} \leq 2.4\times10^{-14}\,\rm erg\ cm^{-2}\ s^{-1}$ (0.5–2.4 keV), assuming a thermal bremsstrahlung spectrum with a temperature $kT = 3\,\rm keV$ as in R94. By inspection of the MOS2 data, there is no evidence of any X-ray source in the vicinity of the position of source D.

Table 5–2 compares the predicted number of source counts which should be detected with *ROSAT*/HRI during the 5030 sec observation, assuming the observed *XMM*/pn-med countrates and the *XMM*/pn source spectra, including both countrate and spectral uncertainties. For the three candidate qLMXBs (XMMU J171433−292747, XMMU J171421−292917 and XMMU J171411−293159), the expected number of counts (20.7±1.5, 3.9±0.9, 11.4±1.0, respectively) are consistent, within Poisson uncertainties, with the number of source counts observed by R94 (15, 7, and 17 respectively).

For source D, which is not detected on *XMM-Newton*, the 3σ upper limit on the number of counts due to an X-ray source at this position (<63 counts, in 11037 sec of integration), implies that <1.8 counts should have been detected with *ROSAT*/HRI, whereas the observed number of counts with *ROSAT*/HRI corresponds to 14 counts at the HRI field centre[1] . In an absence of an error analysis on the number of detected source counts on *ROSAT*, it is not possible to correctly estimate the amount of fading; however, taking the detected number of counts at face value implies that source D faded in luminosity by a factor of ∼10.

In conclusion, the three candidate qLMXBs are consistent with having the same luminosity between the *ROSAT*/HRI observation and the *XMM*/pn observation; and source D appears to have faded by a factor of ∼10.

5.3 The Power-Law Component of Quiescent Low-Mass X-ray Binaries

Two candidate qLMXBs identified in this thesis work (XMMU J171433−292747 in NGC 6304 and XMMU J180916−255426 in NGC 6553) exhibited a strong high-energy excess of counts above the X-ray thermal component on their *XMM-Newton* spectra. These excesses were best fitted with power-law components which were statistically required via F-test probabilities (0.014 and 0.01, respectively). The photon indices were of the order $\alpha \sim 1 - 2$ in both cases, and the flux contribution of the power-law component to the total flux accounted for $\sim 50\%$ in both cases. As mentioned in § 2.3.1, some field qLMXBs have been observed with power-law tail, the physical origin of which is still uncertain. The proposed interpretations are the residual of a recent accretion episode (Grindlay et al. 2001a), the shock

[1] The number of counts given by R94 are corrected for scattering and vignetting by a factor >1, but which is not given by R94. Therefore the number given is that of counts which would have been detected from this source if it had been located at the centre of the FOV

emissions via the emergence of a magnetic field (Campana and Stella 2000), or the intrabinary shock between the winds from the NS and its companion star (Campana et al. 2004a; Bogdanov et al. 2005). The spectra of the field qLMXBs Cen X-4 (Rutledge et al. 2001a) and Aql X-1 (Rutledge et al. 2001b) both revealed power-law components of index $\alpha = 1.0^{+0.6}_{-0.4}$ and $\alpha = 1$ (fixed) which account for 41% and 15% of the total X-ray fluxes (0.5–10 keV), respectively. The power-law fraction has been compared in previous work to the luminosity of sources that are thought to be quiescent NS soft X-ray transient in the field of the Galaxy (Jonker et al. 2004). None of the known qLMXBs in GCs shows such a hard power-law component except for the possible qLMXB in NGC 3201 (Webb et al. 2006). The photon-index for source #16 in NGC 3201 is $\alpha = 1.04^{+0.63}_{-0.63}$ (see Table 2–1). However, this classification requires confirmation with higher S/N spectra.

XMMU J171433$-$292747 was initially characterized as a qLMXB at the distance of NGC 6304, but with an *XMM-Newton* spectrum containing a strong power-law component. However, high-resolution observations with *Chandra* revealed that the power-law component was actually a separate source with $\alpha = 0.8^{+0.7}_{-0.7}$ at a distance of 13″ from the thermal source. The fluxes were also shown to be consistent between the *XMM-Newton* and *Chandra* observations.

For XMMU J180916$-$255426, a *Chandra* observation of NGC 6553 taken on October 30, 2008 but which has not yet been published, may confirm that the power-law component of the X-ray spectra comes from the emission of another close-by unresolved source. If high-resolution observations do not reveal multiple sources in the core of NGC 6553, the high-energy tail of XMMU J180916−255426 would be the first among the population of GC qLMXBs.

5.4 The Location of Quiescent Low-Mass X-ray Binaries in Their Host Globular Clusters

Prior to this thesis work, all qLMXBs known in GCs were located near the core of their host GC. As can be seen on Table 5–3, most known qLMXBs are within $\sim 2\,r_c$ of the GC core centre, except for U24 (at $d_c = 6.8\,r_c$) in NGC 6397 which is a core-collapse cluster with $r_c = 0.05'$, and for the candidate qLMXB source #16 in NGC 3201 (at $d_c = 4.1\,r_c$ with $r_c = 1.43'$), but this classification needs to be confirmed.

Table 5–3: The distances of quiescent low-mass X-ray binaries from their host globular cluster cores

Name	d_c ($'$)	r_c ($'$)	d_c/r_c	References
ωCen	4.38	2.58	1.7	Rutledge et al. 2002b
M13	0.74	0.78	0.95	Gendre et al. 2003a
47 Tuc X7	< 0.37	0.38	< 1.5	Heinke et al. 2003b
47 Tuc X5	< 0.37	0.38	< 1.5	Heinke et al. 2003b
M 28 (#26)	0.05	0.24	0.21	Becker et al. 2003
M 30 A-1	0.03	0.06	0.5	Lugger et al. 2007
NGC 6397 (U24) ^{cc}	0.34	0.05	6.8	Grindlay et al. 2001b
M80 CX2	0.063	0.15	0.42	Heinke et al. 2003a
M80 CX6	0.324	0.15	2.2	Heinke et al. 2003a
NGC 2808 C2	0.08	0.26	0.31	Servillat et al. 2008
NGC 3201 16	5.8	1.43	4.1	Webb et al. 2006

NOTES: This table is a compilation of the positional information of known qLMXBs and candidate qLMXBs in GCs. The columns, from left to right, are the object name (or the GC hosting the qLMXB), the distance of the qLMXB from the optical centre of the GC (in arcminutes), the core radius of the GC (in arcminutes, Harris 1996) and the distance of the qLMXB from the optical centre of the GC in units of core radii. ^{cc} denotes a core-collapse cluster.

Table 5–4: The distances of candidate quiescent low-mass X-ray binaries discovered in this thesis work, from their host globular cluster cores

Name	Host GC	d_c ($'$)	r_c ($'$)	d_c/r_c	Section
CXOU J171432.93−292748.0	NGC 6304	0.20	0.21	0.96	4.1.1
CXOU J171420.88−292916.1	NGC 6304	3.2	0.21	15.2	4.1.2
XMMU J171411−293159	NGC 6304	6.7	0.21	31.8	4.1.3
XMMU J180916−255426	NGC 6553	0.26	0.55	0.47	4.3.1
XMMU J180839−260119	NGC 6553	10.9	0.55	19.9	4.3.2
XMMU J180939−254724	NGC 6553	8.63	0.55	15.7	4.3.3
XMMU J183217−322346	NGC 6637	11.9	0.34	35.0	4.4.1

NOTES: This table is similar to Table 5–3, for the candidate qLMXBs discovered in this thesis work. The column "Section" indicates where the analysis can be found in this thesis. cluster. CXOU J171432.93−292748.0 corresponds to XMMU J171433−292747 (see details in § 4.1.1) and CXOU J171420.88−292916.1 is XMMU J171421−292917 (see § 4.1.2). Five candidate qLMXBs are a large distances ($d_C > 15 r_c$) from the GC cores.

In the six clusters observed and analyzed in this thesis work, five of out the seven candidates are located away from the host core, at $d_c = 15\, r_c$. Two of them, XMMU J180839−260119 in NGC 6553 and XMMU J183217−322346 in NGC 6637) are even outside the tidal radius of the cluster, at distances $d_c = 1.27\, r_t$ and $d_c = 1.43\, r_t$, respectively.

The general postulate for binary systems, either primordials or formed via interaction, argues that they should be found in the densest part of the cluster due to mass segregation (Meylan and Heggie 1997). The presence of those qLMXBs far outside the core radii and even beyond the tidal radius of their respective GC would challenge, if their classification is confirmed, the current theory of qLMXB formation and would require revisiting the theory of binary evolution in GCs.

For example, the two candidates mentioned above, XMMU J180839−260119 and XMMU J183217−322346, could lie on the outskirts of the GC due to some mechanism like binary interactions leading to their ejection from the GC, as was observed for the binary MSP in the NGC 6752 (Bassa et al. 2003). On the other hand, if the candidate qLMXBs are not confirmed, then a more stringent criteria will be required before accepting future X-ray sources as qLMXBs.

CHAPTER 6
Conclusions

The data analysis of the X-ray observations of the six GCs permitted the spectral identification of seven candidate qLMXBs. This number is consistent with the total predicted number of qLMXBs in those six GCs, as indicated by the 49.8% (24.2%) Poisson probability of finding seven candidates or more where a total of 3.06 (2.76) are expected on average, based on previous work (Gendre et al. 2003a and Heinke et al. 2003c, respectively).

The classification was performed on the basis of their X-ray spectra being consistent with NS H-atmosphere models at the distance of their host GCs. The spectral parameters of the identified qLMXBs are shown in Table 4–2, including the best-fit radii and best-fit temperatures. When possible, IR counterparts were tentatively associated with the X-ray sources using the 2MASS Point Source Catalogue.

6.1 NGC 6304

It was found in this thesis work that the GC NGC 6304 hosts three candidate qLMXBs. The NS radii and temperatures obtained for the three candidates were consistent with typical values for quiescent NS binaries and in accordance with the radii of other known field and GCs qLMXBs. No variability was measured from any of the candidates over the timescale of the observation, with weak limits; the large X-ray variability in the *XMM-Newton*/pn background precludes a detailed variability analysis. A comparison with *ROSAT* observations 14 yr prior, found that the fluxes of the candidates were consistent with those of the earlier observation (R94), as would be expected from qLMXBs in this observational context.

CXOU J171432.93−292748.0 is located in the core ($0.79\,r_c$) of the GC. Its spectrum was acceptably fitted with a NS H-atmosphere model with $kT_{\rm eff} = 132^{+23}_{-25}\,{\rm eV}$ and $R_\infty = 7.9^{+6.4}_{-2.2}\,{\rm km}$. The power-law component initially accounted for in the spectrum of XMMU J171433−292747 was shown to be attributed to a separate X-ray source, resolved with the *Chandra X-ray Observatory.* This close-by source, CXOU J171431.86−292745.5, was tentatively classified as a CV based on its photon index, but a deeper exposure will be required to attempt a more precise spectral fitting, using a thermal bremsstrahlung model for example, and confirm this classification.

CXOU J171420.88−292916.1 (XMMU J171421−292917), a second candidate, has a low S/N and correspondingly larger uncertainties for the X-ray spectral parameters used to identify it as a qLMXB candidate: the NS H-atmosphere temperature is $kT_{\rm eff} = 70^{+28}_{-20}\,{\rm eV}$, and $R_\infty = 23^{+69}_{-10}\,{\rm km}$. The best-fit parameters obtained from the *Chandra* observations were consistent with those values. The flux comparison between the *XMM-Newton* and the previous *ROSAT*/HRI observations did not demonstrate any evidence of long term variability, with weak constraints. The unabsorbed flux during the more recent *Chandra* observation, however, was a factor $0.54^{+0.30}_{-0.24}$ (90% confidence) lower than the flux measured during the *XMM-Newton* observation. This is significantly lower than the previously observed flux, and calls into question the classification of this X-ray source as an H-atmosphere qLMXB, since such strong variability is not expected on ∼years timescales, unless a protracted (∼years) long outburst (e.g. $L_{\rm X} \gtrsim 10^{37}\,{\rm erg\ s^{-1}}$) ended recently ($\lesssim 1\,{\rm yr}$) (Rutledge et al. 2002b; Brown and Cumming 2009); there is no evidence supporting this scenario in the present case. A faint 2MASS counterpart ($m_J = 13.063$) is identified (with 99.916% confidence), and it was shown that the X-ray emission is unlikely to emerge from the giant star itself.

Finally, XMMU J171411−293159, a third candidate in NGC 6304, is a bright X-ray source consistent with a NS H-atmosphere spectral model at the distance of the GC. Its measured properties are $kT_{\rm eff} = 115^{+21}_{-16}\,{\rm eV}$ and $R_\infty = 10.7^{+6.3}_{-3.1}\,{\rm km}$. The 2MASS IR counterpart (with 99.988% confidence) appears to belong to the post-asymptotic giant branch; this is the first qLMXB with this type of companion. Other explanations for the source were investigated, concluding that a coronally active field star is not a possible explanation, due to the unusual optical/IR colours and unusual X-ray spectrum. Optical/IR spectroscopy of 2MASS J17141152−2931594 can definitively determine whether the star is a foreground main sequence star, or an evolved post-AGB star at the distance of NGC 6304.

6.2 NGC 6540

The programmed observation of this GC with *XMM-Newton* revealed the presence of a candidate qLMXB. Its spectrum was consistent with a qLMXB at the distance of NGC 6540, and the best-fit parameters were comparable to other known GC qLMXBs. The X-ray source was associated, at 99.19% confidence, with a bright star of magnitude $m_J = 10.629$. However, the star non-zero proper motion was shown to be consistent with a spatial velocity greater that the escape velocity of the GC, therefore refuting the classification.

The X-ray source was present on a longer *XMM-Newton* observation (70 ks of "good time intervals") of a nearby microlensing event, allowing us to obtain the spectrum of the candidate qLMXB with higher S/N. The spectrum was not consistent with the expected thermal spectrum of a qLMXB. This provided further support that XMMU J180530−274212 is not a qLMXB.

6.3 NGC 6553

Three candidates were detected in the FOV of this observation. No variability was measured over the timescale of the observation, with weak constraints.

The candidate qLMXB XMMU J180916−255426, in the core of NGC 6553 was identified with a spectrum that was acceptably fitted with a NS H-atmosphere model with $kT_{\rm eff} = 127^{+7}_{-45}\,$eV and $R_\infty = 6.4^{+5.7}_{-1.4}\,$km, combined with a power-law component of photon index $\alpha = 2.0^{+0.9}_{-1.3}$. The power-law component dominates the spectrum at photon energies above $\sim 2\,$keV, and represents 53% of the observed flux. This contribution, although its source is not perfectly understood, is similar to that found in the spectra of some other qLMXBs in the field of the Galaxy, and is comparable to the power-law contribution to the flux of the qLMXB Cen X-4 (Asai et al. 1996; Rutledge et al. 2001a; Menou and McClintock 2001; Campana et al. 2004b). Another possibility is that of unresolved X-ray sources in the core of the GC. Similarly to what was observed for XMMU J171433−292747 (see § 6.1), a hard source could be close enough to the thermal source that their spectra are merged into a single one, as viewed by *XMM-Newton*. Only a high-resolution observations like those obtained with *Chandra* could differentiate multiple sources.

The two other candidates, XMMU J180839−260119 and XMMU J180939−254724, in this GC are located at distances from the GC core that are not explained by the theory of binary evolution in GCs. They are spectrally consistent with qLMXBs at the distance of NGC 6553: $kT_{\mathrm{eff}} = 98^{+26}_{-20}\,\mathrm{eV}$ and $R_\infty = 13.2^{+15}_{-6.6}\,\mathrm{km}$ for XMMU J180839−260119, $kT_{\mathrm{eff}} = 88^{+80}_{-42}\,\mathrm{eV}$ and $R_\infty = 9\,\mathrm{km}$ (no error bars) for XMMU J180939−254724. However, their locations, at a distance of more than $15\,r_c$ from the cluster core, calls into question their classification. One of them is even located outside the tidal radius, suggesting a possible ejection from the cluster, if the qLMXB classification is confirmed.

The possible association (99.97% confidence) of the candidate XMMU J180839−260119 with a bright star results in an X-ray to J-band flux ratio that is consistent with a coronally active star. However, this does not exclude the qLMXB classification which could be explained by the association with an unexpectedly bright companion star, as postulated for XMMU J171411−293159 and its post-AGB companion.

6.4 NGC 6637

The only candidate found in the observation of this cluster was not a strong candidate, but it was nevertheless identified on the basis of its X-ray spectrum. Even if the X-ray spectral fits indicates consistency with a qLMXB at the distance of NGC 6637 ($kT_{\mathrm{eff}} = 99^{+37}_{-25}\,\mathrm{eV}$ and $R_\infty = 17.4^{+28}_{-6.8}\,\mathrm{km}$), the localization of the source outside the tidal radius of the cluster is difficult to explain from the current theory of binary evolution in GCs. The 81%-confidence association with a possible counterpart 2MASS J18321804−3223488 did not permit one to provide further support or contradiction to the qLMXB classification.

6.5 NGC 6681

In this cluster, an X-ray source was found within the tidal radius and had best-fit parameters and a spectrum in statistical agreement with typical qLMXB values. Its effective temperature is $kT_{\rm eff} = 146^{+57}_{-64}\,$eV and its projected radius is $R_\infty = 10.9^{+12.3}_{-10.9}\,$km, with an H-atmosphere model. However, the classification as a qLMXB was excluded based on the proper motion of an associated bright counterpart 2MASS J18431156−3214096 (with $> 99.99\%$ confidence). The non-zero proper motion of the counterpart resulted in a spatial velocity larger than the escape velocity of the cluster, implying that the star could not be a cluster member. Therefore, this demonstrated a misinterpretation of the X-ray spectrum.

6.6 NGC 7089

No candidate qLMXBs were found following the analysis of the X-ray sources in this cluster. Specifically, none showed spectral consistency with NS H-atmosphere models at the distance of NGC 7089.

6.7 Thesis Work Conclusion

As a more general conclusion, we found seven candidate qLMXBs where we expected 3.06 (Gendre et al. 2003a) or 2.76 (Heinke et al. 2003c). Two X-ray sources, XMMU J180530−274212 in NGC 6540 and XMMU J184311−321409 in NGC 6681, were initially identified as candidate qLMXBs based on their short exposure *XMM-Newton* spectra, but the proper motion of their identified IR counterpart showed inconsistency with cluster membership. This excluded possible classifications as candidate qLMXBs at the distance of the GCs. In addition, XMMU J184311−321409 was in the FOV of a long *XMM-Newton* observations, allowing for high S/N spectral fitting, which demonstrated that the source was not consistent with a qLMXB.

The discovery of candidates outside the tidal radius of the clusters is also problematic since it is not explained by the current theory of binary evolution in GCs which imposes that binary systems sink toward the GC cores due to mass segregation. Their classification can be confirmed or contradicted with deeper X-ray exposures. Also possible is the confirmation of the binary nature of the systems using either ellipsoidal variations via optical photometry, or radial velocity measurements via periodic Doppler shift measurements. In fact, we are in the process of analyzing photometric data from the SMARTS telescope of XMMU J171421−292917 and XMMU J171411−293159 in NGC 6304 to detect possible brightness variations that would confirm the binary nature of the system. In addition, we are also performing the analysis of spectroscopic data of XMMU J171411−293159 from the Gemini South telescope to obtain a possible radial velocity curve, that could also demonstrate that the star is in a binary system.

It was also noticed during the course of this thesis work that the moderate S/N obtained with the short *XMM-Newton* observations performed could lead to erroneous identifications of X-ray sources. More specifically, the spectrum of XMMU J180530−274212 was initially interpreted as that of a qLMXB but the spectrum obtained with a deeper exposure demonstrated its inconsistency with a NS H-atmosphere model.

Finally, a series of tests were performed to accumulate supporting or refuting evidences required to identify qLMXBs:

1. The spectral analysis demonstrating consistency with H-atmosphere models is the required test to characterize the X-ray sources.
2. The association with an optical/IR counterpart, like a star from the 2MASS catalogue unveil several analyses.
3. The calculation of X-ray to optical/IR flux ratios to compare with that of X-ray active stars, can exclude such a classification and provide further support to the qLMXB identification.
4. The demonstration that the X-ray spectrum is inconsistent with that of coronally active stars can be performed using the ratio of emission measures of a 2-temperature plasma model.
5. The search for the proper motion of the stellar companion in the TYCHO-2 catalogue permits the calculation of the spatial velocity, and therefore can exclude a possible cluster membership. That would absolutely contradicts a qLMXB candidacy.
6. The evidence of ellipsoidal variations and periodic radial velocities of the companion star can demonstrate the binary nature of the system, arguing in favor of the qLMXB classification.
7. The IR/optical spectrum of the star can also determine the spectral class of the object. A spectrum typical of that of an active galactic nuclei would

irrefutably exclude the classification of the source as a qLMXB. Also contradictory with this classification would be a spectrum typical of a dwarf main-sequence star.

The confirmation with higher S/N data of the candidates found in this thesis work will provide a larger sample of qLMXBs suitable for dense EoS contraints. More specifically, obtaining measurements of the radii of the candidates with 5–10% precision are required to have a better understanding of the behavior of dense matter inside neutron stars. Such high precision measurements will be possible with an upcoming *Chandra* observation of the globular cluster NGC 6304 in 2010.

References

K. A. Arnaud. XSPEC: The First Ten Years. In G. H. Jacoby and J. Barnes, editors, *Astronomical Data Analysis Software and Systems V*, volume 101 of *Astronomical Society of the Pacific Conference Series*, pages 17–+, 1996.

K. Asai, T. Dotani, K. Mitsuda, R. Hoshi, B. Vaughan, Y. Tanaka, and H. Inoue. ASCA Observations of Soft X-Ray Transients in Quiescence : X1608-52 and CEN X-4. *PASJ*, 48:257–263, April 1996.

K. Asai, T. Dotani, R. Hoshi, Y. Tanaka, C. R. Robinson, and K. Terada. ASCA Observations of Transient X-Ray Sources in Quiescence. *PASJ*, 50:611–619, December 1998.

W. Baade and F. Zwicky. Remarks on Super-Novae and Cosmic Rays. *Physical Review*, 46:76–77, July 1934. doi: 10.1103/PhysRev.46.76.2.

C. G. Bassa, F. Verbunt, M. H. van Kerkwijk, and L. Homer. Optical identification of the companion to PSR J1911-5958A, the pulsar binary in the outskirts of NGC 6752. *A&A*, 409:L31–L34, October 2003. doi: 10.1051/0004-6361:20031339.

W. Becker, D. A. Swartz, G. G. Pavlov, R. F. Elsner, J. Grindlay, R. Mignani, A. F. Tennant, D. Backer, L. Pulone, V. Testa, and M. C. Weisskopf. Chandra X-Ray Observatory Observations of the Globular Cluster M28 and Its Millisecond Pulsar PSR B1821-24. *ApJ*, 594:798–811, September 2003. doi: 10.1086/376967.

L. R. Bedin, G. Piotto, J. Anderson, S. Cassisi, I. R. King, Y. Momany, and G. Carraro. ω Centauri: The Population Puzzle Goes Deeper. *ApJL*, 605: L125–L128, April 2004. doi: 10.1086/420847.

L. Bildsten, E. E. Salpeter, and I. Wasserman. The fate of accreted CNO elements in neutron star atmospheres - X-ray bursts and gamma-ray lines. *ApJ*, 384: 143–176, January 1992. doi: 10.1086/170860.

T. Bloecker. Stellar evolution of low- and intermediate-mass stars. II. Post-AGB evolution. *A&A*, 299:755–+, July 1995.

S. Bogdanov, J. E. Grindlay, and M. van den Berg. An X-Ray Variable Millisecond Pulsar in the Globular Cluster 47 Tucanae: Closing the Link to Low-Mass X-Ray Binaries. *ApJ*, 630:1029–1036, September 2005. doi: 10.1086/432249.

S. Bogdanov, J. E. Grindlay, and G. B. Rybicki. Thermal X-Rays from Millisecond Pulsars: Constraining the Fundamental Properties of Neutron Stars. *ApJ*, 689: 407–415, December 2008. doi: 10.1086/592341.

E. F. Brown and A. Cumming. Mapping crustal heating with the cooling lightcurves of quasi-persistent transients. *ArXiv e-prints*, January 2009.

E. F. Brown, L. Bildsten, and R. E. Rutledge. Crustal Heating and Quiescent Emission from Transiently Accreting Neutron Stars. *ApJL*, 504:L95+, September 1998. doi: 10.1086/311578.

E. M. Cackett, R. Wijnands, M. Linares, J. M. Miller, J. Homan, and W. H. G. Lewin. Cooling of the quasi-persistent neutron star X-ray transients KS 1731-260 and MXB 1659-29. *M.N.R.A.S.*, 372:479–488, October 2006. doi: 10.1111/j.1365-2966.2006.10895.x.

S. Campana and L. Stella. On the Bolometric Quiescent Luminosity and Luminosity Swing of Black Hole Candidate and Neutron Star Low-Mass X-Ray Transients. *ApJ*, 541:849–859, October 2000. doi: 10.1086/309493.

S. Campana, S. Mereghetti, L. Stella, and M. Colpi. X-ray variability in the quiescent state of Centaurus X-4. *A&A*, 324:941–942, August 1997.

S. Campana, L. Stella, S. Mereghetti, M. Colpi, M. Tavani, D. Ricci, D. D. Fiume, and T. Belloni. Aquila X-1 from Outburst to Quiescence: The Onset of the Propeller Effect and Signs of a Turned-on Rotation-powered Pulsar. *ApJL*, 499: L65+, May 1998. doi: 10.1086/311357.

S. Campana, L. Stella, S. Mereghetti, and D. Cremonesi. BeppoSAX observation of Cen X-4 in quiescence. *A&A*, 358:583–586, June 2000.

S. Campana, P. D'Avanzo, J. Casares, S. Covino, G. Israel, G. Marconi, R. Hynes, P. Charles, and L. Stella. Indirect Evidence of an Active Radio Pulsar in the Quiescent State of the Transient Millisecond Pulsar SAX J1808.4-3658. *ApJL*, 614:L49–L52, October 2004a. doi: 10.1086/425495.

S. Campana, G. L. Israel, L. Stella, F. Gastaldello, and S. Mereghetti. The Variable Quiescence of Centaurus X-4. *ApJ*, 601:474–478, January 2004b. doi: 10.1086/380194.

F. Caputo. Globular clusters. *Reports on Progress in Physics*, 48:1235–1282, September 1985. doi: 10.1088/0034-4885/48/9/001.

B. W. Carroll and D. A. Ostlie. *An Introduction to Modern Astrophysics*. 1996.

W. Cash. Parameter estimation in astronomy through application of the likelihood ratio. *ApJ*, 228:939–947, March 1979. doi: 10.1086/156922.

J. Chadwick. Possible Existence of a Neutron. *Nat.*, 129:312–+, February 1932. doi: 10.1038/129312a0.

G. W. Clark. X-ray binaries in globular clusters. *ApJL*, 199:L143–L145, August 1975. doi: 10.1086/181869.

R. Cornelisse, R. Wijnands, and J. Homan. An XMM-Newton observation of the neutron star X-ray transient 2S 1803-245 in quiescence. *M.N.R.A.S.*, 380: 1637–1641, October 2007. doi: 10.1111/j.1365-2966.2007.12207.x.

J. Cottam, F. Paerels, and M. Mendez. Gravitationally redshifted absorption lines in the X-ray burst spectra of a neutron star. *Nat.*, 420:51–54, November 2002. doi: 10.1038/nature01159.

A. P. Cowley and P. C. Schmidtke. The Strange Case of the X-Ray Binary 2129+47. *AJ*, 99:678–+, February 1990. doi: 10.1086/115363.

J. H. J. de Bruijne, R. Hoogerwerf, and P. T. de Zeeuw. A Hipparcos study of the Hyades open cluster. Improved colour-absolute magnitude and Hertzsprung-Russell diagrams. *A&A*, 367:111–147, February 2001. doi: 10.1051/0004-6361:20000410.

R. C. Dempsey, J. L. Linsky, J. H. M. M. Schmitt, and T. A. Fleming. The ROSAT All-Sky Survey of active binary coronae. II - Coronal temperatures of the RS Canum Venaticorum systems. *ApJ*, 413:333–338, August 1993. doi: 10.1086/173001.

R. Di Stefano and S. Rappaport. Predictions of a population of cataclysmic variables in globular clusters. *ApJ*, 423:274–293, March 1994. doi: 10.1086/173805.

J. M. Dickey and F. J. Lockman. H I in the Galaxy. *Ann. Rev. A&A*, 28:215–261, 1990. doi: 10.1146/annurev.aa.28.090190.001243.

P. D. Edmonds, C. O. Heinke, J. E. Grindlay, and R. L. Gilliland. Hubble Space Telescope Detection of a Quiescent Low-Mass X-Ray Binary Companion in 47 Tucanae. *ApJL*, 564:L17–L20, January 2002. doi: 10.1086/338776.

E. Ergma, S. C. Lundgren, and J. M. Cordes. A Millisecond Pulsar Progenitor to an Ultracompact Low-Mass X-Ray Binary. *ApJL*, 475:L29+, January 1997. doi: 10.1086/310448.

W. D. Evans, R. D. Belian, and J. P. Conner. Observations of the Development and Disappearance of the X-Ray Source Centaurus XR-4. *ApJL*, 159:L57+, January 1970. doi: 10.1086/180477.

E. L. Fitzpatrick. Correcting for the Effects of Interstellar Extinction. *PASP*, 111: 63–75, January 1999. doi: 10.1086/316293.

A. Fruscione, J. C. McDowell, G. E. Allen, N. S. Brickhouse, D. J. Burke, J. E. Davis, N. Durham, M. Elvis, E. C. Galle, D. E. Harris, D. P. Huenemoerder, J. C. Houck, B. Ishibashi, M. Karovska, F. Nicastro, M. S. Noble, M. A. Nowak, F. A. Primini, A. Siemiginowska, R. K. Smith, and M. Wise. CIAO: Chandra's data analysis system. In *Society of Photo-Optical Instrumentation Engineers (SPIE) Conference Series*, volume 6270 of *Society of Photo-Optical Instrumentation Engineers (SPIE) Conference Series*, July 2006. doi: 10.1117/12.671760.

G. Garmire. X-Ray Astronomy. *New York Academy Sciences Annals*, 140:172–174, December 1966. doi: 10.1111/j.1749-6632.1966.tb50957.x.

B. Gendre, D. Barret, and N. Webb. Discovery of a quiescent neutron star binary in the globular cluster M 13. *A&A*, 403:L11–L14, May 2003a. doi: 10.1051/0004-6361:20030423.

B. Gendre, D. Barret, and N. A. Webb. An XMM-Newton observation of the globular cluster Omega Centauri. *A&A*, 400:521–531, March 2003b. doi: 10.1051/0004-6361:20021845.

R. Giacconi, H. Gursky, F. R. Paolini, and B. B. Rossi. Evidence for x Rays From Sources Outside the Solar System. *Physical Review Letters*, 9:439–443, December 1962. doi: 10.1103/PhysRevLett.9.439.

R. Giacconi, E. Kellogg, P. Gorenstein, H. Gursky, and H. Tananbaum. An X-Ray Scan of the Galactic Plane from UHURU. *ApJL*, 165:L27+, April 1971. doi: 10.1086/180711.

R. Giacconi, S. Murray, H. Gursky, E. Kellogg, E. Schreier, and H. Tananbaum. The Uhuru catalog of X-ray sources. *ApJ*, 178:281–308, December 1972. doi: 10.1086/151790.

R. Giacconi, S. Murray, H. Gursky, E. Kellogg, E. Schreier, T. Matilsky, D. Koch, and H. Tananbaum. The Third UHURU Catalog of X-Ray Sources. *ApJ Supp.*, 27:37–+, February 1974. doi: 10.1086/190288.

R. Giacconi, G. Branduardi, U. Briel, A. Epstein, D. Fabricant, E. Feigelson, W. Forman, P. Gorenstein, J. Grindlay, H. Gursky, F. R. Harnden, J. P. Henry, C. Jones, E. Kellogg, D. Koch, S. Murray, E. Schreier, F. Seward, H. Tananbaum, K. Topka, L. Van Speybroeck, S. S. Holt, R. H. Becker, E. A. Boldt, P. J. Serlemitsos, G. Clark, C. Canizares, T. Markert, R. Novick, D. Helfand, and

K. Long. The Einstein /HEAO 2/ X-ray Observatory. *ApJ*, 230:540–550, June 1979. doi: 10.1086/157110.

O. Y. Gnedin, H. Zhao, J. E. Pringle, S. M. Fall, M. Livio, and G. Meylan. The Unique History of the Globular Cluster ω Centauri. *ApJL*, 568:L23–L26, March 2002. doi: 10.1086/340319.

D. E. Graessle, I. N. Evans, K. Glotfelty, X. H. He, J. D. Evans, A. H. Rots, G. Fabbiano, and R. J. Brissenden. The Chandra X-ray Observatory Calibration Database (CALDB): Building, Planning, and Improving. *Chandra News*, 14: 33–+, March 2007.

J. E. Grindlay, C. Heinke, P. D. Edmonds, and S. S. Murray. High-Resolution X-ray Imaging of a Globular Cluster Core: Compact Binaries in 47Tuc. *Science*, 292:2290–2295, June 2001a. doi: 10.1126/science.1061135.

J. E. Grindlay, C. O. Heinke, P. D. Edmonds, S. S. Murray, and A. M. Cool. Chandra Exposes the Core-collapsed Globular Cluster NGC 6397. *ApJL*, 563: L53–L56, December 2001b. doi: 10.1086/338499.

M. Guainizzi. XMM-SOC-CAL-TN-0018, available at http://xmm.vilspa.esa.es/external/xmm_sw_cal/calib/documentation/index.shtml. 2008.

S. Guillot, R. E. Rutledge, L. Bildsten, E. F. Brown, G. G. Pavlov, and V. E. Zavlin. X-ray spectral identification of three candidate quiescent low-mass X-ray binaries in the globular cluster NGC 6304. *M.N.R.A.S.*, 392:665–681, January 2009. doi: 10.1111/j.1365-2966.2008.14076.x.

S. Gupta, E. F. Brown, H. Schatz, P. Möller, and K.-L. Kratz. Heating in the Accreted Neutron Star Ocean: Implications for Superburst Ignition. *ApJ*, 662: 1188–1197, June 2007. doi: 10.1086/517869.

P. Haensel and J. L. Zdunik. Nuclear composition and heating in accreting neutron-star crusts. *A&A*, 404:L33–L36, June 2003. doi: 10.1051/0004-6361:20030708.

P. Haensel and J. L. Zdunik. Models of crustal heating in accreting neutron stars. *A&A*, 480:459–464, March 2008. doi: 10.1051/0004-6361:20078578.

P. Haensel and J. L. Zdunik. Non-equilibrium processes in the crust of an accreting neutron star. *A&A*, 227:431–436, January 1990.

D. Haggard, A. M. Cool, J. Anderson, P. D. Edmonds, P. J. Callanan, C. O. Heinke, J. E. Grindlay, and C. D. Bailyn. Hubble Space Telescope Advanced Camera for Surveys Imaging of ω Centauri: Optical Counterpart for the Quiescent Low-Mass X-Ray Binary. *ApJ*, 613:512–516, September 2004. doi: 10.1086/421549.

B. Haisch and J. H. M. M. Schmitt. Advances in Solar-Stellar Astrophysics. *PASP*, 108:113–+, February 1996. doi: 10.1086/133700.

W. E. Harris. A Catalog of Parameters for Globular Clusters in the Milky Way. *AJ*, 112:1487–+, October 1996. doi: 10.1086/118116.

M. Harwit. *Astrophysical Concepts*. 2006.

A. Heger, C. L. Fryer, S. E. Woosley, N. Langer, and D. H. Hartmann. How Massive Single Stars End Their Life. *ApJ*, 591:288–300, July 2003. doi: 10.1086/375341.

C. O. Heinke, J. E. Grindlay, P. D. Edmonds, D. A. Lloyd, S. S. Murray, H. N. Cohn, and P. M. Lugger. A Chandra X-Ray Study of the Globular Cluster M80. *ApJ*, 598:516–526, November 2003a. doi: 10.1086/378884.

C. O. Heinke, J. E. Grindlay, D. A. Lloyd, and P. D. Edmonds. X-Ray Studies of Two Neutron Stars in 47 Tucanae: Toward Constraints on the Equation of State. *ApJ*, 588:452–463, May 2003b. doi: 10.1086/374039.

C. O. Heinke, J. E. Grindlay, P. M. Lugger, H. N. Cohn, P. D. Edmonds, D. A. Lloyd, and A. M. Cool. Analysis of the Quiescent Low-Mass X-Ray Binary Population in Galactic Globular Clusters. *ApJ*, 598:501–515, November 2003c. doi: 10.1086/378885.

C. O. Heinke, G. B. Rybicki, R. Narayan, and J. E. Grindlay. A Hydrogen Atmosphere Spectral Model Applied to the Neutron Star X7 in the Globular Cluster 47 Tucanae. *ApJ*, 644:1090–1103, June 2006. doi: 10.1086/503701.

J. W. T. Hessels, S. M. Ransom, I. H. Stairs, P. C. C. Freire, V. M. Kaspi, and F. Camilo. A Radio Pulsar Spinning at 716 Hz. *Science*, 311:1901–1904, March 2006. doi: 10.1126/science.1123430.

A. Hewish, S. J. Bell, J. D. H. Pilkington, P. F. Scott, and R. A. Collins. Observation of a Rapidly Pulsating Radio Source (Reprinted from Nature, February 24, 1968). *Nat.*, 224:472–+, November 1969. doi: 10.1038/224472b0.

E. Høg, C. Fabricius, V. V. Makarov, S. Urban, T. Corbin, G. Wycoff, U. Bastian, P. Schwekendiek, and A. Wicenec. The Tycho-2 catalogue of the 2.5 million brightest stars. *A&A*, 355:L27–L30, March 2000.

M. Hunsch, J. H. M. M. Schmitt, and W. Voges. The ROSAT all-sky survey catalogue of optically bright late-type giants and supergiants. *A&A Supp.*, 127: 251–255, January 1998. doi: 10.1051/aas:1998347.

P. Hut, S. McMillan, J. Goodman, M. Mateo, E. S. Phinney, C. Pryor, H. B. Richer, F. Verbunt, and M. Weinberg. Binaries in globular clusters. *PASP*, 104: 981–1034, November 1992. doi: 10.1086/133085.

H. Inoue. The X-ray astronomy satellite 'ASCA'. *Experimental Astronomy*, 4:1–10, 1993. doi: 10.1007/BF01581810.

J. J. M. in't Zand, M. H. van Kerkwijk, D. Pooley, F. Verbunt, R. Wijnands, and W. H. G. Lewin. Identification of the Optical and Quiescent Counterparts to the Bright X-Ray Transient in NGC 6440. *ApJL*, 563:L41–L44, December 2001. doi: 10.1086/338361.

G. H. Jacoby, J. A. Morse, L. K. Fullton, K. B. Kwitter, and R. B. C. Henry. Planetary Nebulae in the Globular Cluster PAL 6 and NGC 6441. *AJ*, 114: 2611–+, December 1997. doi: 10.1086/118671.

R. D. Jeffries, P. A. Evans, J. P. Pye, and K. R. Briggs. An XMM-Newton observation of the young open cluster NGC 2547: coronal activity at 30 Myr. *M.N.R.A.S.*, 367:781–800, April 2006. doi: 10.1111/j.1365-2966.2005.09988.x.

P. G. Jonker, D. K. Galloway, J. E. McClintock, M. Buxton, M. Garcia, and S. Murray. Optical and X-ray observations of the neutron star soft X-ray transient XTE J1709-267. *M.N.R.A.S.*, 354:666–674, November 2004. doi: 10.1111/j.1365-2966.2004.08246.x.

P. G. Jonker, C. G. Bassa, and S. Wachter. The quasi-persistent neutron star soft X-ray transient 1M 1716-315 in quiescence. *M.N.R.A.S.*, 377:1295–1300, May 2007a. doi: 10.1111/j.1365-2966.2007.11689.x.

P. G. Jonker, D. Steeghs, D. Chakrabarty, and A. M. Juett. The Cold Neutron Star in the Soft X-Ray Transient 1H 1905+000. *ApJL*, 665:L147–L150, August 2007b. doi: 10.1086/521079.

L. J. Kaluzienski, S. S. Holt, E. A. Boldt, and P. J. Serlemitsos. Recurrent X-ray outbursts from Aquila X-1. *Nat.*, 265:606–+, February 1977. doi: 10.1038/265606a0.

T. Kitamura, M. Matsuoka, S. Miyamato, M. Nakagawa, M. Oka, Y. Ogawara, and K. Takagishi. Observation of a New X-Ray Source. *Nat.*, 224:784–+, November 1969. doi: 10.1038/224784a0.

M. Kramer, I. H. Stairs, R. N. Manchester, M. A. McLaughlin, A. G. Lyne, R. D. Ferdman, M. Burgay, D. R. Lorimer, A. Possenti, N. D'Amico, J. M. Sarkissian, G. B. Hobbs, J. E. Reynolds, P. C. C. Freire, and F. Camilo. Tests of General Relativity from Timing the Double Pulsar. *Science*, 314:97–102, October 2006. doi: 10.1126/science.1132305.

J. M. Lattimer and M. Prakash. Neutron Star Structure and the Equation of State. *ApJ*, 550:426–442, March 2001. doi: 10.1086/319702.

J. M. Lattimer and M. Prakash. The Physics of Neutron Stars. *Science*, 304: 536–542, April 2004. doi: 10.1126/science.1090720.

J. M. Lattimer and M. Prakash. Neutron star observations: Prognosis for equation of state constraints. *Phys. Rep.*, 442:109–165, April 2007. doi:

10.1016/j.physrep.2007.02.003.

W. H. G. Lewin, J. van Paradijs, and E. P. J. van den Heuvel, editors. *X-ray binaries*, 1995.

P. M. Lugger, H. N. Cohn, C. O. Heinke, J. E. Grindlay, and P. D. Edmonds. Chandra X-Ray Sources in the Collapsed-Core Globular Cluster M30 (NGC 7099). *ApJ*, 657:286–301, March 2007. doi: 10.1086/507572.

P. Marigo, L. Girardi, A. Bressan, M. A. T. Groenewegen, L. Silva, and G. L. Granato. Evolution of asymptotic giant branch stars. II. Optical to far-infrared isochrones with improved TP-AGB models. *A&A*, 482:883–905, May 2008. doi: 10.1051/0004-6361:20078467.

E. Masana, C. Jordi, and I. Ribas. Effective temperature scale and bolometric corrections from 2MASS photometry. *A&A*, 450:735–746, May 2006. doi: 10.1051/0004-6361:20054021.

J. E. McClintock, R. Narayan, and G. B. Rybicki. On the Lack of Thermal Emission from the Quiescent Black Hole XTE J1118+480: Evidence for the Event Horizon. *ApJ*, 615:402–415, November 2004. doi: 10.1086/424474.

K. Menou and J. E. McClintock. The Quiescent Emission Spectrum of Centaurus X-4 and Other X-Ray Transients Containing Neutron Stars. *ApJ*, 557:304–310, August 2001. doi: 10.1086/321665.

G. Meylan and D. C. Heggie. Internal dynamics of globular clusters. *A&A Rev.*, 8: 1–143, 1997. doi: 10.1007/s001590050008.

M. C. Miller, F. K. Lamb, and D. Psaltis. Constraints on the Equation of State of Neutron Star Matter from Observations of Kilohertz QPOs. In L. Scarsi,

H. Bradt, P. Giommi, and F. Fiore, editors, *The Active X-ray Sky: Results from BeppoSAX and RXTE*, pages 123–+, 1998.

D. G. Monet, S. E. Levine, B. Canzian, H. D. Ables, A. R. Bird, C. C. Dahn, H. H. Guetter, H. C. Harris, A. A. Henden, S. K. Leggett, H. F. Levison, C. B. Luginbuhl, J. Martini, A. K. B. Monet, J. A. Munn, J. R. Pier, A. R. Rhodes, B. Riepe, S. Sell, R. C. Stone, F. J. Vrba, R. L. Walker, G. Westerhout, R. J. Brucato, I. N. Reid, W. Schoening, M. Hartley, M. A. Read, and S. B. Tritton. The USNO-B Catalog. *AJ*, 125:984–993, February 2003. doi: 10.1086/345888.

J. Montalbán, A. Miglio, A. Noels, N. Grevesse, and M. P. di Mauro. Solar Model with CNO Revised Abundances. In D. Danesy, editor, *SOHO 14 Helio- and Asteroseismology: Towards a Golden Future*, volume 559 of *ESA Special Publication*, pages 574–+, October 2004.

F. Özel, T. Güver, and D. Psaltis. The Mass and Radius of the Neutron Star in EXO 1745−248. *ApJ*, 693:1775–1779, March 2009. doi: 10.1088/0004-637X/693/2/1775.

F. Paerels. Pressure Broadening of Absorption Lines in Neutron Star Atmospheres and Prospects for Measuring Neutron Star Masses and Radii. *ApJL*, 476:L47+, February 1997. doi: 10.1086/310485.

R. Pallavicini and N. E. White. *X-ray astronomy with EXOSAT*. 1988.

D. Pooley, W. H. G. Lewin, S. F. Anderson, H. Baumgardt, A. V. Filippenko, B. M. Gaensler, L. Homer, P. Hut, V. M. Kaspi, J. Makino, B. Margon, S. McMillan, S. Portegies Zwart, M. van der Klis, and F. Verbunt. Dynamical Formation of Close Binary Systems in Globular Clusters. *ApJL*, 591:

L131–L134, July 2003. doi: 10.1086/377074.

M. Rajagopal and R. W. Romani. Model Atmospheres for Low-Field Neutron Stars. *ApJ*, 461:327–+, April 1996. doi: 10.1086/177059.

S. Rappaport, D. Dewey, A. Levine, and L. Macri. ROSAT Observations of Nine Globular Clusters. *ApJ*, 423:633–+, March 1994. doi: 10.1086/173841.

A. Renzini and F. Fusi Pecci. Tests of evolutionary sequences using color-magnitude diagrams of globular clusters. *Ann. Rev. A&A*, 26:199–244, 1988. doi: 10.1146/annurev.aa.26.090188.001215.

H. R. Richman. X-Ray Spectra of Cataclysmic Variables from ROSAT. *ApJ*, 462: 404–+, May 1996. doi: 10.1086/177161.

G. H. Rieke and M. J. Lebofsky. The interstellar extinction law from 1 to 13 microns. *ApJ*, 288:618–621, January 1985. doi: 10.1086/162827.

S. Rosswog and M. Bruggen. *Introduction to High-Energy Astrophysics*. September 2000.

R. E. Rutledge, L. Bildsten, E. F. Brown, G. G. Pavlov, and V. E. Zavlin. The Thermal X-Ray Spectra of Centaurus X-4, Aquila X-1 , and 4U 1608-522 in Quiescence. *ApJ*, 514:945–951, April 1999. doi: 10.1086/306990.

R. E. Rutledge, L. Bildsten, E. F. Brown, G. G. Pavlov, and V. E. Zavlin. A Method for Distinguishing between Transiently Accreting Neutron Stars and Black Holes, in Quiescence. *ApJ*, 529:985–996, February 2000. doi: 10.1086/308303.

R. E. Rutledge, L. Bildsten, E. F. Brown, G. G. Pavlov, and V. E. Zavlin. The Quiescent X-Ray Spectrum of the Neutron Star in Centaurus X-4 Observed with

Chandra/ACIS-S. *ApJ*, 551:921–928, April 2001a. doi: 10.1086/320247.

R. E. Rutledge, L. Bildsten, E. F. Brown, G. G. Pavlov, and V. E. Zavlin. Quiescent Thermal Emission from the Neutron Star in Aquila X-1. *ApJ*, 559: 1054–1059, October 2001b. doi: 10.1086/322361.

R. E. Rutledge, L. Bildsten, E. F. Brown, G. G. Pavlov, and V. E. Zavlin. Variable Thermal Emission from Aquila X-1 in Quiescence. *ApJ*, 577:346–358, September 2002a. doi: 10.1086/342155.

R. E. Rutledge, L. Bildsten, E. F. Brown, G. G. Pavlov, and V. E. Zavlin. A Possible Transient Neutron Star in Quiescence in the Globular Cluster NGC 5139. *ApJ*, 578:405–412, October 2002b. doi: 10.1086/342306.

L. Scarsi. SAX overview. *A&A Supp.*, 97:371–383, January 1993.

J. Secker. A statistical investigation into the shape of the globular cluster luminosity distribution. *AJ*, 104:1472–1481, October 1992. doi: 10.1086/116332.

M. Servillat, N. A. Webb, and D. Barret. XMM-Newton observations of the Galactic globular clusters NGC 2808 and NGC 4372. *A&A*, 480:397–407, March 2008. doi: 10.1051/0004-6361:20078327.

A. S. H. Shevchuk, D. R. Fox, R. J. Letcavage, M. Turner, and R. E. Rutledge. A *Swift* Survey of Candidate High $L_{\rm X}/L_{\rm opt}$ Sources from the *ROSAT* Bright Source Catalog – The Initial Ninety Targets. *In Prep.*, 2009.

I. S. Shklovsky. On the Nature of the Source of X-Ray Emission of SCO XR-1. *ApJL*, 148:L1+, April 1967. doi: 10.1086/180001.

K. P. Singh, S. A. Drake, and N. E. White. RS CVn Versus Algol-Type Binaries: A Comparative Study of Their X-Ray Emission. *AJ*, 111:2415–+, June 1996.

doi: 10.1086/117975.

N. Siódmiak, M. Meixner, T. Ueta, B. E. K. Sugerman, G. C. Van de Steene, and R. Szczerba. Hubble Space Telescope Snapshot Survey of Post-AGB Objects. *ApJ*, 677:382–400, April 2008. doi: 10.1086/529115.

S. L. Snowden and J. H. M. M. Schmitt. The ROSAT diffuse X-ray background survey. *A&Sp.Sc.*, 171:207–212, September 1990. doi: 10.1007/BF00646848.

L. Strüder, U. Briel, K. Dennerl, R. Hartmann, E. Kendziorra, N. Meidinger, E. Pfeffermann, C. Reppin, B. Aschenbach, W. Bornemann, H. Bräuninger, W. Burkert, M. Elender, M. Freyberg, F. Haberl, G. Hartner, F. Heuschmann, H. Hippmann, E. Kastelic, S. Kemmer, G. Kettenring, W. Kink, N. Krause, S. Müller, A. Oppitz, W. Pietsch, M. Popp, P. Predehl, A. Read, K. H. Stephan, D. Stötter, J. Trümper, P. Holl, J. Kemmer, H. Soltau, R. Stötter, U. Weber, U. Weichert, C. von Zanthier, D. Carathanassis, G. Lutz, R. H. Richter, P. Solc, H. Böttcher, M. Kuster, R. Staubert, A. Abbey, A. Holland, M. Turner, M. Balasini, G. F. Bignami, N. La Palombara, G. Villa, W. Buttler, F. Gianini, R. Lainé, D. Lumb, and P. Dhez. The European Photon Imaging Camera on XMM-Newton: The pn-CCD camera. *A&A*, 365:L18–L26, January 2001. doi: 10.1051/0004-6361:20000066.

J. Thorstensen, P. Charles, and S. Bowyer. The optical counterpart of Aquila X-1 /3U 1908+00/. *ApJL*, 220:L131–L134, March 1978. doi: 10.1086/182651.

J. A. Tomsick, W. A. Heindl, D. Chakrabarty, J. P. Halpern, and P. Kaaret. Keck Measurement of the XTE J2123-058 Radial Velocity Curve. *ApJL*, 559: L123–L126, October 2001. doi: 10.1086/323752.

J. A. Tomsick, D. M. Gelino, J. P. Halpern, and P. Kaaret. The Low Quiescent X-Ray Luminosity of the Neutron Star Transient XTE J2123-058. *ApJ*, 610: 933–940, August 2004. doi: 10.1086/421865.

J. A. Tomsick, D. M. Gelino, and P. Kaaret. The Low Quiescent X-Ray Luminosity of the Transient X-Ray Burster EXO 1747-214. *ApJ*, 635:1233–1238, December 2005. doi: 10.1086/497587.

J. A. Tomsick, D. M. Gelino, and P. Kaaret. Uncovering the Nature of the X-Ray Transient 4U 1730-22: Discovery of X-Ray Emission from a Neutron Star in Quiescence with Chandra. *ApJ*, 663:461–467, July 2007. doi: 10.1086/518239.

G. Ushomirsky and R. E. Rutledge. Time-variable emission from transiently accreting neutron stars in quiescence due to deep crustal heating. *M.N.R.A.S.*, 325:1157–1166, August 2001. doi: 10.1046/j.1365-8711.2001.04515.x.

E. Valenti, F. R. Ferraro, and L. Origlia. Near-Infrared Properties of 24 Globular Clusters in the Galactic Bulge. *AJ*, 133:1287–1301, April 2007. doi: 10.1086/511271.

M. van den Berg, G. Tagliaferri, T. Belloni, and F. Verbunt. A Chandra observation of the old open cluster M 67. *A&A*, 418:509–523, May 2004. doi: 10.1051/0004-6361:20031642.

S. van den Bergh. Globular clusters and dwarf spheroidal galaxies. *M.N.R.A.S.*, 385:L20–L22, March 2008. doi: 10.1111/j.1745-3933.2008.00424.x.

J. van Paradijs, F. Verbunt, T. van der Linden, H. Pedersen, and W. Wamsteker. Spectroscopic observations of the optical counterpart of Centaurus X-4. *ApJL*, 241:L161–L164, November 1980. doi: 10.1086/183382.

J. van Paradijs, F. Verbunt, R. A. Shafer, and K. A. Arnaud. Soft X-ray transients in quiescence - Observations of AQL X-1 and CEN X-4. *A&A*, 182:47–50, August 1987.

F. Verbunt. Binary Evolution and Neutron Stars in Globular Clusters. In G. Piotto, G. Meylan, S. G. Djorgovski, and M. Riello, editors, *New Horizons in Globular Cluster Astronomy*, volume 296 of *Astronomical Society of the Pacific Conference Series*, pages 245–+, 2003.

F. Verbunt and C. Bassa. X-ray sources in globular clusters. *Chinese Journal of Astronomy and Astrophysics Supplement*, 3:225–234, December 2003.

F. Verbunt, T. Belloni, H. M. Johnston, M. van der Klis, and W. H. G. Lewin. ROSAT observations of soft X-ray transients in quiescence. *A&A*, 285:903–911, May 1994.

O. Vilhu and F. M. Walter. Chromospheric-coronal activity at saturated levels. *ApJ*, 321:958–966, October 1987. doi: 10.1086/165689.

W. Voges, B. Aschenbach, T. Boller, H. Brauninger, U. Briel, W. Burkert, K. Dennerl, J. Englhauser, R. Gruber, F. Haberl, G. Hartner, G. Hasinger, E. Pfeffermann, W. Pietsch, P. Predehl, J. Schmitt, J. Trumper, and U. Zimmermann. Rosat All-Sky Survey Faint Source Catalogue. *IAU Circ.*, 7432:3–+, May 2000.

N. A. Webb and D. Barret. Constraining the Equation of State of Supranuclear Dense Matter from XMM-Newton Observations of Neutron Stars in Globular Clusters. *ApJ*, 671:727–733, December 2007. doi: 10.1086/522877.

N. A. Webb, P. J. Wheatley, and D. Barret. XMM-Newton X-ray and optical observations of the globular clusters M 55 and NGC 3201. *A&A*, 445:155–165, January 2006. doi: 10.1051/0004-6361:20053010.

J. M. Weisberg and J. H. Taylor. The Relativistic Binary Pulsar B1913+16: Thirty Years of Observations and Analysis. In F. A. Rasio and I. H. Stairs, editors, *Binary Radio Pulsars*, volume 328 of *Astronomical Society of the Pacific Conference Series*, pages 25–+, July 2005.

R. Wijnands, C. O. Heinke, and J. E. Grindlay. A Chandra Observation of the Globular Cluster Terzan 1: The Neutron Star X-Ray Transient X1732-304 in Quiescence. *ApJ*, 572:1002–1005, June 2002. doi: 10.1086/340366.

H. Wolter. Spiegelsysteme streifenden Einfalls als abbildende Optiken für Röntgenstrahlen. *Annalen der Physik*, 445:94–114, 1952. doi: 10.1002/andp.19524450108.

P. M. Woods and C. Thompson. *Soft gamma repeaters and anomalous X-ray pulsars: magnetar candidates*, pages 547–586. April 2006.

M. D. Young, R. N. Manchester, and S. Johnston. A radio pulsar with an 8.5-second period that challenges emission models. *Nat.*, 400:848–849, August 1999. doi: 10.1038/23650.

V. E. Zavlin, G. G. Pavlov, and Y. A. Shibanov. Model neutron star atmospheres with low magnetic fields. I. Atmospheres in radiative equilibrium. *A&A*, 315: 141–152, November 1996.